DOT/FAA/AR-01/33

Office of Aviation Research
Washington, D.C. 20591

Investigation of Thick Bondline Adhesive Joints

June 2001

Final Report

This document is available to the U.S. public through the National Technical Information Service (NTIS), Springfield, Virginia 22161.

U.S. Department of Transportation
Federal Aviation Administration

NOTICE

This document is disseminated under the sponsorship of the U.S. Department of Transportation in the interest of information exchange. The United States Government assumes no liability for the contents or use thereof. The United States Government does not endorse products or manufacturers. Trade or manufacturers names appear herein solely because they are considered essential to the objective of this report. This document does not constitute FAA certification policy. Consult your local FAA aircraft certification office as to its use.

This report is available at the Federal Aviation Administration William J. Hughes Technical Centers Full-Text Technical Reports page: actlibrary.tc.faa.gov in Adobe Acrobat portable document format (PDF).

Technical Report Documentation Page

1. Report No.	2. Government Accession No.	3. Recipients Catalog No.
DOT/FAA/AR-01/33		

4. Title and Subtitle	5. Report Date
INVESTIGATION OF THICK BONDLINE ADHESIVE JOINTS	June 2001
	6. Performing Organization Code
7. Author(s)	8. Performing Organization Report No.
J.S. Tomblin, C. Yang, and P. Harter	
9. Performing Organization Name and Address	10. Work Unit No. (TRAIS)
Wichita State University 1845 N. Fairmount Wichita, KS 67260-0093	11. Contract or Grant No. IA031
12. Sponsoring Agency Name and Address	13. Type of Report and Period Covered
U.S. Department of Transportation Federal Aviation Administration Office of Aviation Research Washington, DC 20591	Final Report
	14. Sponsoring Agency Code ACE-110

15. Supplementary Notes

The Federal Aviation Administration William J. Hughes Technical Center Technical Monitor was Peter Shyprykevich.

16. Abstract

In recent years, the use of polymer matrix composite materials as primary structural components has risen, especially in the general aviation (GA) industry. The use of composites not only results in weight savings, but also reduces part counts, joining operations, and results in significant savings in assembly, storage, and inspection. However, joining of some integral parts is still required. GA aircraft industry also uses bonded joints with bondline thicknesses much greater than the 0.01in. that was standard in aircraft bonded joints. For composites, there are two methods of joining: bonding and mechanical fastening. Of the two, adhesively bonding composite structures is the preferred method for a variety of reasons. There are several adhesive test methods that are used to determine the in situ properties of an adhesive joint for use in design. From these methods, ASTM D 1002, D 3165, and D 5656 were evaluated in this investigation with the substrate materials of 2024-T3 phosphoric anodized aluminum, carbon/epoxy quasi-isotropic laminate, and fiberglass/epoxy quasi-isotropic laminate. Bondline thicknesses from 0.010-0.160 inch were evaluated for three paste adhesive systems using different test methods and substrate materials. The apparent shear strength given by the test methods investigated was found to be highly dependent on adherend bending stiffness, which directly effects the peel stress distributions in the adhesive layer. Thin-adherend specimens, regardless of bondline thickness, yielded lower apparent shear strengths than the thick adherend specimens and gave misleading information when comparing the apparent shear strengths of different adhesive systems. The adhesive shear-stress behavior was characterized over the range of bond thicknesses and environmental conditions and several recommendations and correction factors were offered for the thick-adherend test method.

Due to reformulations in the base adhesives and the low glass transition temperatures, which were found during this study, the adhesives investigated in the report may not be representative of the current adhesive formulations used in production of GA aircraft. However, the adhesive mechanical properties reflect the correct trends for the effect of adhesive thickness and environment.

17. Key Words	18. Distribution Statement
Composite materials, Bonded joints, Adhesive test methods, Bondline thickness	This document is available to the public through the National Technical Information Service (NTIS), Springfield, Virginia 22161.

19. Security Classif. (of this report)	20. Security Classif. (of this page)	21. No. of Pages	22. Price
Unclassified	Unclassified	106	

TABLE OF CONTENTS

LIST OF FIGURES

LIST OF TABLES

EXECUTIVE SUMMARY

In recent years, the use of polymer matrix composite materials as primary structural components has risen, especially in the general aviation (GA) industry. The use of composites not only results in weight savings, but also reduces part counts, joining operations, and results in significant savings in assembly, storage, and inspection. However, joining of some integral parts is still required. GA aircraft industry also uses bonded joints with bondline thicknesses much greater than the 0.01in. that was standard in aircraft bonded joints. For composites, there are two methods of joining: bonding and mechanical fastening. Of the two, adhesively bonding composite structures is the preferred method for a variety of reasons. There are several adhesive test methods that are used to determine the in situ properties of an adhesive joint for use in design. From these methods, ASTM D 1002, D 3165, and D 5656 were evaluated in this investigation with the substrate materials of 2024-T3 phosphoric anodized aluminum, carbon/epoxy quasi-isotropic laminate, and fiberglass/epoxy quasi-isotropic laminate. Bondline thicknesses from 0.010-0.160 inch were evaluated for three paste adhesive systems using different test methods and substrate materials. The apparent shear strength given by the test methods investigated was found to be highly dependent on adherend bending stiffness, which directly effects the peel stress distributions in the adhesive layer. Thin-adherend specimens, regardless of bondline thickness, yielded lower apparent shear strengths than the thick adherend specimens and gave misleading information when comparing the apparent shear strengths of different adhesive systems. The adhesive shear-stress behavior was characterized over the range of bond thicknesses and environmental conditions and several recommendations and correction factors were offered for the thick-adherend test method.

Due to reformulations in the base adhesives and the low glass transition temperatures, which were found during this study, the adhesives investigated in the report may not be representative of the current adhesive formulations used in production of GA aircraft. However, the adhesive mechanical properties reflect the correct trends for the effect of adhesive thickness and environment.

1. INTRODUCTION.

The development of composite materials and their production methods have made significant strides over the last 15 years. In the mid 1990s, a major revitalization of the general aviation (GA) industry began to take place. This lead to new applications of polymer matrix composites for a large percentage of both the secondary and primary GA structures. The new small aircraft, spurred by the revitalization of the GA industry, rely heavily on the use of secondary bonded construction. Moreover, there is a trend towards the use of substantially larger bond layer thicknesses (up to 0.160 in.) for which there is little structural performance data available.

As in any aircraft, the assembly of the structure from its constituent parts involves bonded joints, mechanically fastened joints, or a combination of the two. However, for their parts, mechanically fastening composite materials is undesirable due to large diameter/thickness ratios. Mechanical fasteners also tend to be inefficient in load transfer, resulting in areas of high stress concentration. Adhesive joints, on the other hand, tend to be more structurally efficient in that they provide better opportunities to eliminate stress concentrations.

Some of the advantages of using adhesive-bonded joints compared to other joining methods have been given by Kuno, Vinson, and others [1, 2, 3, and 4]:

- Weight and cost savings from using thinner gage materials in the joint.
- Number of production parts can be reduced.
- Manufacturing procedures like milling, machining, forming, and riveting can be reduced or eliminated.
- Adhesive bonds provide a high strength-to-weight ratio with three times the shearing force of riveted joints.
- Improved aerodynamic surfaces and visual appearance.
- Excellent electrical and thermal insulation properties.
- Superior fatigue resistance.
- Allows for variations in coefficients of thermal expansion when joining materials.
- Adhesive joints can distribute the load over a larger area and can take advantage of the ductile response of the adhesive to reduce peak stresses.

It is evident that there are many advantages to using adhesive bonds compared to mechanical fasteners; however, it is difficult to analyze, design, and optimize adhesive bonded joints.

There are many adhesive test methods in use today, but few can generate directly applicable design allowable data for the adhesive system. In order to properly design a joint, the design engineer needs to characterize the adhesive behavior. Once an adhesive has been selected, the

adhesive shear stress-strain data must be characterized over the range of design temperatures and moisture contents.

The most widely used adhesive-bond test specimen is the 0.5-inch single overlap tension test (ASTM D 1002) [5]. The failure mode of the joint is rarely determined by the shear strength of the adhesive but is largely the result of joint deflections and rotations and induced peel stresses. Data from single overlap tension test specimen cannot be used to obtain directly applicable adhesive shear design data but are often used for screening material to compare several adhesives systems and the effects of the environment on the adhesive properties in the selection process of the adhesive. Another similar thin-adherend test specimen is the notched sandwich ASTM D 3165 specimen [6].

To find the shear stress-strain behavior of an adhesive, there are two common test methods employed: the napkin-ring test specimen and the thick-adherend lap shear specimen ASTM D 5656 [7]. The napkin-ring test specimen is seldom used for reasons that will be discussed. This leaves the experimenter with the thick-adherend single-lap shear specimen. A specifically designed extensometer by Raymond Krieger, called the KGR-1, is a popular device used in the aerospace industry for determining in situ adhesive shear properties [8]. This device is designed to measure the shear deformation of a thin adhesive layer in a thick-adherend lap shear specimen. Advantages of this device include:

- Cost-effective, simple, and reusable device
- Can test large groups of specimens for statistical confidence
- Measures the entire nonlinear elastic-plastic spectrum of the adhesive behavior

To use adhesives in certified primary structures, the adhesive modulus and strength must be determined experimentally and under a range of environments. In addition, the use of large bond layer thicknesses pose many questions as to the performance of a thin bond compared to a thicker one. The present investigation evaluated the common test methods used for adhesive characterization. An evaluation of the effect of bondline thickness on the adhesive joint strength and the shear stress-strain behavior was made, including the effect of temperature and moisture.

1.1 LITERATURE REVIEW.

The following review is intended to provide insight into earlier work in the area of the behavior of adhesive joints, both experimentally and analytically.

1.1.1 Analytical Work.

Volkersen developed one of the earliest analytical models of a single-lap adhesively bonded joint in 1938, which assumed only shear deformation in the adhesive [9]. In his analysis, Volkersen determined that shear transfer of the axial stresses in the adherends resulted in what was termed “shear lag,” or a parabolic variation of the shear stress across the lap region. Goland and Reissner conducted further analytical work in the field in 1944 [10]. Their analysis provided important insight into the effect of peel stresses on the strength of adhesive joints and the consequences of bending deflections of the joint due to load path eccentricity. Kutscha and Kutscha and Hofer reviewed other developments in 1961 and 1969, respectively [11 and 12].

A full survey of subsequent work related to the original study by Goland and Reissner is provided by Adams and Wake [13]. Vinson also provides a good literature review in the area of bonding polymer composites [3].

Guess and Gerstle made further steps in the development of analytical models in the 1970s when they compared different test methods both experimentally and analytically [14]. Hart-Smith began modeling the behavior of the single lap joint based on a continuum model and Volkersen's shear lag model [15-18]. Vinson states that in 1975, "Oplinger went far to organize the maze of publications to date on bonded joints. He concluded that it is necessary to include transverse shear deformation, transverse normal strain, temperature effects, nonlinear adherend and adhesive behavior, and viscoelastic behavior to model an adhesive joint of any configuration" [3, 19, and 20]

In recent years, Yang, et al. studied double-lap composite joints under cantilevered bending [21]. Furthermore, Yang and Pang have proposed models for single lap joints under cylindrical bending and tension using laminated anisotropic plate theory [22].

This investigation is also coupled with the development of two models. The first by Yang, et al. [23] involves the evaluation of the thick-adherend specimen. Experimental results from this investigation were used in conjunction with a finite element model to propose adjustments to the ASTM D 5656 test method, which will be discussed further in section 1.2 [23]. Another study by Yang and others involves the development and verification of a model for stress analysis and failure prediction for thin adherend, thick adhesive single lap joints using composite adherends [24].

1.1.2 Experimental Work.

Properly designed adhesive joints should not be critical in the adhesive layer. Instead, the adherend should be designed to fail before the adhesive. In order to achieve this, knowledge of the mechanical properties, particularly the stiffness of the adhesive, is required for design. Several common test methods have been developed that are used to find the strength and modulus properties of the adhesive [5, 6, and 7]. These properties can then be used in the design and analysis of the adhesive-bonded joint. The test methods used to find these properties have been debated and investigated to some extent.

The aforementioned studies done by Guess, et al. [14] found that the adhesive shear strengths measured using the ASTM D 1002 lap shear specimen were too low. This well known fact was further substantiated in their experiments. They also found that the stress gradients through the adhesive layer are of great importance when analyzing and designing adhesive joints. Kriegers KGR-1 extensometer along with the thick-adherend lap shear specimen, aimed to eliminate (or significantly reduce) the peel stresses in the joint in order to improve the shear stress distribution [8]. Adams and Wake found that there was a large discrepancy between the shear modulus found by the KGR-1 extensometer and bulk adhesive values [13]. Post, et al. used moirè interferometry to examine the thick-adherend specimen and found the shear stress distribution to be nearly uniform [25]. Kassapoglou and Adelmann found that error was introduced through slippage of the KGR-1 measuring points and in the specimen calibration procedure [26]. More recently, Tsai, et al. found that much of the error associated with the KGR-1 specimen can be

eliminated by making the load path more centric using notched loading pins or a steel bushing in the pin hole [2]. By comparing the results of the KGR-1 extensometer with strain gage data and moirè interferometry, they found that a KGR-1 extensometer can provide a reasonably accurate measurement of the adhesive shear modulus if the test specimens are loaded centrically.

Previous studies also found that both normal and shear stress concentrations along the length of the adhesive layer are reduced with increased adherend thickness, increased adherend to adhesive modulus ratio, and decreased bond lengths.

1.2 DIFFERENT ADHESIVE TEST METHODS.

There are several commonly used ASTM test standards that are used to obtain adhesive properties. These methods are listed as follows:

- ASTM D 1002 “Standard Method of Test for Strength Properties of Adhesives in Shear by Tension Loadings (Metal-to-Metal)” [5].

- ASTM D 3165, “Strength Properties of Adhesives in Shear by Tension Loading of Single-Lap-Joint Laminated Assemblies” [6].

- ASTM D 5656, “Thick Adherend Metal Lap-Shear Joints for Determination of Stress-Strain Behavior of Adhesives in Shear by Tension Loading” [7].

Another common but less used method is ASTM E 229, the so called “napkin ring test” where bulk adhesive specimens are tested in torsion. This method is not used as often as the others due to a lack in torsional testing machines, high cost-per-test-item, and the specimen configuration is considerably different from those seen in aircraft structures.

The configuration of the three lap-shear test joints can be seen in figures 1 through 3. All three tests specimens are loaded in tension, which in turn places the adhesive in the gage section under shear. However, eccentricity is induced due to the specimen geometry when the specimens are loaded. The adherends rotate as a result of the bending moment in order to align themselves in the load direction. This is illustrated in figure 4. The adherend rotation in turn introduces peel stresses in the adhesive. These peel stresses are most significant in the vicinity of the joint edges and eventually lead to failure of the adhesive joint. ASTM D 5656 specimens have the least amount of adherend rotation and adhesive peel stresses due to the higher bending rigidity and larger adherend cross-sectional area.

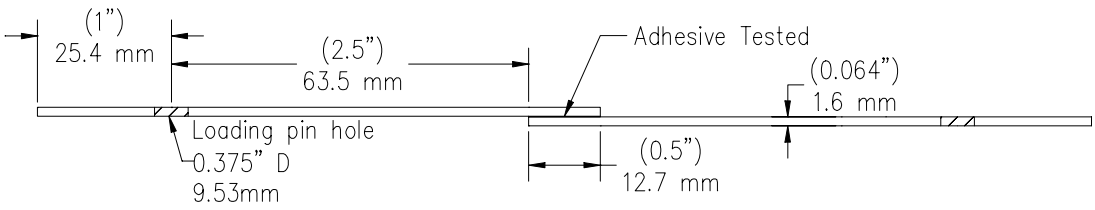

FIGURE 1. ASTM D 1002 TEST SPECIMEN PROFILE [24]

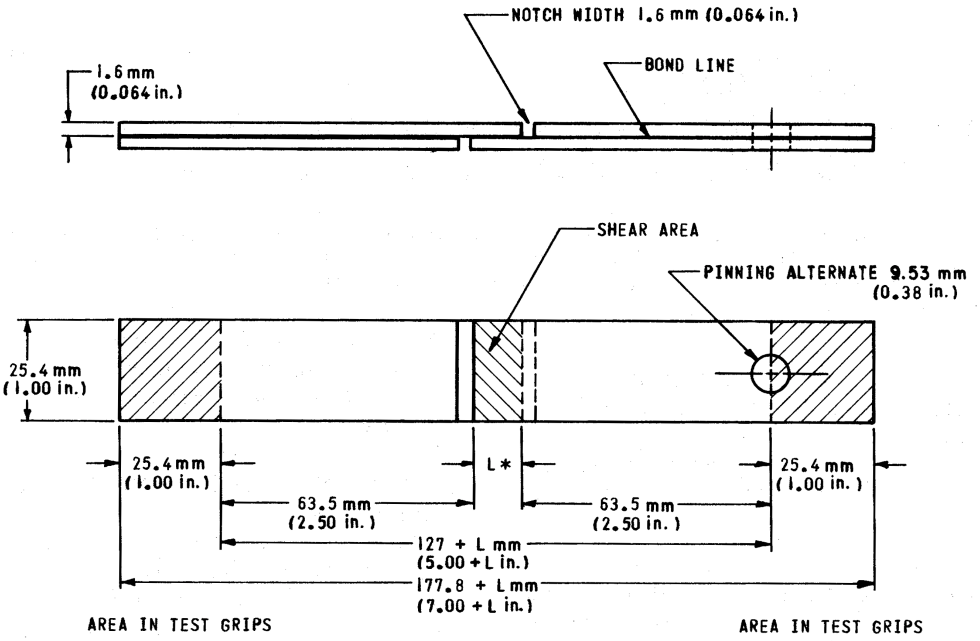

FIGURE 2. ASTM D 3165 TEST SPECIMEN PROFILE [6]

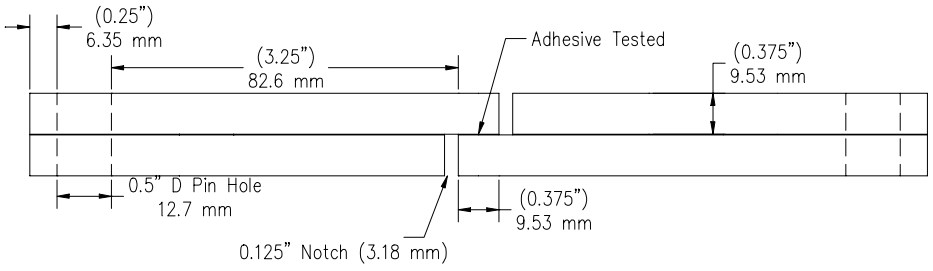

FIGURE 3. ASTM D 5656 TEST SPECIMEN PROFILE [24]

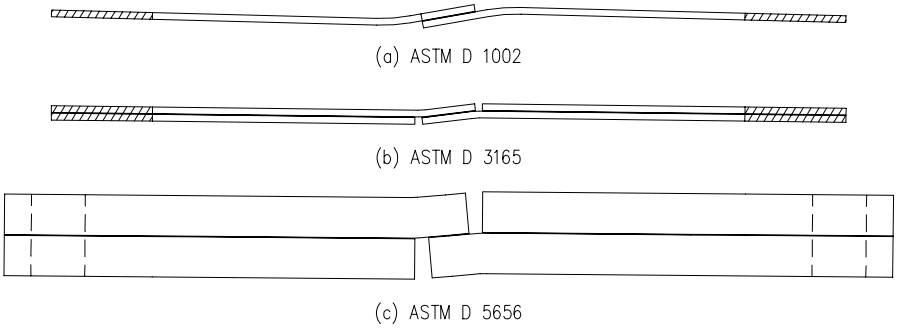

FIGURE 4. DEPICTION OF TEST SPECIMEN DEFORMATION WHILE LOADED [24]

The peel stresses in these specimens, especially ASTM D 1002 and D 3165, present a problem for the design engineer who is interested in finding adhesive properties. Indeed, adhesive shear modulus values and shear strengths cannot be easily determined from the two thin-adherend test methods. They are only capable of providing relative joint strengths when comparing different adhesive systems, and even then can provide "false" results as found by Guess, et al. and also in this investigation [14]. Only the ASTM D 5656 specimen can provide information about the adhesive shear modulus and yield strength. Using an appropriate measuring device, such as the KGR-1 or the KGR-type extensometers used in this investigation, adhesive stress-strain curves can be obtained form the ASTM D 5656 test specimen. From these stress-strain curves, engineering design data can be obtained.

1.3 FAILURE MODES OF ADHESIVE JOINTS.

In order to gain a full understanding of the properties of the adhesive and the joint being investigated, the mode of failure must be characterized. In adhesive technology, there are three typical characterizations for the failure mode of an adhesive joint:

a. Cohesive Failure: A cohesive failure is characterized by failure of the adhesive itself (see figure 5).

b. Adhesive Failure: An adhesive failure is characterized by a failure of the joint at the adhesive/adherend interface. This is typically caused by inadequate surface preparation, chemically and/or mechanically. Specimens that fail adhesively tend to have excessive peel stresses that lead to failure and often do not yield a strength value for the adhesive joint, but rather indicate unsuitable surface qualities of the adherend (see figure 5).

c. Substrate Failure: A substrate failure occurs when the adherend fails instead of the adhesive. In metals, this occurs when the adherend yields. In composites, the laminate typically fails by way of interlaminar failure, i.e., the matrix in between plies fails. A substrate failure indicates that the adhesive is stronger than the adherend in the joint being tested. This is a desirable situation in practical design, but not when determination of adhesive behavior is being studied.

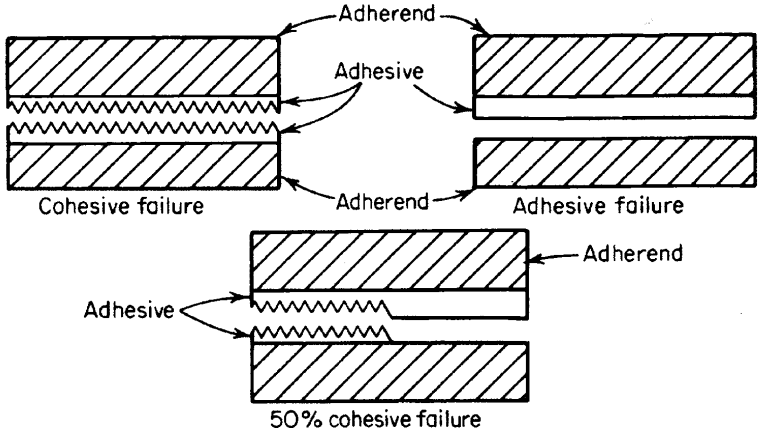

FIGURE 5. COHESIVE AND ADHESIVE FAILURES OF BONDLINE

1.4 TEST MATRICES.

In order to reach the objectives of this investigation, two test matrices were used. The first test matrix was designed primarily to (1) evaluate the common tests methods used for adhesive characterization, (2) evaluate the use of different substrate materials, and (3) to evaluate the effect of bondline thickness on the adhesive joint strength and modulus. Test matrix 1, shown in table 1, made use of three different substrate materials, three test methods, three adhesive systems, and four different bondline thicknesses. All tests for this test matrix were Room Temperature Dry (RTD) with the moisture content as fabricated.

TABLE 1. TEST MATRIX 1: EVALUATION OF COMMON TEST METHODS, DIFFERENT ADHEREND MATERIALS, AND ADHESIVE JOINT PROPERTIES VS BONDLINE THICKNESS

Nominal Bondline Thickness[1]	Adherend Type	Test Methods	Minimum Number of Replicates per Test Condition[2]
0.015″	Aluminum Alloy (2024-T3)	ASTM D 1002 ASTM D 3165 ASTM D 5656	3
0.040″			3
0.080″			3
0.120″			3
0.015″	Carbon Fabric[3]	ASTM D 1002[4] ASTM D 3165	3
0.040″			3
0.080″			3
0.120″			3
0.015″	E-Glass Fabric[3]	ASTM D 1002[4] ASTM D 3165	3
0.040″			3
0.080″			3
0.120″			3
Number of Tests per Resin System			84

Notes:
1. Tolerances on bondline thickness shall be ±0.002″.
2. Test temperature = 70° ±5°F, Moisture content = as fabricated.
3. Only used with Hysol EA9394 adhesive system.
4. Initially proposed but later rejected because of unsatisfactory failure mode.

The substrate materials used in this investigation consisted of the following:

- 2024-T351 Aluminum Alloy—0.064″ thick and 0.375″ thick
- 7-ply quasi-isotropic carbon/epoxy (C/Ep) laminate of 0.068″ average thickness.
- 7-ply quasi-isotropic E-fiberglass/epoxy (Gl/Ep) laminate of 0.069″ average thickness

Ply properties for the composite substrates are given in appendix E. The composite laminates were manufactured according the procedures as outlined in appendix E. The 2024-T351 aluminum was purchased in bulk sheet (0.064 in. thick) or bulk plate form (0.378 in. thick) and handbook material properties were used.

Four different bondline thicknesses were chosen over a range of 0.010″-0.120″ to investigate the effect of bondline thickness with respect to failure mode. As stated before, bondline thicknesses within this range are of interest to the GA industry. There were three paste adhesive systems used: (1) a two-part paste adhesive manufactured by Martin G. Sheufler GmbH, designated MGS A100/B100; (2) a two-part paste adhesive manufactured by PTM&W Industries Inc., designated PTM&W ES6292; and (3) a two-part paste adhesive manufactured by Hysol Inc., designated Hysol EA9394. The first two adhesives listed are of particular interest to GA companies that manufacture small airplanes, but had no baseline data at the time of this investigation. The Hysol system is a derivative of an adhesive system that has been used for military applications and has empirical data available for comparison purposes.

The objective of the second test matrix was to evaluate the adhesive joint strength as a function of bondline thickness when influenced by temperature and moisture effects. The effects of cold, room, and elevated temperatures as well as high moisture content were studied. Test matrix 2 can be broken down into two submatrices. The first submatrix, 2-A, shown in table 2, was designed to study the effect of environmental condition on the adhesive joint strength as a function of bondline thickness. This submatrix used the ASTM D 3165 specimen configuration with carbon/epoxy adherends. Both the MGS and the PTM&W adhesives were evaluated using test matrix 2-A. The second submatrix, 2-B, shown in table 3, used 2024-T3 ASTM D 5656 specimens to study the effect of environmental condition on the adhesive characteristics of the MGS adhesive. Only one adhesive bondline thickness (0.015″) was used for this submatrix.

TABLE 2. TEST MATRIX 2-A: STUDY OF ENVIRONMENTAL EFFECTS AND BONDLINE THICKNESS ON ADHESIVE JOINT STRENGTH

Nominal Bondline Thickness[1]	Test Method[2]	Number of Replicates Per Test Condition			
		CTD[3]	RTD[4]	ETD[5,7]	ETW[6,8]
0.015″	ASTM D 3165[9]	5	5	10	10
0.080″	ASTM D 3165[9]	5	5	10	10
0.160″	ASTM D 3165[9]	5	5	10	10
Total Number of Tests		180			

Notes:
1. Tolerances on bondline thickness were ±0.002″.
2. Adherend materials: ASTM D 5656 – 2024-T3 Aluminum, ASTM D 3165 - C/Ep laminate.
3. Test temperature = -65 ±5°F, Moisture content = as fabricated*
4. Test temperature = 70 ±5°F, Moisture content = as fabricated*
5. Test temperature = 160 ±5°F, Moisture content = as fabricated*
6. Test temperature = 160 ±5°F, Moisture content = 1000 hrs at 145°F, 85% relative humidity (RH)
7. Test temperature = 200 ±5°F, Moisture content = as fabricated*
8. Test temperature = 200 ±5°F, Moisture content = 1000 hrs at 145°F, 85% RH
9. MGS and PTM&W adhesives tested.

* Dry specimens are “as fabricated” specimens that have been maintained at ambient conditions in an environmentally controlled laboratory.

TABLE 3. TEST MATRIX 2-B: STUDY OF ENVIRONMENTAL EFFECTS ON ADHESIVE CHARACTERISTICS

Nominal Bondline Thickness[1]	Test Method[2]	Number of Replicates Per Test Condition			
		CTD[3]	RTD[4]	ETD[5,7]	ETW[6,8]
0.015″	ASTM D 5656[9]	5	5	10	10
Total Number of Tests		30			

Notes:
1. Tolerances on bondline thickness were ± 0.002″.
2. Adherend materials: ASTM D 5656 – 2024-T3 Aluminum, ASTM D 3165 - C/Ep laminate.
3. Test temperature = -65 ± 5°F, Moisture content = as fabricated*
4. Test temperature = 70 ± 5°F, Moisture content = as fabricated*
5. Test temperature = 160 ± 5°F, Moisture content = as fabricated*
6. Test temperature = 160 ± 5°F, Moisture content = 1000 hrs at 145°F, 85% relative humidity (RH)
7. Test temperature = 200 ± 5°F, Moisture content = as fabricated*
8. Test temperature = 200 ± 5°F, Moisture content = 1000 hrs at 145°F, 85% RH
9. MGS adhesive only tested.

* Dry specimens are “as fabricated” specimens that have been maintained at ambient conditions in an environmentally controlled laboratory.

1.5 OTHER TASKS INCLUDED IN THIS INVESTIGATION.

It should be noted that several subtasks were also carried out during this investigation. Bulk adhesive specimens were made to gather baseline information about the three paste adhesives used in this investigation. The “neat” adhesive properties such as tensile modulus, Poisson’s ratio, and the glass transition temperatures of both wet and dry adhesive specimens were obtained using various existing test methods. An in-depth discussion about the procedures and results of these bulk adhesive tests is offered in appendix D and in section 3.1.1.2.

The experimental results from this investigation were also used in conjunction with current studies by Yang, et al. [23]. Experimental data from this investigation was used in the development of an analytical model to determine the stress and strain distributions of adhesive-bonded composite single-lap joints under tension. Data from the ASTM D 5656 tests were used to develop correction factors for the ASTM D 5656 test method via an finite element (FE) model [23]. The results of that study are presented in section 2.6, where the correction factors based on the experimental results from this investigation and the finite element model by Yang, et al. are discussed.

2. CHARACTERIZATION OF THE ADHESIVE SHEAR STRESS-STRAIN RELATIONSHIP.

2.1 ASTM D 5656—THICK-ADHEREND SINGLE-LAP SHEAR SPECIMEN.

The ASTM D 5656 test specimen is commonly used obtain the shear stress-strain behavior of structural adhesives. This section discusses the use of this test method for this investigation, as well as the fabrication, testing, and data reduction procedures used within the investigation.

Figure 6 shows the configuration of the ASTM D 5656 specimen as specified in the test method. All the specimens tested in this investigation were made to the dimensions outlined in ASTM D 5656 unless specified otherwise in this document.

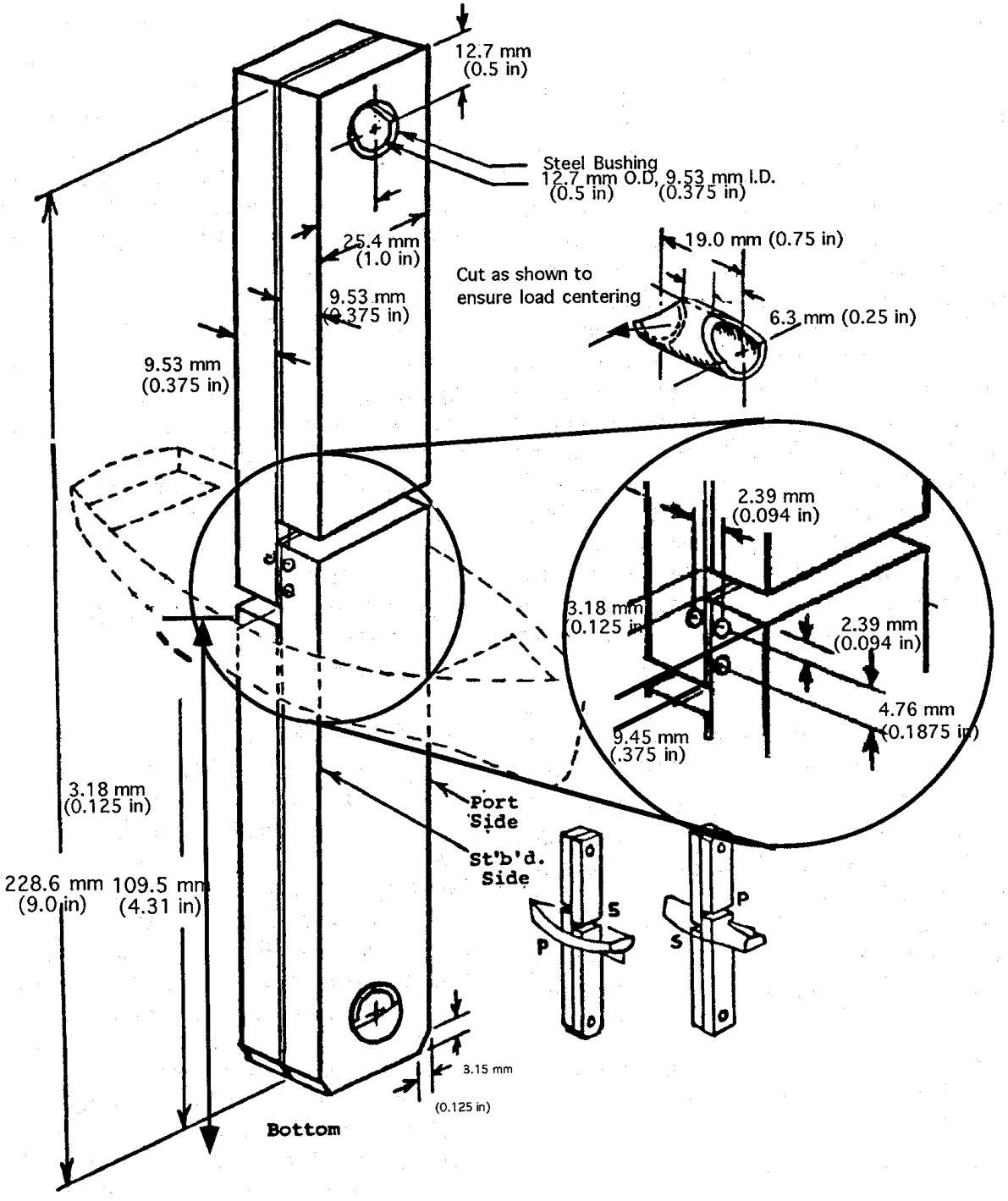

FIGURE 6. ASTM D 5656 SPECIFICATIONS FOR SPECIMEN DIMENSIONS

Using this test method, four different adhesives were investigated. The first adhesive tested was the FM-300K film adhesive. This adhesive was used to validate the KGR-type extensometers used for this test method. A discussion of the KGR-type devices used for characterizing the adhesive shear stress-strain behavior in this investigation is offered in section 2.8. The other three adhesives investigated are structural paste adhesives of interest to the GA industry. Table 4 gives a summary of all ASTM D 5656 specimens used in this investigation.

TABLE 4. SUMMARY OF ALL ASTM D 5656 SPECIMENS USED IN THE INVESTIGATION

Nominal Bondline Thickness[1]	Adhesive[2]	Number of Replicates Per Test Condition (per adhesive system)			
		CTD[3]	RTD[4]	ETD[5,7]	ETW[6,8]
0.007″	FM-300 (film)		6		
0.010″	EA9394, ES9232, A100/B100		5		
0.040″	EA9394, ES9232, A100/B100		5		
0.080″	EA9394, ES9232, A100/B100		5		
0.120″	EA9394, ES9232, A100/B100		5		
0.013″	A100/B100	5	5	10	10
Total Number of Tests		106			

Notes:
1. Tolerances on bondline thickness were ±0.002″.
2. Manufacturers: FM-300 (Cytec), EA9394 (Hysol), ES9232 (PTM&W), A100/B100 (MGS)
3. Test temperature = -65 ±5°F, Moisture content = as fabricated*
4. Test temperature = 70 ±5°F, Moisture content = as fabricated*
5. Test temperature = 160 ±5°F, Moisture content = as fabricated*
6. Test temperature = 160 ±5°F, Moisture content = 1000 hrs at 145°F, 85% relative humidity (RH)
7. Test temperature = 200 ±5°F, Moisture content = as fabricated*
8. Test temperature = 200 ±5°F, Moisture content = 1000 hrs at 145°F, 85% RH

* Dry specimens are “as fabricated” specimens that have been maintained at ambient conditions in an environmentally controlled laboratory.

ASTM D 5656 provides the experimenter with several different options for the choice of the adherend. For this investigation, the adherend was chosen to be aluminum alloy 2024-T351. This material was chosen for several reasons, including ease of machining compared to other materials, time and cost of machining, and familiarity with surface preparation and priming procedures.

2.2 THE KGR-TYPE EXTENSOMETER.

This section addresses the validation of the KGR-type extensometer used in this investigation for gathering adhesive shear strain data. A small fixture was designed and machined at Wichita State University (WSU) to be attached to a Mechanical Test Systems (MTS) axial extensometer, model number 632.11B-20. The fixture attached to an extensometer is shown in figure 7.

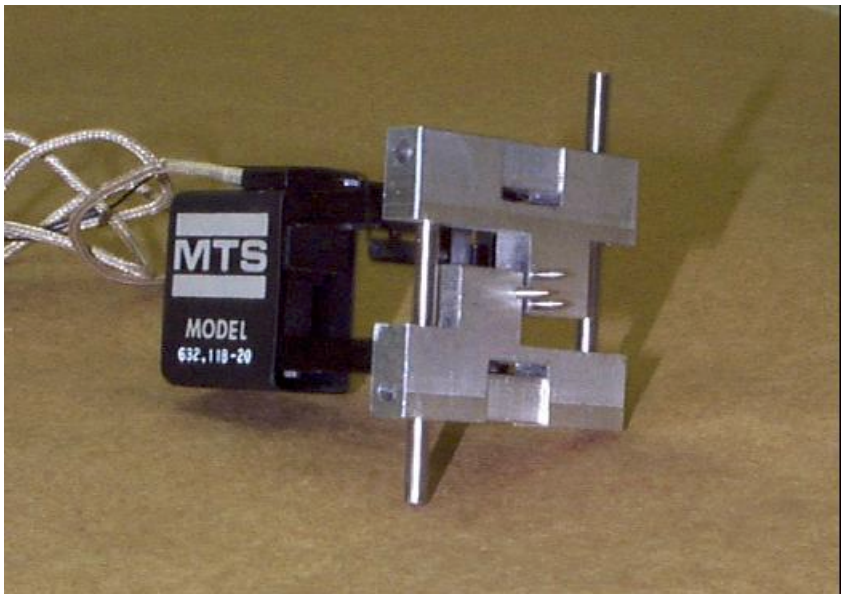

FIGURE 7. THE ORIGINIAL KGR-TYPE EXTENSOMETER

The KGR-1 device is designed to measure the relative displacement between two points, across the adhesive using a three-pin configuration as shown in figure 6. The third pin is used to align the device during loading when rotation occurs. The WSU device uses the same general concept as the KGR-1 device; however, several modifications were made to enable the device to collect more accurate data, which will now be discussed.

The KGR-type device was used to gather data for characterizing the stress-strain relationship of adhesives to be investigated using ASTM D 5656 test specimens. The ASTM specifications are designed around the KGR-1 device, which has a three-pin configuration that rests on the surface of the ASTM specimen. Initially, the fixture used for this investigation was made with the same three-pin configuration. However, initial tests showed that large scatter resulted in many of the tests which could be attributed to:

- Slippage of the mounting pins on the surface of the ASTM D 5656 specimen.
- Stretching of the adherend between the holes under the tensile load [23]. Although the stretching of the adherend is very small, the error caused by this slippage is quite considerable, because the displacement due to the shear strain of the adhesive is also very small.
- Rotation of the KGR-type fixture while under load. Even small rotations are significant due to the small displacements being measured.

It was decided that these discrepancies could be reduced in two ways: (1) adding a fourth pin to reduce any unwanted rotation of the device (described later), and (2) drilling small holes into the adherend of the same size as the pins. By drilling mounting holes into the adherend, any slippage of the measuring pins on the surface of the specimen was eliminated. Moreover, the need for any spring force used in mounting the devices was eliminated, since the fixtures could

slide into the predrilled holes. The pin diameter holes were drilled to a depth of 0.15″ into the adherend. Upon testing, the KGR-type device was mounted to the specimens by inserting the pins into the holes. Inserting the device into the mounting holes proved to eliminate most of the scatter due to slippage during the tests.

An extra mounting hole was also added to the specimen for more accurate measurements at low loads. During initial tests with the KGR-type device, it was difficult to get accurate readings for stresses under 1000 psi (where the initial modulus data was recorded). Displacements in this region are extremely small (on the order of 0.0003″-0.0005″) and any slack, slippage, rotation, or noise in the system can obscure the data substantially. To help reduce any slack in the system, an extra pin was added to the original fixture shown in figure 7, which helped substantially in getting readings for the initial stress-strain behavior of the adhesive. It should be noted that the addition of the extra pin causes the KGR-type device to gather reading from the midpoint instead of the quarter-point.

2.3 SURFACE PREPARATION AND BONDING PROCEDURE.

All aluminum specimens for this test method were fabricated using the procedure outlined below. A large plate (4′ by 12′ by 0.378″) of the raw material was purchased and rough cut with a circular saw into 10″ by 10″ panels, taking care to keep track of the grain direction. These subpanels were surface ground to 0.365″ in order to remove the oxidation layer and any slight bowing of the material.

In practice, metals receive some kind of surface preparation treatment before bonding to aid in adhesion and to protect the surface from corrosion. For this reason, the surface ground panels were phosphoric anodized and bond primed by Cessna Aircraft Co. following ASTM D 3933 [27].

Once the aluminum was finished with the anodization process, it was ready for bonding. The aluminum panels were cleaned with acetone prior to bonding. All subpanels that used paste adhesives were fitted with spacers at this point. Figure 8 shows the general configuration of the spacers on the adherend-bonding surface. The test section was located and marked to aid in the spacer placement, and aligned with the grain direction of the aluminum. The spacers were affixed to one of the subpanels using double-sided tape and care was taken to keep all spacers out of the overlap section. For the validation of the KGR-type extensometers, FM-300K film adhesive with a cloth carrier was used, therefore, no spacers were needed to control the bondline thickness. At this point, the subpanels were ready for the application of the adhesive.

For the validation specimens, the thawed film adhesive was placed on one of the panels with the second panel being placed on top immediately. The edges of the assembly were taped with flash breaker tape and two thermocouples were attached at the bondline in order to monitor the temperature at the bondline during the cure. The finished assembly was then wrapped in separator film and breather and vacuum bagged. An autoclave was used to cure the bagged assembly. The assembly was cured at 350°F for 75 minutes at 50 psi in an autoclave using the thermocouple readings at the bondline as the parameters for the cure cycle. Once the cure cycle was complete, the assembly was removed from the autoclave and vacuum bagged.

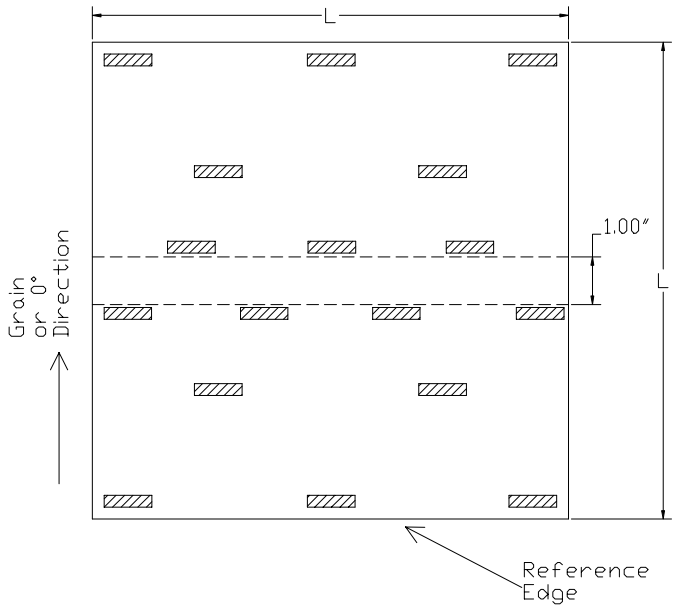

FIGURE 8. SCHEMATIC SHOWING GENERAL LOCATION OF THE SPACERS ON THE ADHEREND SURFACE PRIOR TO BONDING
(Spacers denoted as hatched rectangles. L is 10″ for ASTM D 5656.)

For all other ASTM D 5656 specimens used in this investigation, a paste adhesive was used. After mixing the adhesive as outlined in appendix B, a thin layer is applied to one surface of each subpanel. This thin, continuous layer assures that the entire surface is wetted and helps the adhesive to spread uniformly. Adhesive was then added uniformly over the entire surface of the subpanel that had been fitted with spacers until it reaches a level just above the spacers. Special care was taken to keep the amount of air bubbles trapped in the adhesive to a minimum.

Once the adhesive was applied completely, one edge of the subpanel without spacers was lined up on top of the other subpanel and was slowly placed down from one edge to the other. This minimizes the chances for air to be trapped between the two subpanels. The reference edge was then fixed using flash breaker tape. The bonded assembly was secured in other places with tape and then placed between two pieces of separator film.

After trying several methods, it was found that the best way to assure that the subpanels were sitting firmly atop the bondline spacers was to use a hydraulic press. The wrapped assembly was placed on the lower platen of a large hydraulic press. The press was slowly closed and then ramped up to a load of 6-7 kip at room temperature and kept there for 5 minutes. This gives the excess adhesive time to flow out, and in so doing, allows for the top plate of aluminum to sit firmly atop the bondline spacers. After the platens were lowered, the bonded assembly was removed and placed on top of a large aluminum caul plate, which was then vacuum bagged. The vacuum bag holds the assembly in place during the cure cycle.

The assembly was cured for three hours at 120°F, allowed to cool to room temperature, and then removed from the vacuum bag. For the Hysol EA9394 adhesive system, the bonded panels were

ready for machining. An additional postcure segment of 175°F for 5 hours was used for both the MGS and PTM&W adhesives (per Cirrus Design specifications).

2.4 SPECIMEN FABRICATION PROCEDURE.

Once the cure cycle was complete, the bonded assembly was ready to be machined into individual specimens. The first step was to remove any adhesive from the reference edge and the adherend faces by hand filing. The next step in the process was to drill the holes where the load was applied. The panel was aligned and mounted on the bed of a Bridgeport CNC machine. The holes were drilled and reamed to size using abundant coolant to ensure that the specimen was not overheated in the machining process. The drilled panels were removed from the CNC machine and rough cut into 1.25″ wide strips on a band saw. The strips were cut oversize to avoid overheating and stressing of the bondline.

After the band saw roughing cut, the specimens were labeled using the scheme outlined in appendix C and returned individually to the CNC machine to machine the final width, length, and slot dimensions per figure 6. TiN-coated end mills were used for most milling operations in order to reduce cutter wear due to the abrasive nature of the adhesives. Because a computer-controlled machine was used, high accuracy and repeatability was achieved in the machining process. It also drastically reduced the time of machining, compared to manually machining the specimens.

The final step in the machining process was to drill the KGR-type extensometer mounting holes. The placement of these holes is shown in figure 9. The holes were drilled on the CNC machine as well to assure their exact placement according to specification.

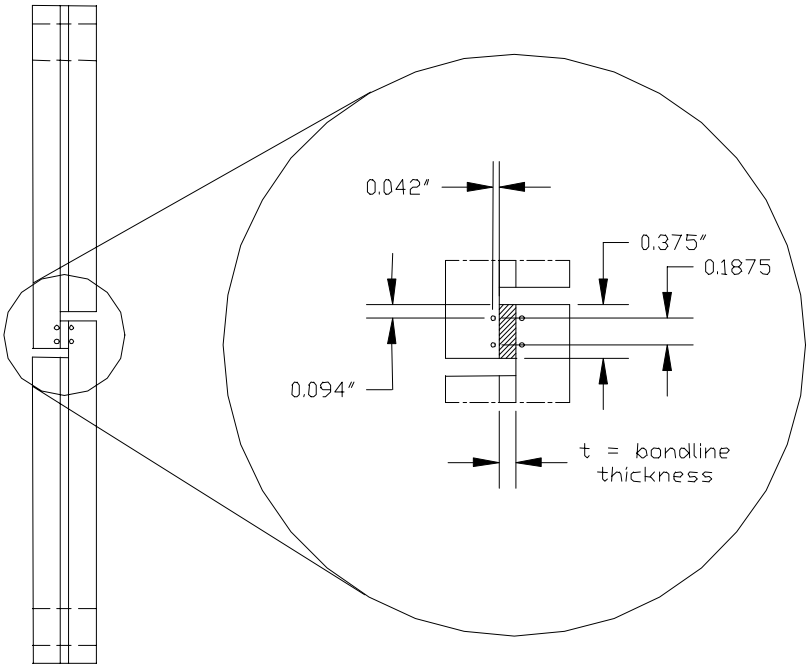

FIGURE 9. LOCATION OF THE MOUNTING HOLES ON THE ASTM D 5656 SPECIMEN

In addition to adding an extra mounting pin, the distance between the pins had to be modified for this investigation. The ASTM specifications call for a distance of 0.094 inch from center to center across the adhesive thickness (see figure 6). However, this investigation included several different bondline thicknesses ranging from 0.007″-0.160″. Because of this, it was decided that for all bondline thicknesses, the distance from the center of each hole to the adherend/substrate interface would remain constant. A distance of 0.042″ from the center of the mounting holes to the interface was decided on by assuming that the ASTM specifications were for a specimen with bondline thickness equal to 0.010″. By choosing a constant value for this distance, the amount of aluminum that was deformed for each test, regardless of bondline thickness, remained constant for all tests. This proved to be an important attribute for the finite element modeling correction factors discussed in section 2.6.

After completing all of the above steps in the fabrication and machining processes, the ASTM D 5656 specimens were ready for the testing phase. The specimen testing procedure is discussed in full in section 2.5.

2.5 SPECIMEN TESTING PROCEDURE.

After the machining process, specimens had to be dimensioned prior to testing. Measurements were taken for the width, length, and thickness of the bondline at the test section. Measurements for the width and length of overlap were taken using precision calipers and recorded digitally on a spreadsheet to eliminate any errors introduced by manual input. Thickness measurements were taken using a micrometer and recorded digitally as well. Bondline thickness measurements were found by taking the total thickness of the specimen at the gage section and then subtracting the thickness of the adherends, which were measured with a micrometer prior to bonding. Two measurements were taken for each parameter and were recorded. Calculations were carried out using the average of the two recordings for each parameter.

Part of this investigation included characterizing the adhesive shear stress-strain relationship as a function of environmental conditioning. All specimens for the RTD, CTD, and ETD tests were ready for testing immediately after the measurement process. ETW test specimens required moisture conditioning after the measurement phase before they were tested.

All testing was carried out on a universal 5.5 kip MTS test stand. All tests used displacement control at a rate of 0.05 in/min as per ASTM specifications. Data for the crosshead displacement, load, and both KGR-type extensometers were collected using TestWorks™ software.

Each specimen was attached to a clevis test fixture as shown in figure 10. One-half-inch steel bushings were inserted into the loading holes, followed by 0.375″ steel dowel pins which attach the specimen to the clevis arrangement. Tsai, et al. found in their experiments on load eccentricity, that using the bushing/pin (or a notched pin) configuration led to the least amount of eccentricity during loading [2].

The KGR-type extensometers were mounted onto the specimens using the predrilled guide holes. Initial trial tests of the FM-300 film adhesive used the three-hole configuration along with small

springs that were attached to the fixtures to hold them in place during the test. This proved to be insufficient in providing accurate readings for the initial stress-strain relationship of the adhesive. Therefore, an additional pin was added to the fixture as mentioned before and the springs were no longer needed. This four-pin configuration was used for the remainder of the investigation.

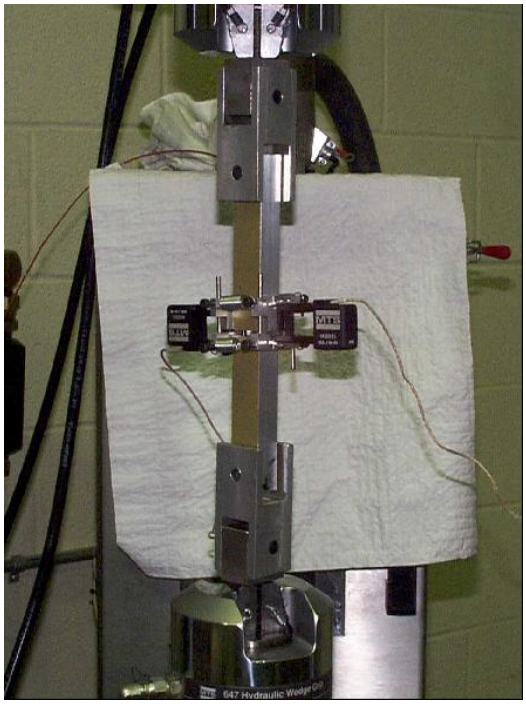

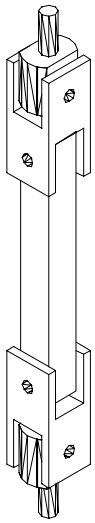

FIGURE 10. PICTURE AND SCHEMATIC DRAWING OF THE ASTM D 5656 SPECIMEN MOUNTED IN THE CLEVIS FIXTURE. CLEVIS ARRANGEMENT ALLOWS ROTATIONAL ALIGNMENT ON THREE AXES.

Once the KGR-type devices were fixed to the specimen, testing was initiated. The computer recorded the load, crosshead displacement, time, and both extensometer readings. The testing could be plotted in real time so that any irregularities could be seen and recorded during the test. In addition, tests could be stopped or paused in the event that a fixable irregularity occurred. It should be mentioned that if a test was interrupted or stopped, it was noted so that it could be discarded if necessary. If the specimen was then retested, it was only done if the initial load was within the linear elastic range of the adhesive. After the test was finished, the maximum load was recorded by hand and the specimen was removed from the clevis fixtures.

Environmental testing was carried out in much the same manner as RTD specimens. An environmental chamber was used to control the test temperature to within ±5°F. After the chamber had reached the test temperature, the specimens were mounted and instrumented in the same manner as before. In addition, a thermocouple was placed on the specimen to record the temperature at the test section. Three time values were recorded for each test. First, the time to reach the test temperature was recorded. After the specimen reached the test temperature, it was allowed to soak for 2-3 minutes. This soak time was also recorded. At this point, the specimen was tested and the test temperature was recorded. The final time recorded was the test time.

2.6 DATA REDUCTION.

Reduction of the data from each test was carried out using the procedure discussed in this section. In addition, FE analysis carried out by Yang, et al. in conjunction with this investigation, added additional correction factors which will also be discussed [23].

The first step in the data reduction phase was to import the raw data for the crosshead displacement, load, and both KGR-type extensometer readings into Microsoft (MS) Excel from a text file. A data filtering program was made using FORTRAN that filtered noise out of the original data. Vibrations from the actuator caused the data to have some scatter, which was quite apparent in the low stress regions. After some investigation, it was found that noisy data could be filtered out using a simple routine that removed any actuator displacements that were less than the previous ones. The filtered data was sent to a spreadsheet, and the data from the extensometers was then corrected to set the initial point at zero. This was necessary in case the extensometers began collecting data at some value above or below zero, which occurred frequently. Next, the shear stress, τ_i, on the adhesive at each point was calculated using equation 1 below.

$$\tau_i = P_i / A \tag{1}$$

where P_i is the load and A is the initial overlap area (length times width). The next step in the process is to find the adhesive shear strain.

A correction for the displacement of the adherend that occurs between the pins and the adherend/adhesive interface, δ_m, is found by using equation 2 from the ASTM standard,

$$\delta_m = \frac{p-t}{p} M \frac{L}{1000} \tag{2}$$

where p is the average point gap and t is the bondline thickness. M is the metal displacement at 1000 lbf as found from the all aluminum dummy sample and L is the load at displacement δ_a. Refer to figure 11 for a schematic definition of p and t.

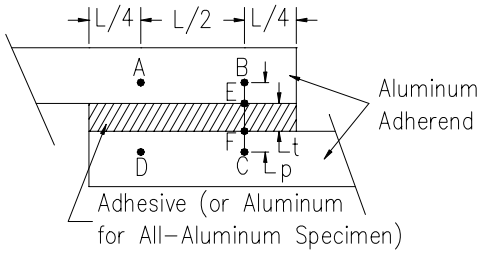

FIGURE 11. ZOOMED IN VIEW OF GAGE SECTION BEFORE LOADING—POINTS A, B, C, AND D ARE THE QUARTER POINT MOUNTING LOCATIONS FOR THE KGR-TYPE EXTENSOMETER [23]

The shear strain, γ_i, at each point is calculated using equation 3, taken from the ASTM standard, assuming small angle theory,

$$\gamma_i = \frac{\delta_a - \delta_m}{t} \tag{3}$$

where δ_a is the measured displacement of the KGR-type extensometer and δ_m is the ASTM correction factor for the adherend displacement that occurs between the measuring points and the adherend/adhesive interface. Refer to figure 12 for a schematic view of this relationship.

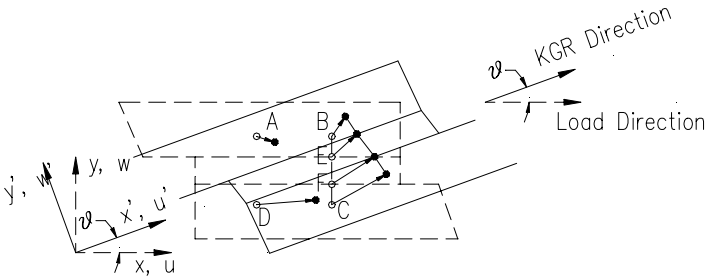

FIGURE 12. ZOOMED IN VIEW OF GAGE SECTION WHILE LOAD IS APPLIED
(Note the movement of the measuring points due to rotation and stretching) [23]

Finite element modeling of the all aluminum dummy specimen by Yang, et al. [23] showed that equation 2 is insufficient in correcting for the shear displacement of the adherend. An additional correction factor must be applied to the metal displacement as offered by Yang. This correction factor, F_a, corrects the ASTM term δ_m for the effect of rotation and stretching of the dummy specimen. Each of the all aluminum dummy specimens had a different simulated bondline thickness, $t_{simulated}$, corresponding to the thicknesses under investigation. Because a nonconstant shear strain exists between the points of measurement in the dummy specimen, multiplying the ASTM term δ_m by the correction factor F_a corrects for the actual displacement of the adherend between the measuring points and the adhesive interface. The reader is directed to this reference where a more detailed explanation of this correction factor can be found [23]. Equation 4 shows the

$$\delta_m = \frac{p - t}{p} M \frac{L}{1000} F_a \tag{4}$$

where F_a is the relationship between the all aluminum correction factor and the simulated bondline thickness for $t_{simulated}$ in inches.

$$F_a = -1.73 t_{simulated} + 1.065 \tag{5}$$

One final correction is needed before a graph can be made showing the adhesive shear stress versus shear strain relationship. This final correction is a calibration constant that is

device dependent. An explanation of how the KGR-type devices were calibrated is offered in appendix B. The measured displacement of each KGR-type device, δ_a, was multiplied by the calibration correction factor corresponding to each particular device. This being done, the adhesive shear strain data was completely corrected and ready to plot.

An example of an adhesive shear stress-strain plot is shown in figure 13. A variation of this graph yields the adhesive shear modulus, G, which is shown in figure 14. The adhesive shear modulus is found by

$$G_{ASTM} = \frac{\tau}{\gamma} \tag{6}$$

where τ is the adhesive shear stress from equation 1, and γ is the adhesive shear strain from equation 3. In order to find the shear modulus from the adhesive shear stress-strain graph, a curve fit is applied to the initial linear section of the stress-strain curve. This is illustrated in figure 14, where the data points for the average reading of both KGR-type devices were curve fit. MS Excel fits the data and computes the equation of the line that fits the data. The slope of this line is the $G_{ASTM.}$

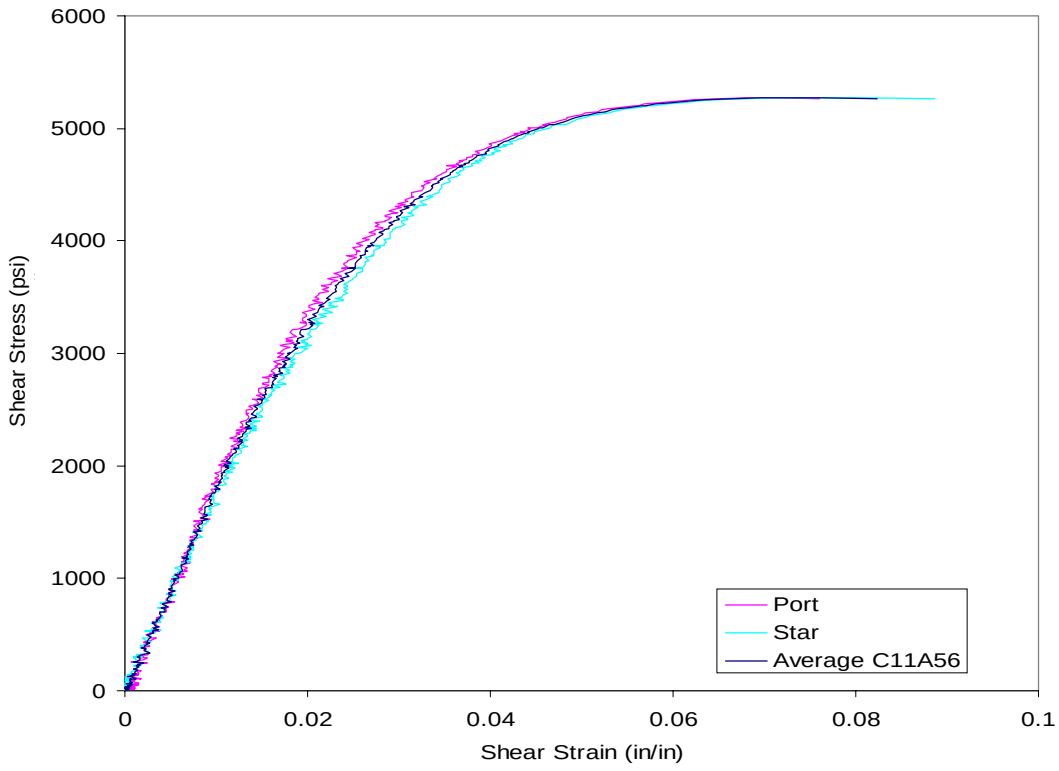

FIGURE 13. EXAMPLE OF AN ADHESIVE SHEAR STRESS-STRAIN CHART
(This chart shows the readings from both KGR-type devices and the average reading (MGS adhesive, t = 0.013″, RTD test))

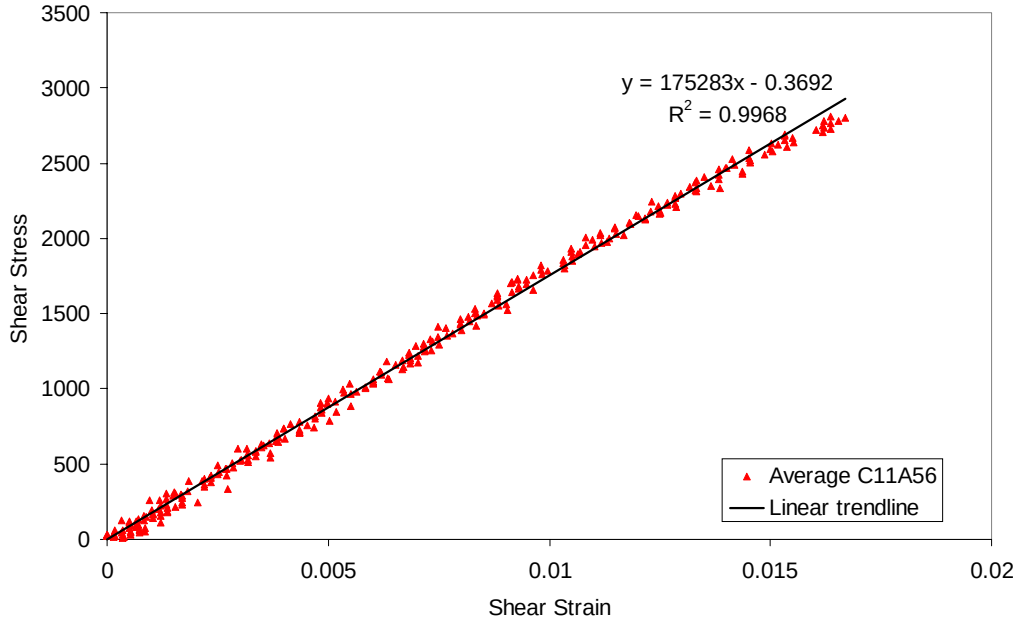

FIGURE 14. EXAMPLE OF AN ADHESIVE SHEAR STRESS-STRAIN CHART FROM WHICH THE SHEAR MODULUS, *G*, IS FOUND FROM THE SLOPE OF THE LINEAR CURVE FIT
(MGS adhesive, $T = 0.013''$, RTD test)

Comparison of experimental data from this investigation with the analytical model developed by Yang, et al. showed that the G_{ASTM} can deviate as much as 20% from the G_{true}, the value of the adhesive shear modulus assumed in finite element computations [23]. It was found that due to the nonuniformity of the shear strain along the overlap length, the calculated shear modulus, G_{ASTM}, varies with the adhesive bondline thickness and the stiffness of the adhesive. In order to correct for this variation, a linear function between G_{true} and G_{ASTM} was obtained using a nonlinear regression among the data points.

$$G_{recovered} = C_1 G_{ASTM} + C_2 \tag{7}$$

The coefficients C_1 and C_2 are functions of the bondline thickness in the form of

$$\begin{aligned} C_1 &= 1.28t^{0.068} \\ C_2 &= -0.07 + 10.58e^{-83.62t} \end{aligned} \tag{8}$$

Where t is in inches and G_{ASTM} is ksi. Yang, et al. found that after this correction is applied, the $G_{recovered}$ has an error of less than 1.5% when compared with G_{true} from the FE model [23].

2.7 DUMMY SPECIMEN TESTING.

This section discusses the results of the various aluminum dummy specimens tested in this investigation. These specimens were tested as discussed in section 2.5 in order to provide the correction factor, *M*, for equation 2. This correction factor is used in the ASTM D 5656 test method to correct for the metal displacement, δ_m.

As suggested by the ASTM standard, it is necessary to correct for the adherend displacement that occurs during the testing of the ASTM D 5656 specimen. As mentioned previously, this displacement is very small in a macro sense. However, when compared with the adhesive displacement, the displacement due to the adherend will cause significant error if ignored.

Several different all aluminum dummy specimens were manufactured to correspond to the different bondline thicknesses under investigation. All aluminum specimens were made with simulated bondline thicknesses of 0.012″, 0.040″, 0.080″, and 0.120″. These were all tested within the elastic range of the aluminum, and the load and extensometer data was collected. An example of this data plotted is shown in figure 15.

After the data is plotted, it is curve fit so that the term *M,* the displacement of the adherend at 1000 lbs, can be calculated for use in equation 2. Figure 15 shows the adherend deformation for an all aluminum dummy specimen with a $t_{simulated}$ of 0.012″, which can be approximated linearly. At a load of 1000 pounds, the displacement of the adherend is 0.0001″. Table 5 shows the displacement of the all aluminum dummy specimens corresponding to the simulated bondline thickness, $t_{simulated}$.

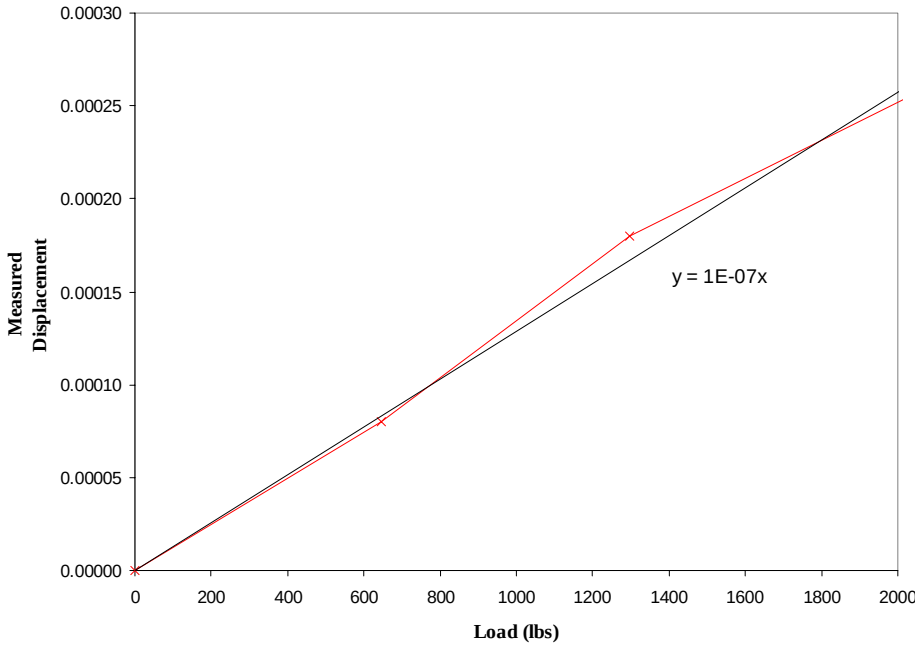

FIGURE 15. EXAMPLE OF GRAPH SHOWING THE DEFORMATION OF THE METAL ADHEREND WITH RESPECT TO THE LOAD
(The data is fit with a linear fit so that the displacement at 1000 lbs can be found)

TABLE 5. VALUES OF *M* FOR EQUATION 2 FOR EACH SIMULATED BONDLINE THICKNESS

$t_{simulated}$ (inches)	Displacement of Aluminum Dummy Specimen at 1000 lbs. (inches)
0.012	$10.0*10^{-5}$
0.040	$9.0*10^{-5}$
0.080	$8.0*10^{-5}$
0.122	$7.0*10^{-5}$

2.8 KGR-TYPE DEVICE VALIDATION STUDY.

Before the designed and fabricated KGR-type device could be used for this study, it was necessary to conduct a validation. The data collected by the device needed to be compared with the data gathered by an actual KGR-1 device. Boeing Phantom Works [28 and 29] supplied a shear stress vs strain chart for tests that were conducted on Cytec FM-300K film adhesive using a KGR-1 device.

A small amount of FM-300K was donated by Cessna Aircraft Company to be used for this study. Several test specimens were fabricated and tested as described in sections 2.4 and 2.5 respectively. Initial tests with these specimens yielded scattered data that did not match the baseline data from reference 27. It was at this time that it was decided to drill the guide holes into the adherend as discussed previously. Several specimens were made this way and tested using the three-pin configuration. At the time of the validation testing, only one extensometer was providing data due a faulty strain cartridge, but both were attached to the specimen in accordance with the ASTM.

The adhesive shear stress and strain data were calculated using equations 1, 2, and 3 per ASTM specifications. None of the corrections to ASTM D 5656 offered by Yang, equations 5, 7, and 8, were applied to the data because the data [27] was reduced using the ASTM equations only. The stress-strain curves for three specimens tested using the KGR-type extensometers were averaged and are plotted along with the data [27] in figure 16.

It can be seen from the figure that the data gathered by the WSU fixture fit the provided data rather well. The shear modulus data was found to be within 5% of the baseline data [27]. The maximum shear stresses for both curves are relatively close as well. Based on this comparison, it was decided that the modified devices were capable of characterizing the adhesive shear stress-strain relationship.

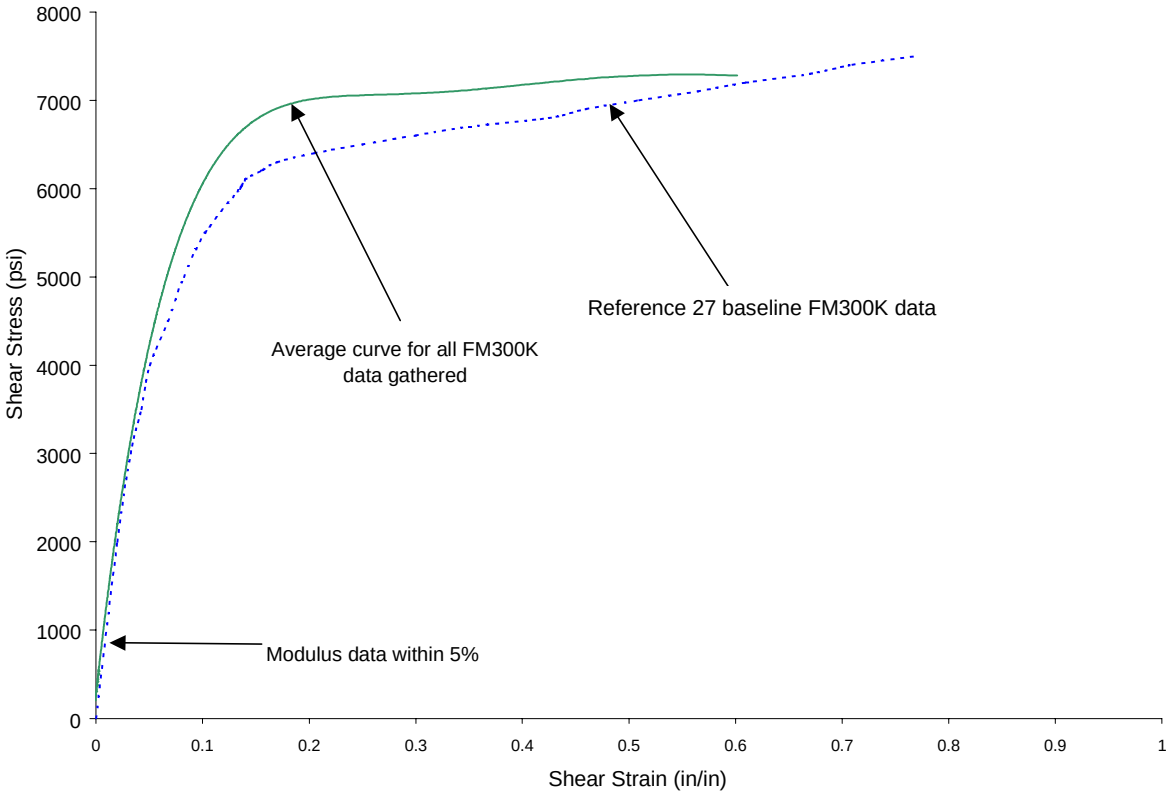

FIGURE 16. COMPARISON OF FM-300 ADHESIVE SHEAR STRESS VS STRAIN DATA COLLECTED USING THE WSU KGR-TYPE DEVICE COMPARED WITH DATA GATHERED BY BOEING PHANTOM WORKS USING A KGR-1 DEVICE

2.9 THIN-ADHEREND SINGLE-LAP SHEAR TEST SPECIMENS.

Thin-adherend lap shear test specimens are the most widely used in industry for adhesive strength determination. The more commonly used ASTM D 1002 test specimen and the ASTM D 3165 test specimen are intended for determining the comparative shear strengths of adhesives in large area joints. These test methods are useful in that the joint configuration closely simulates the actual joint configuration of many bonded assemblies. Moreover, they are also useful as in-process quality control tests for laminated assemblies. Caution should be employed when using the apparent strength values obtained from these tests, because different adhesives may respond differently in different joints [13,14].

This section will discuss the different procedures used in this investigation to prepare and test all of the thin-adherend single-lap shear specimens. Topics discussed will include adherend preparation, bonding procedures, specimen fabrication procedures for both aluminum and composite test specimens, and the testing procedures used in this investigation.

2.10 SPECIMEN CONFIGURATION.

The configuration of both the ASTM D 1002 test specimen and the ASTM D 3165 test specimen are shown again in figures 17 and 18 for the readers convenience. Both test methods use thin metal (or composite) adherends to characterize the apparent shear strengths of adhesive joints.

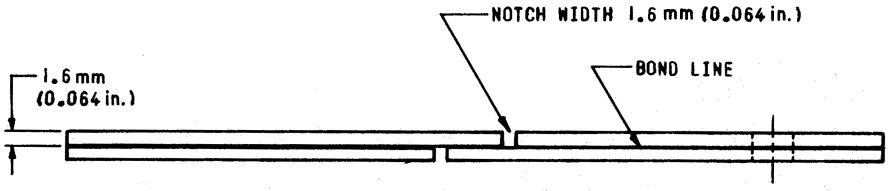

FIGURE 17. ASTM D 1002 SPECIMEN PROFILE

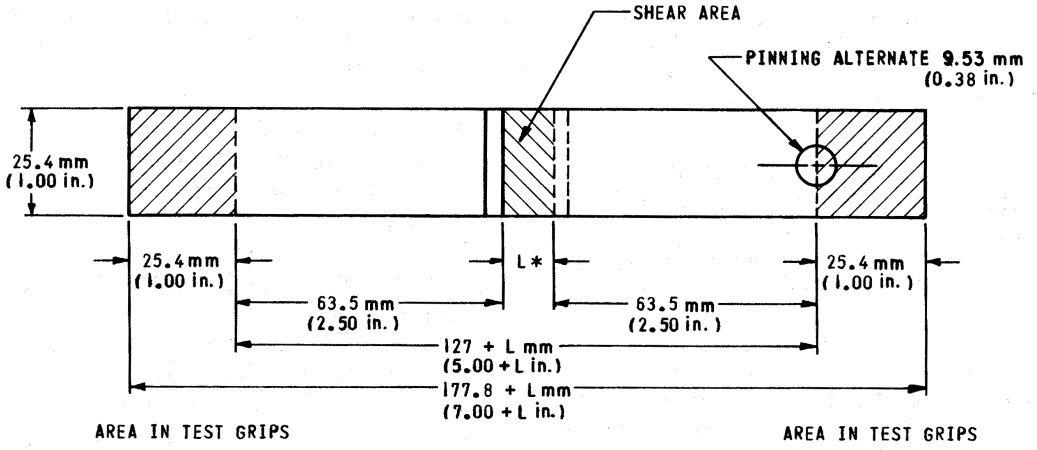

FIGURE 18. ASTM D 3165 SPECIMEN

2.11 SPECIMEN FABRICATION.

This investigation used three different adherend types for both the ASTM D 3165 and ASTM D 1002 test specimen. The adherend types used were (1) 0.064″ thick 2024-T351 aluminum, (2) ≈0.068″ thick quasi-isotropic carbon/epoxy (C/Ep) 7-ply laminate, and (3) ≈0.068″ thick quasi-isotropic fiberglass/epoxy (Gl/Ep) 7-ply laminate. This section will describe procedures that were used to fabricate all the test specimens used throughout the investigation.

2.11.1 Surface Preparation.

The strength of an adhesive bond relies greatly on the adhesion quality at the adhesive/adherend interface. If the substrate is metal, provisions must be taken to protect the material from environmental degradation as well as providing a surface conducive to bonding. Composite surfaces must also be prepared for bonding by removing any surface contaminants and providing a surface with good surface adhesion features.

2.11.1.1 Aluminum Adherend Preparation.

Both ASTM D 3165 and ASTM D 1002 test methods suggest the use of 2024-T351 aluminum for a substrate material. For this investigation, a large sheet (4″ by 12″ by 0.064″) of bare 2024-T351 was purchased for use on all ASTM D 3165 specimens. For the ASTM D 1002 specimens, Cessna Aircraft donated prefabricated material that is specifically used for this type of test specimens.

The large sheet of aluminum was sheared into 10″ by 10″ panels and sent to Cessna Aircraft to be phosphoric anodized and bond primed on the Cessna production line according to ASTM D 3933 [27]. This procedure produces a surface more conducive to bonding and protects it from environmental attack prior to bonding.

After receiving the primed panels for both test methods from Cessna, they were cleaned with acetone and fitted with spacers. For the ASTM D 3165 subpanels, spacers were fitted to the subpanels in a similar fashion as described in section 2.3. Figure 19 shows the spacer configuration used on all ASTM D 3165 subpanels. The test section was aligned with the grain direction of the subpanels and was marked to assure that none of the spacers would be placed in the gage section.

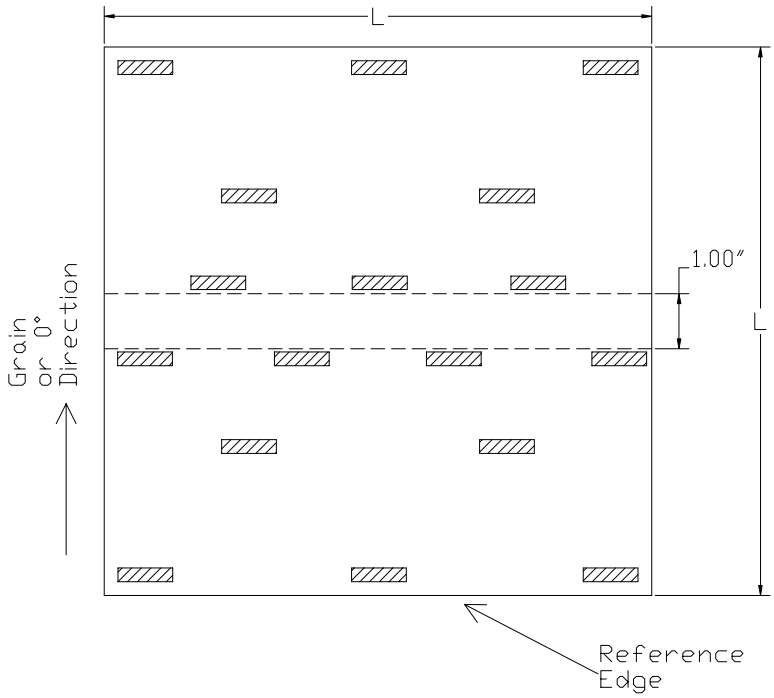

FIGURE 19. SCHEMATIC VIEW OF SPACER PLACEMENT ON AN ASTM D 3165 SUBPANEL (L is the length/width of the subpanel)

ASTM D 1002 subpanels were fitted with spacers as shown in figure 20. The location of the spacers was marked so that no specimens were taken from those parts. The subpanels were ready to be bonded after placement of the spacers is complete.

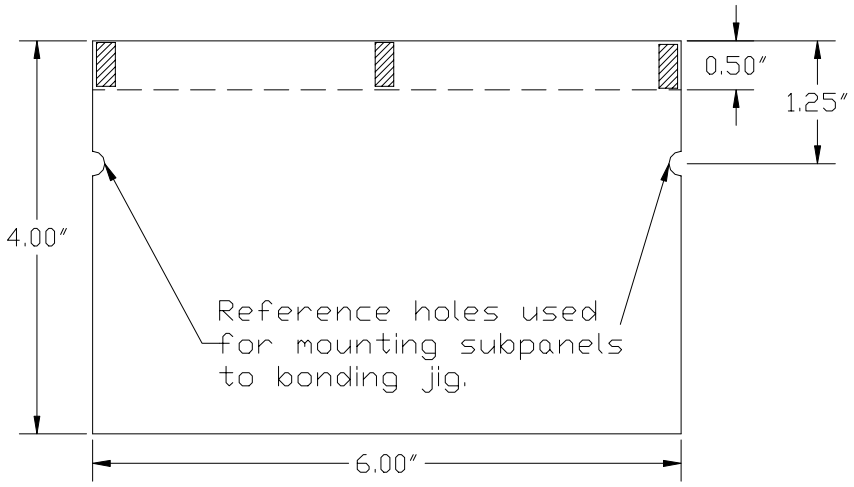

FIGURE 20. SCHEMATIC VIEW OF SPACER PLACEMENT ON AN ASTM D 1002 SUBPANEL

2.11.1.2 Composite Adherend Preparation.

Two different types of composite adherends were used in this investigation. This section will deal only with the surface preparation of the composite adherends. The reader is directed to appendix E for a detailed explanation of the composite adherend lay-up and fabrication procedures.

Typically, composite surfaces must be altered to some extent prior to secondary bonding. The surfaces of a composite laminate are often very smooth, especially on a tool-side surface. This smooth, glass-like surface provides few surface features for the adhesive to mechanically fasten itself. In addition, residue left on the surface from separator film or peel ply used in the curing process can cause poor adhesion. For these reasons, composite laminates commonly go through some type of surface preparation phase prior to secondary bonding.

In practice, there exists a quick check for surface adhesion qualities. A surface that is deemed sufficient for secondary bonding must be a water “break-free” surface. A break-free surface implies that if water is poured on a surface held at an angle, it will not bead up or break. This is understood best when one thinks of water being poured on a piece of slightly tilted glass. The water will bead up on the glass and continue its ascent. This is due to the lack of surface tension. On a break-free surface, the water will not bead up due to the increased surface tension caused by the roughened surface, and it will wet the entire surface.

Most composite secondary bonding procedures call for some type of surface roughening preparation. Mechanical abrasion, i.e., hand sanding or low-pressure grit blasting, is the most common way of preparing a composite laminate surface for secondary bonding. For this investigation, an automated grit blaster, which controls feed rate (ft/min) and blast pressure (psi), was available for surface preparation. The blasting medium was aluminum oxide, which produces a much more jagged surface structure than other blasting media like glass beads.

Both the C/Ep and Gl/Ep laminates for ASTM D 3165 were cut into 9″ square subpanels. A reference edge was marked on all subpanels designating the 0° direction of the composite laminate as described in appendix E. The composite subpanels were then run through the blaster at 50 psi several times each. This pressure was found to roughen the surface sufficiently without damaging the fibers. The subpanels were rotated 90° on each subsequent run through the blaster to assure even blasting. The panels were then rinsed and scrubbed by hand with a Scotch pad to remove any leftover blast media. A quick water break test was run on each subpanel to assure the proper surface adhesion qualities, and then the subpanels were dried in an oven at 100°F.

After being dried, the subpanels were cleaned thoroughly with acetone. Spacers were fitted to the composite subpanels in the same manner as the aluminum subpanels described in the previous section (see figure 19). After a final acetone wipe, the subpanels were ready to be bonded.

2.11.2 Bonding Procedure for ASTM D 1002 Subpanels.

The procedure for bonding both aluminum and composite adherend ASTM D 1002 subpanels was the same and is described in this section. As was previously mentioned, the subpanels for ASTM D 1002 specimens were fabricated with prepunched/drilled alignment holes as shown in figure 20. A thick aluminum plate was fitted with four dowel pins that were used to align and hold the subpanels during the bonding process. The subpanel with spacers were placed and secured to the jig first. A thin layer of adhesive was applied to the overlap area to assure proper wetting of the surface and then more adhesive was added until it reached the desired thickness. After application of the adhesive, the top subpanel was slid into position using the alignment pins. Two clamps were used to make sure that the top panel sat directly on the spacers, and a thick piece of metal was used to distribute the clamping load over the entire gage section. The clamped assembly was then oven cured at 120°F for 3 hours. The MGS and PTM&W adhesives received a final postcure of 175°F for 5 hours. The bonded subpanel was ready to be machined at this point.

2.11.3 Bonding Procedure for ASTM D 3165 Subpanels.

Bonding of the ASTM D 3165 subpanels, both aluminum and composite, was carried out in the same manner as was the paste adhesive bonding of the ASTM D 5656 subpanels described in section 2.3. The only differences are the adherend thickness and subpanel dimensions.

After applying the adhesive and securing the reference edge, the assembly was wrapped in separator film, placed on a flat aluminum plate, and vacuum bagged. It was found that vacuum pressure alone was not always enough to press the upper adherend completely down onto the bondline spacers. For this reason, the vacuum-bagged assembly was placed in a hydraulic press and pressure was slowly increased to 6-7 kip and held for approximately 3 minutes to allow all the excess adhesive between the two subpanels to flow out completely. After removing the assembly from the press, it was placed directly into an oven for curing at 120°F for 3 hours. The MGS and PTM&W adhesives received a final postcure of 175°F for 5 hours. The bonded assembly was ready to be machined into specimens after its removal from the vacuum bag.

2.11.4 ASTM D 1002 Aluminum Adherend Specimen Machining Procedure.

The bonded aluminum ASTM D 1002 subpanel from which specimens are taken from is depicted in figure 21. The first step in the machining process was to remove any excess adhesive that had flowed out of the test section in the bonding process. The subpanel was secured to the base of a milling machine, taking care to line up the reference edge with a preindicated reference block. A 1/2″ cutter at high speed and low feed was then used to remove all of the adhesive spew from the subpanel. This was done to both sides of the bonded assembly.

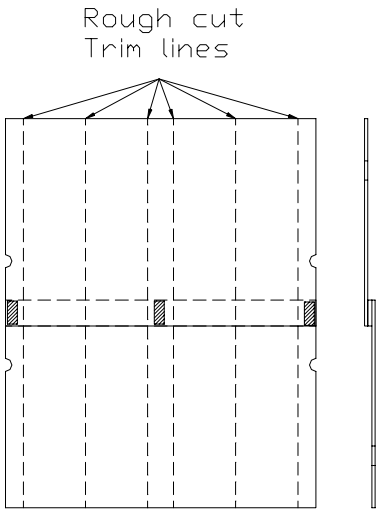

FIGURE 21. SCHEMATIC OF BONDED ALUMINUM ASTM D 1002 SUBPANEL SHOWING LOCATION OF SPACERS AND ROUGH-CUT TRIM LINES FOR EACH SPECIMEN

After the adhesive spew was removed, the subpanel was rough cut into four specimens on a band saw. Care was taken during this process to minimize any vibrations that could damage the adhesive bond. The rough-cut specimens were returned to the milling machine individually where they were machined to their final width. Each specimen was lined up using the reference edge, and a cutter was used to machine the aluminum specimen to its final width of 1 inch. Any sharp edges were filed down by hand, and the specimens were labeled as outlined in appendix C.

The last step in the machining process was to drill the loading holes. A drill jig used to align and clamp the specimens during drilling was designed and fabricated for this purpose. After the jig was mounted and indicated on the milling machine, the specimens were clamped down individually, and the holes were drilled and reamed to the final diameter of 1/2″. Finally, any rough edges were removed by hand. At this point, the test specimens are ready to be dimensioned and tested.

2.11.5 ASTM D 1002 Composite Adherend Specimen Machining Procedure.

The bonded ASTM D 1002 composite subpanel is similar to the aluminum subpanel. The same procedure discussed in the previous section was used to remove any adhesive spew outside of the test section.

After removing the excess adhesive, a new reference edge was cut along the length of the subpanel. Using this new reference edge, specimens were cut oversize on a specimen cutter to a width of 1.25″. Spacers were used when clamping the specimens due to the asymmetry of the ASTM D 1002 specimen. If spacers were not used, the upper adherend would bend and could in turn produce unwanted stresses in the joint. The oversized specimens were then surface ground to the final width of one inch. The final step in the process was to drill the loading pin holes. These holes were drilled using the same drill jig as previously described.

2.11.6 ASTM D 3165 Aluminum Adherend Specimen Machining Procedure.

Figure 22 shows a schematic of the bonded ASTM D 3165 aluminum subpanel. After removing the bonded assembly from the vacuum bag, excess adhesive had to be removed from the reference edge before the machining process could begin. This was achieved by removing the flash breaker tape that was placed on the reference edge to hold the unbonded panels together during the cure cycle. If this was not possible, the excess adhesive was filed by hand until the tape can be removed.

The bonded subpanel was then aligned and fixed to a CNC milling machine, where it received the first of several computer-controlled operations. The loading holes for all the specimens were drilled into the subpanel as shown in figure 22. The holes were drilled first because they were used in subsequent steps of the machining process.

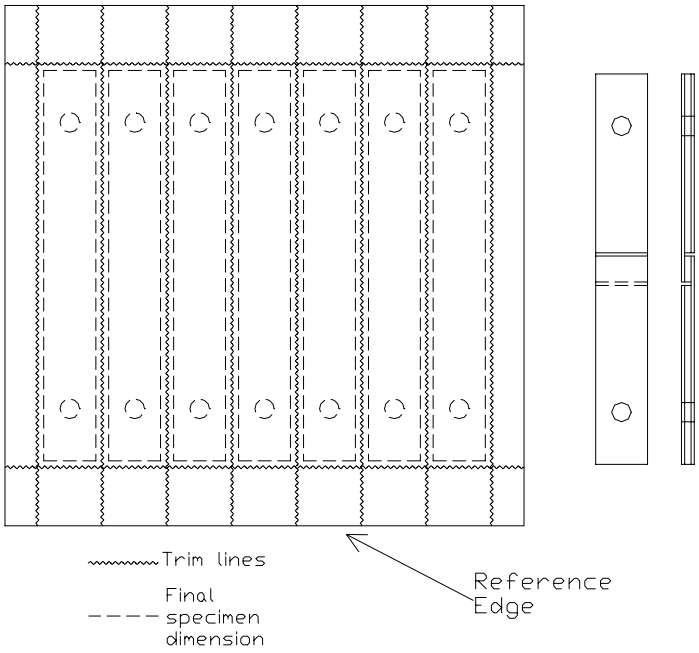

FIGURE 22. SCHEMATIC OF THE BONDED ALUMINUM ASTM D 3165 SUBPANEL

The drilled subpanel could then be removed from the CNC machine and taken to a band saw where the individual specimens were rough cut from the subpanel. Figure 22 shows how the specimens were cut from the bonded subpanel. Again, care was taken so as to minimize any

vibrations caused by the cutting process. The cutting process yielded seven individual specimens from each subpanel. The strips were cut oversize to avoid overheating and stressing of the bondline. Approximately 1/8″ of material was left on each side of both the width and length after the rough cut was made. At this point, any rough edges were removed by filing and the specimens were labeled according to appendix C. The specimens were then ready to be returned to CNC machine for final machining of the width, length, and slots.

In order to achieve the tolerances required for this test specimen, especially the slotted regions, a holding jig similar to the one used for the ASTM D 5656 specimens was devised. Using the existing loading holes as reference points, each individual specimen was attached to the jig and machined to its final width and length. The final operation was to slot the specimen on each side with a 1/16″ cutter. To avoid breaking this small of a cutter, it was necessary to make several depth cuts before the slot was complete; approximately one cut per 0.02″ of material to be removed. It should be noted that all machining processes used coolant to assure that the specimens were not overheated. The specimens were filed after the slotting was completed and were then ready to be dimensioned and tested.

2.11.7 ASTM D 3165 Composite Adherend Specimen Machining Procedure.

The machining procedures for the composite ASTM D 3165 subpanels differed from the aluminum procedures quite substantially. Figure 23 gives a schematic view of the bonded composite subpanel and the machining operations required to make individual specimens. The first step in the composite adherend procedure is the same as the aluminum adherend procedure. Either removing the flash breaker tape or hand filing must remove any adhesive from reference edge 1 and the adherend faces.

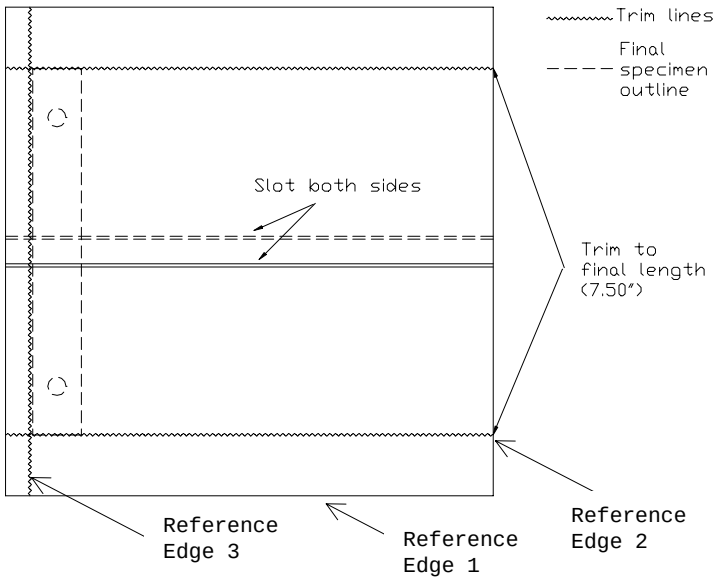

FIGURE 23. SCHEMATIC OF THE COMPOSITE ADHEREND ASTM D 3165 SUBPANEL DEPICTING THE DIFFERENT MACHINING PROCEDURES

All cutting operations specific to composite adherends were carried out using diamond-tipped circular blades. Following removal of excess adhesive, the bonded assembly was aligned and clamped to the bed of a modified milling machine where it was trimmed to the final specimen length, yielding reference edge 2.

The next step in the process was to slot the subpanel. For the composite adherend subpanels, the slotting was done to the entire subpanel at once, instead of on each individual specimen. The subpanel was repositioned, realigned with reference edge 2 and clamped securely to the bed for the slotting operation. Since the adherend thickness was measured prior to bonding, the blade was raised up off the surface of the bed to approximately 0.002″ higher than the thickness of the adherends. It was decided that it would be better to leave a small amount of adhesive in the slot area rather than cutting into the adherend surface. A slot was made on each side of the subpanel in this manner. It should be noted that the blade used for slotting had a radius of approximately 0.031″. This, in turn, left a fillet on the adhesive within the slot, which is illustrated in figure 24.

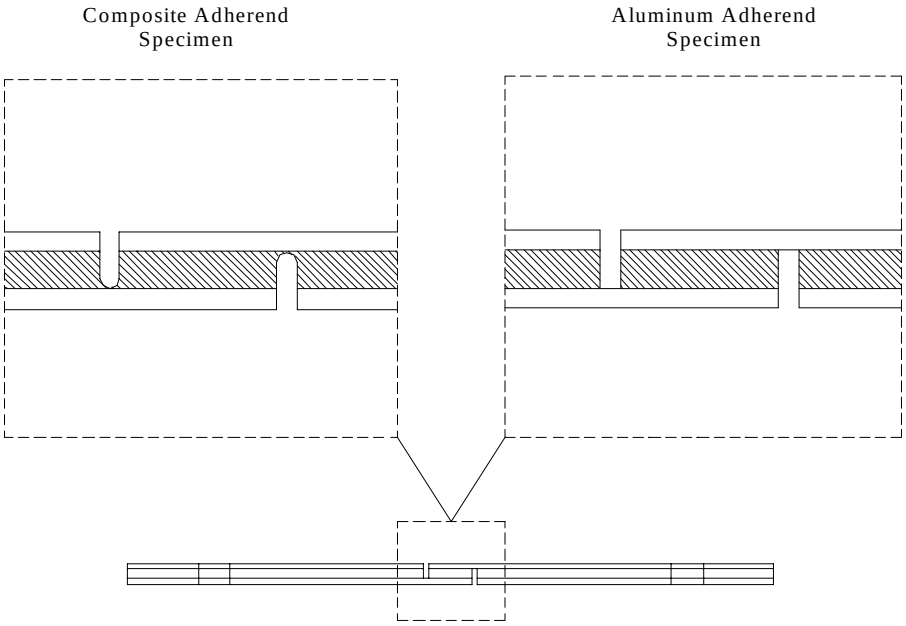

FIGURE 24. DEPICTION OF AN ASTM D 3165 COMPOSITE ADHEREND TEST SPECIMEN SHOWING THE FILLET IN THE SLOT

Following the completion of the slotting operation, the subpanel received its final reference edge, 3, on the milling machine. Subsequently, this new reference edge was used to cut the individual specimens to a width of 1.035″ on a specimen-cutting machine. Each subpanel typically yielded 6-7 test specimens. Once cut, the test specimens were labeled as outlined in appendix C and transferred to a surface grinder where they were ground to the final width of 1 inch. The final machining operation for the composite adherend specimens was to drill the loading pinholes. This was achieved using the same drill jig and technique described in section 2.11.4. After drilling the loading-pin holes, the specimens were ready to be dimensioned and tested.

2.12 SPECIMEN TESTING.

Testing of ASTM D 3165 and ASTM D 1002 specimens, regardless of adherend type, followed the same procedure. Both methods give the tester the option of loading the specimens by clamping them or via a pin load. For this investigation, all test samples were loaded via pin loading for several reasons.

Loading the specimens by clamping can result in unwanted torques, bending, and axial loads if the clamps are not aligned properly. Clamping is also undesirable when the tests are performed at other temperatures than RT, because the stretching and/or contracting of the test specimens due to temperature can induce unwanted loads when under displacement control. Finally, clamping of the specimens should be done under load control, so that the adhesive gage area is not stressed during clamping, while testing is done in displacement control. Switching between the two types of control would add several time consuming steps in the testing process.

Prior to testing, each specimen must be dimensioned for use in calculations and to assure conformity to the dimension standards set out in the ASTM guideline. Measurements for each specimen were taken and recorded for the width, length, and thickness of the bondline at the test section. The same procedure for taking measurements that was discussed in section 2.5 was used for all specimens in this investigation. Any specimens that required moisture absorption for environmental tests were inserted into the environmental chamber at this point.

The testing configuration for the ASTM D 3165 specimens was much the same as that discussed in section 2.5. A similar clevis fixture was attached to the 5.5-kip test stand so that the specimens could be mounted by pin. The specimens were attached to the clevis arrangement using the 0.375″ pin and special spacers that align the specimen in the center of the clevis.

Testing was carried out using displacement control and loading the specimens at 0.05 in/min. Data for the load and crosshead displacement was plotted in real time and saved for each specimen. After specimen failure, the maximum load value and the failure mode were recorded, and the specimen was removed from the clevis arrangement. Environmental testing was carried out as described in section 2.5.

Both the ASTMs discussed in this section yield only strength values. They require only one calculation to be carried out, which is shown below.

$$\tau_{max} = P_{max} / A \tag{9}$$

P_{max} is the maximum load recorded for the test, A is the overlap shear area and τ_{max} is the maximum shear stress of the overlap region found using the particular test method.

3. RESULTS AND DISCUSSION.

This section will present and discuss the experimental results gathered from all tests carried out during this investigation.

3.1 ASTM D 5656 RESULTS.

Section 2 of this document provided the reader with an in-depth look into the ASTM D 5656 specimen. This section will discuss the results from all ASTM D 5656 specimens tested in this investigation.

3.1.1 Test Matrix 1.

In test matrix 1 (see table 1), thick-adherend lap shear specimens were used to characterize the shear stress-strain behavior of the adhesive using the KGR-type extensometer. Three adhesives were characterized at RTD using four bondline thicknesses. The results from these tests will be presented for both the apparent shear strength of the adhesive and the adhesive shear stress-strain behavior.

3.1.1.1 Apparent Shear Strength Results—Thick-Adherend Lap Shear.

The apparent shear strengths for different bondline thicknesses from the thick-adherend lap shear specimens were found for all three adhesive systems. The average values for no less than three replicates are shown in figure 25, and the values for each specimens maximum apparent shear strength, average bondline thickness, and failure mode are given in tables 6 through 8. It can be seen from the figure that Hysol paste adhesive had the largest apparent shear strength of the three paste adhesives, with the MGS adhesive being next and the PTM&W paste adhesive being the least strongest, according to the results from the thick-adherend tests.

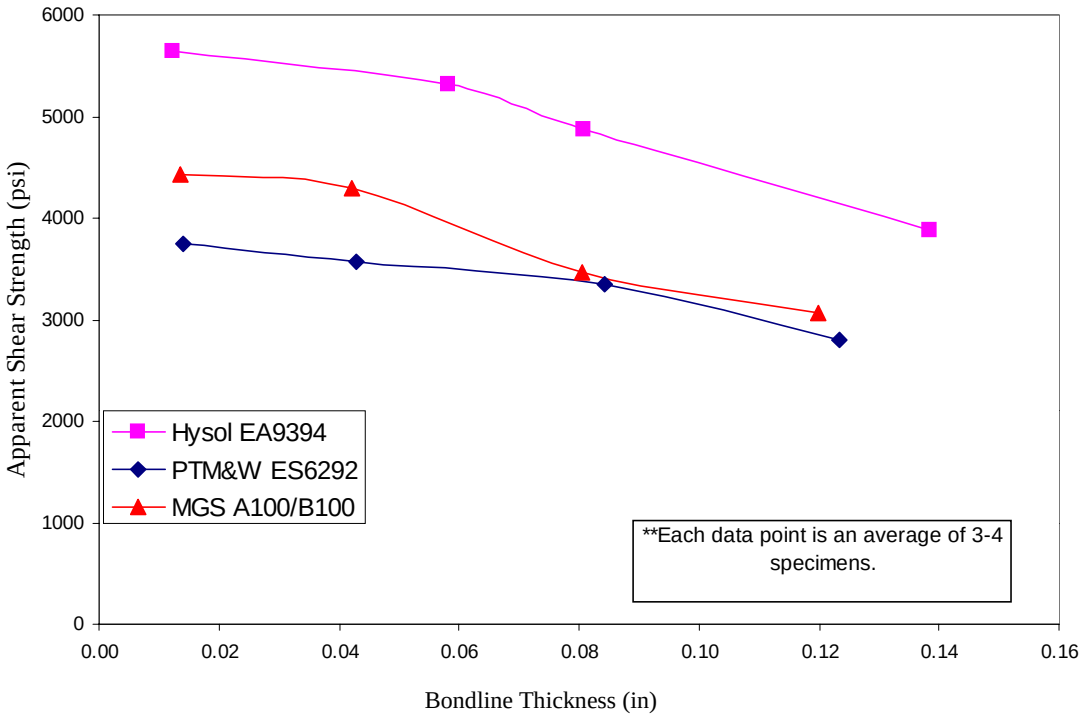

FIGURE 25. APPARENT SHEAR STRENGTH VERSUS BONDLINE THICKNESS FOR ASTM D 5656 SPECIMENS (All three adhesive systems)

TABLE 6. LIST OF THICK-ADHEREND TEST SPECIMENS FROM TEST MATRIX 1 FOR HYSOL EA9394 PASTE ADHESIVE

Adhesive System	Specimen Name	Max. App. Shear Strength (psi)	Avg. Bondline Thickness (in.)	Failure Mode
Hysol EA9394	A11A11	5802.2	0.0135	Cohesive
	A11A13	5957.9	0.0105	Cohesive/Adhesive
	A11A14	5310.2	0.0120	Cohesive/Adhesive
	A11A15	5505.8	0.0135	Cohesive/Adhesive
	A11B11	5448.5	0.0600	Cohesive/Adhesive
	A11B12	5143.8	0.0500	Cohesive/Adhesive
	A11B13	5327.6	0.0580	Cohesive/Adhesive
	A11B14	5359.7	0.0645	Cohesive/Adhesive
	A11C11	4777.6	0.0815	Cohesive/Adhesive
	A11C12	4829.2	0.0785	Cohesive/Adhesive
	A11C13	4997.2	0.0820	Cohesive/Adhesive
	A11D11	3687.7	0.1355	Adhesive/Cohesive
	A11D12	4088.6	0.1395	Adhesive/Cohesive
	A11D13	3856.5	0.1405	Adhesive

TABLE 7. LIST OF THICK-ADHEREND TEST SPECIMENS FROM TEST MATRIX 1 FOR PTM&W ES6292 PASTE ADHESIVE

Adhesive System	Specimen Name	Max. App. Shear Strength (psi)	Avg. Bondline Thickness (in.)	Failure Mode
PTM&W ES6292	B11A11	3665.1	0.0130	Cohesive
	B11A12	3665.1	0.0130	Cohesive
	B11A13	3993.3	0.0155	Cohesive
	B11A14	3661.6	0.0145	Cohesive
	B11B21	3614.0	0.0435	Cohesive/Adhesive
	B11B22	3521.5	0.0430	Cohesive/Adhesive
	B11B23	3621.0	0.0430	Cohesive/Adhesive
	B11B24	3532.8	0.0425	Cohesive/Adhesive
	B11B25	3546.7	0.0420	Cohesive/Adhesive
	B11C11	3237.7	0.0830	Cohesive/Adhesive
	B11C12	3323.9	0.0853	Cohesive/Adhesive
	B11C13	3418.6	0.0855	Cohesive/Adhesive
	B11C14	3415.7	0.0830	Cohesive/Adhesive
	B11D11	2860.2	0.1240	Adhesive/Cohesive
	B11D12	2770.5	0.1225	Adhesive/Cohesive
	B11D13	2750.5	0.1222	Cohesive/Adhesive
	B11D14	2807.5	0.1250	Cohesive/Adhesive

TABLE 8. LIST OF THICK-ADHEREND TEST SPECIMENS FROM TEST MATRIX 1 FOR MGS A100/B100 PASTE ADHESIVE

Adhesive System	Specimen Name	Max. App. Shear Strength (psi)	Avg. Bondline Thickness (in.)	Failure Mode
MGS A100/ B1000	C11A11	3971.8	0.0130	Cohesive
	C11A12	4607.5	0.0135	Cohesive
	C11A13	4817.6	0.0140	Cohesive
	C11A14	4321.0	0.0140	Cohesive
	C11B12	4325.3	0.0420	Cohesive/Adhesive
	C11B14	4413.1	0.0420	Cohesive/Adhesive
	C11B15	4163.5	0.0425	Cohesive/Adhesive
	C11C12	3372.2	0.0810	Cohesive/Adhesive
	C11C13	3666.6	0.0785	Cohesive/Adhesive
	C11C15	3368.2	0.0820	Cohesive/Adhesive
	C11D11	3072.8	0.1210	Cohesive/Adhesive
	C11D12	3055.5	0.1200	Cohesive/Adhesive
	C11D13	3050.1	0.1190	Cohesive/Adhesive

The general trend for all three adhesives shows that as the adhesive bond grows greater in thickness, the apparent shear strength of the joint is decreased. Because the bondline is thicker, the eccentricity of the load path increases. This, in turn, produces more peel stresses in the vicinity of the edge of the overlaps in the thicker bondline specimens. A result of these extra peel stresses is seen in the failure modes of the test specimens (see tables 6-8). The thinnest bondlines (0.015 in.) failed almost completely cohesively, which is a good indication of failing the adhesive by shear. On the other hand, the thickest bonds failed adhesively close to or over 50% of the overlap area, which indicates that the tensile stresses in the overlap region led to failure. For all adhesive systems, the percent of cohesive failure over the overlap area decreased as the bond grew thicker.

3.1.1.2 Adhesive Shear Stress-Strain Characterization.

The adhesive shear stress-strain behavior for all three adhesives was characterized as a function of bondline thickness in test matrix 1 (table 1). The results from these tests were used in the development of the correction factors proposed in the paper by Yang, et al. [23]. The first adhesive to be characterized was the FM-300K film adhesive, which was used in the validation study discussed in section 2.8. After the KGR-type device was perfected, the three paste adhesives were tested.

After testing all of the thick adherend specimens from test matrix 1, the adhesive shear stress-strain charts in appendix F were created using the procedure outlined previously in this document. From these charts, a line could be fit to the linear elastic region of the stress-strain curve, and from this, the initial adhesive shear modulus was found for each test sample. Figures 26 through 28 show the average values of the corrected initial adhesive shear modulus as a function of bondline thickness. Also shown for comparison purposes is the adhesive shear

modulus found by using the ASTM equation only, without the corrections offered by Yang, et al. [23] and the modulus found from the bulk adhesive specimens. Tables 9 through 11 give three modulus values for each specimen from which shear modulus data was taken from, where G_{ASTM} is the ASTM modulus from equation 6, $G\text{-}F_a$ is the corrected modulus using equation 5, and $G_{recovered}$ is the recovered modulus using the correction factors from Yang, et al. equation 7.

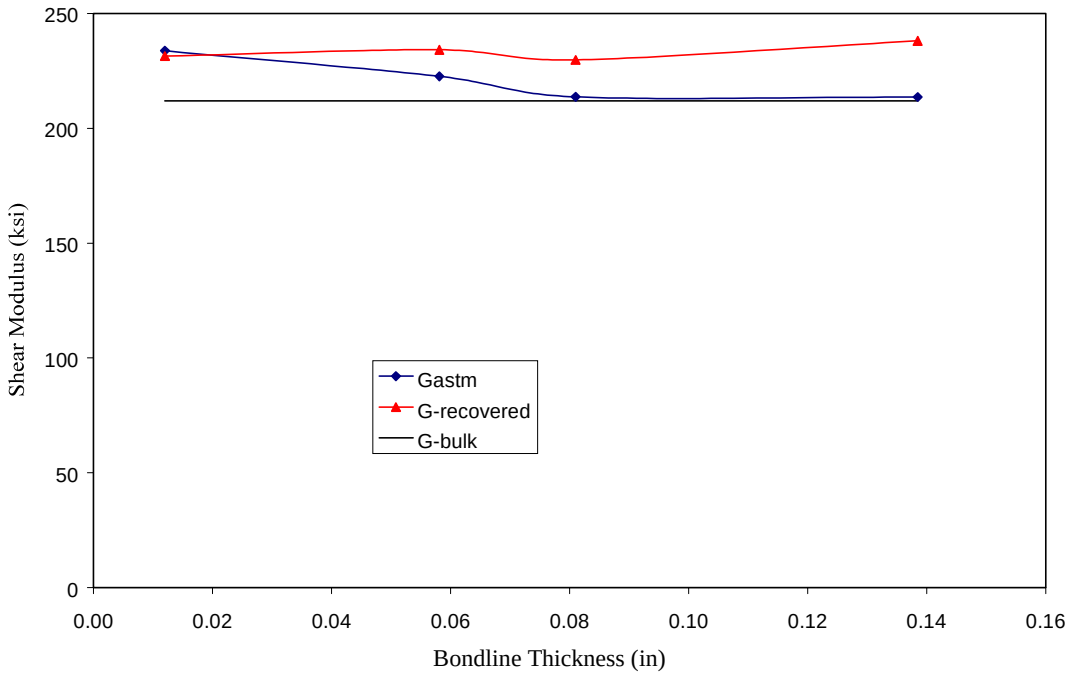

FIGURE 26. HYSOL EA9394 AVERAGE INITIAL ADHESIVE SHEAR MODULUS AS A FUNCTION OF BONDLINE THICKNESS (RTD)

TABLE 9. SHEAR MODULUS DATA FOR HYSOL EA9394 PASTE ADHESIVE FROM RTD THICK-ADHEREND TEST SPECIMENS

Specimen Name	Avg. Bondline Thickness (in)	G_{ASTM} (ksi)	$G\text{-}F_a$ Corrected (ksi)	$G_{recovered}$ (ksi)
A11A12	0.0105	281.772	292.660	279.126
A11A15	0.0135	185.683	188.917	183.796
A11B12	0.0500	197.722	197.400	206.196
A11B13	0.0580	235.861	235.242	248.119
A11B14	0.0645	234.235	233.612	248.151
A11C12	0.0785	199.298	198.724	213.894
A11C13	0.0820	228.077	227.465	245.561
A11D11	0.1355	213.590	213.115	238.050

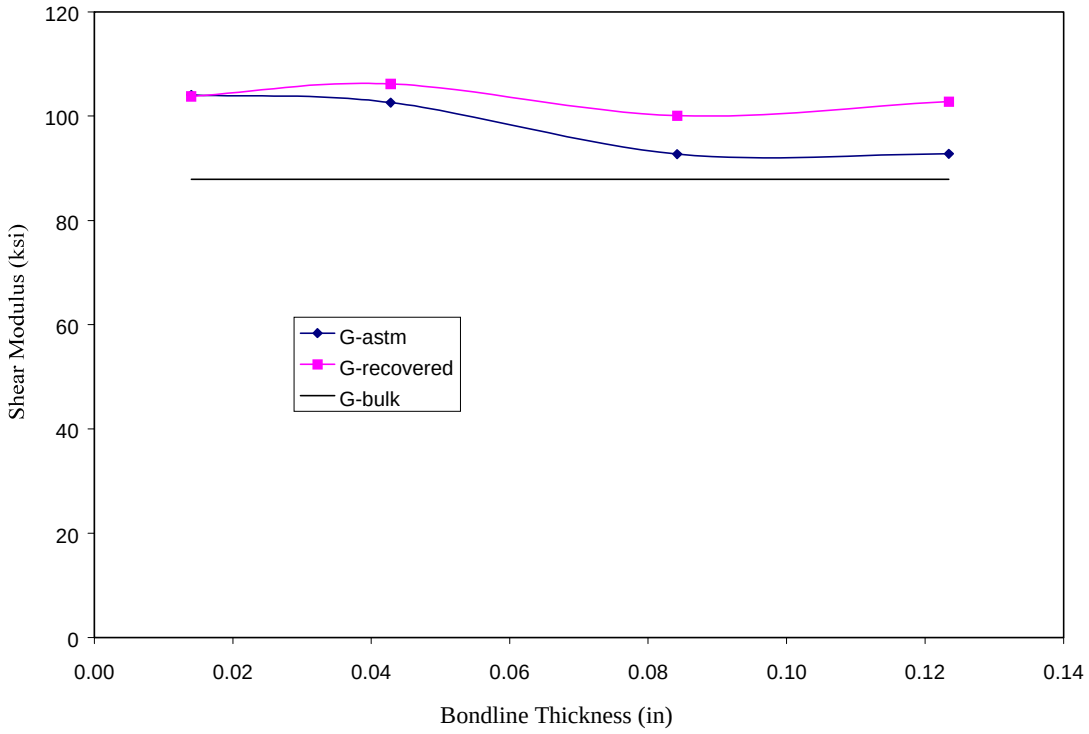

FIGURE 27. PTM&W ES6292 AVERAGE INITIAL ADHESIVE SHEAR MODULUS AS A FUNCTION OF BONDLINE THICKNESS (RTD)

TABLE 10. SHEAR MODULUS DATA FOR PTM&W ES6292 PASTE ADHESIVE FROM RTD THICK-ADHEREND TEST SPECIMENS

Specimen Name	Avg. Bondline Thickness (in)	G_{ASTM} (ksi)	G-F_a Corrected (ksi)	$G_{recovered}$ (ksi)
B11A12	0.0130	138.500	140.400	137.257
B11A13	0.0155	87.990	88.573	88.224
B11A14	0.0145	85.702	86.335	85.942
B11B21	0.0435	98.295	98.248	101.822
B11B22	0.0430	108.727	108.664	112.518
B11B24	0.0425	108.872	108.820	112.602
B11B25	0.0420	94.563	94.527	97.778
B11C11	0.0830	87.930	87.828	94.856
B11C12	0.0853	96.992	96.827	104.770
B11C13	0.0855	87.333	87.232	94.401
B11C14	0.0830	98.628	98.500	106.390
B11D11	0.1240	110.392	110.250	122.375
B11D12	0.1225	81.712	81.635	90.520
B11D13	0.1222	86.901	86.813	96.248
B11D14	0.1250	92.018	91.921	102.075

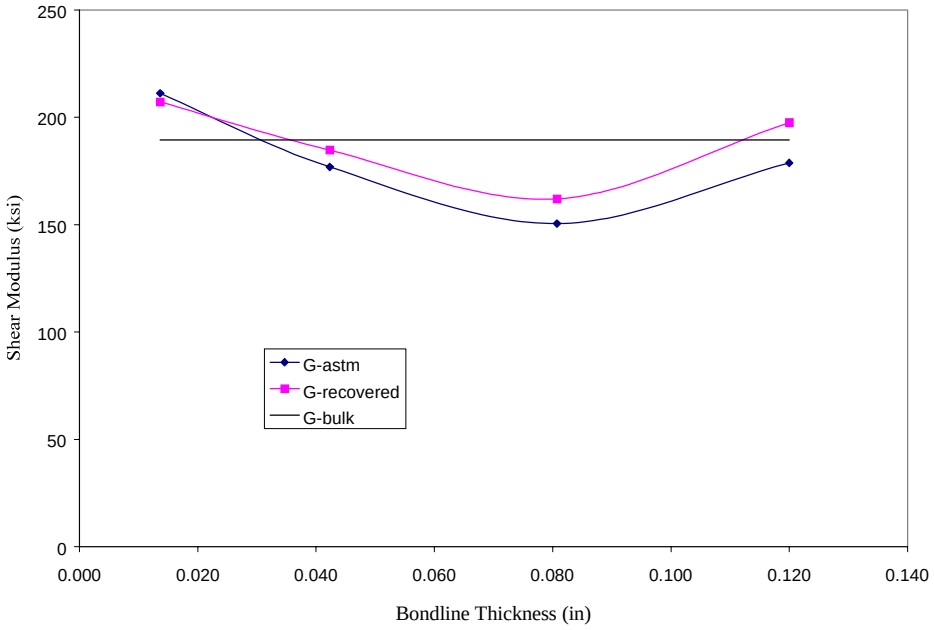

FIGURE 28. MGS A100/B100 AVERAGE INITIAL ADHESIVE SHEAR MODULUS AS A FUNCTION OF BONDLINE THICKNESS (RTD)

TABLE 11. SHEAR MODULUS DATA FOR MGS A100/B100 PASTE ADHESIVE FROM RTD THICK-ADHEREND TEST SPECIMENS

Specimen Name	Avg. Bondline Thickness (in)	G_{ASTM} (ksi)	G-F_a Corrected (ksi)	$G_{recovered}$ (ksi)
C11A11	0.0130	233.587	236.682	228.986
C11A12	0.0135	188.911	190.672	185.472
C11B11	0.0430	183.667	191.512	198.137
C11B12	0.0420	188.775	188.630	194.872
C11B14	0.0420	156.720	156.624	161.849
C11B15	0.0425	178.522	178.387	184.439
C11C12	0.0810	155.348	155.015	167.190
C11C13	0.0785	148.326	148.022	159.308
C11C14	0.0815	151.250	150.936	162.857
C11C15	0.0820	147.326	147.030	158.706
C11D12	0.1200	176.442	176.084	195.056
C11D13	0.1190	181.184	180.805	200.174

For all three adhesive systems, it appears that the shear modulus changes as the bondline thickness increases if one uses the ASTM D 5656 test. This is more readily apparent in the G_{ASTM} curves for the Hysol and PTM&W adhesives, where the shear modulus seems to decrease as the bond thickness increases. The $G_{recovered}$ curves, on the other hand, have been corrected for the irregularities induced by thicker bondlines and appear to be closer to a constant shear modulus value as would be expected.

3.1.2 Test Matrix 2-B.

The objective of test matrix 2-B (table 3), was to characterize the apparent shear strength and adhesive shear stress-strain relationship at various environmental conditions using the thick-adherend lap shear specimen and a bondline thickness of 0.015 inch. For this part of the investigation, only the MGS adhesive was characterized.

3.1.2.1 Apparent Shear Strength Results.

The apparent shear strength as a function of environment was found using thick adherend specimens in test matrix 2-B. The bondline thickness used was 0.015 inch for all environmental conditions. Figure 29 shows the results from the environmental testing carried out on the thick-adherend specimens. The average apparent shear strength for each data set is shown as a function of environmental test condition. Tables 12 through 17 show the strength values for each specimen tested in this test matrix. It can be seen that as the temperature increases, the apparent shear strength of the adhesive decreases. Moreover, if moisture is introduced into the specimen, the strength decrease is even more dramatic. This trend is backed up by the T_g values found for the adhesive. The dry T_g for this adhesive system was found to be just over the 160°F test temperature, and the figure shows that after that threshold is crossed, the strength values diminish. This is even more evident when looking at the wet T_g value for the adhesive, which was found to be well below the 160°F mark. The data show that the adhesive strength drops significantly between the dry and wet 160°F specimens, which is to be expected.

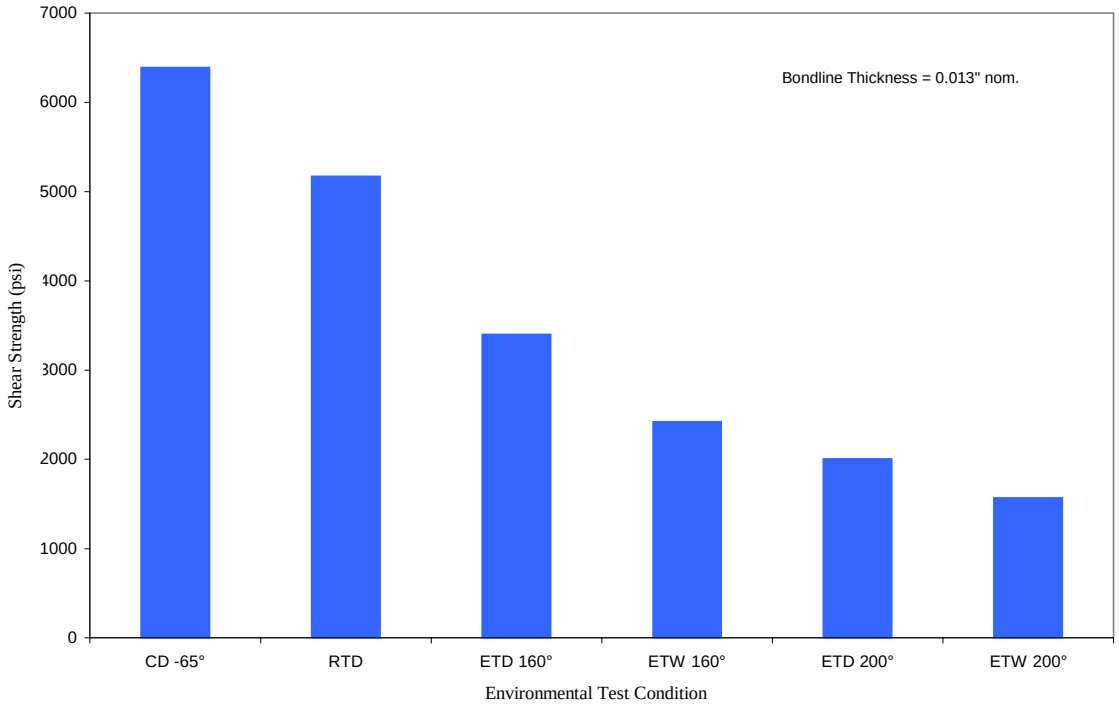

FIGURE 29. APPARENT SHEAR STRENGTH VERSUS ENVIRONMENTAL CONDITION FOR THICK-ADHEREND LAP SHEAR SPECIMENS (MGS adhesive)

TABLE 12. LIST OF COLD DRY -65°F THICK-ADHEREND LAP SHEAR SPECIMENS TESTED IN TEST MATRIX 2-B (MGS adhesive—maximum apparent shear strength)

Environmental Condition	Specimen Name	Max. App. Shear Strength (psi)	Avg. Bondline Thickness (in.)	Failure Mode
Cold Dry -65°F	C11A22	6903.1	0.012	Adhesive
	C11A31	6645.2	0.014	Adhesive
	C11A43	6467.0	0.013	Adhesive
	C11A55	6109.2	0.015	Adhesive
	C11A74	5831.8	0.011	Adhesive

TABLE 13. LIST OF RTD THICK-ADHEREND LAP SHEAR SPECIMENS IN TEST MATRIX 2-B (MGS adhesive—maximum apparent shear strength)

Environmental Condition	Specimen Name	Max. App. Shear Strength (psi)	Avg. Bondline Thickness (in.)	Failure Mode
Room Temperature Dry	C11A53	5062.0	0.016	Cohesive
	C11A56	5281.0	0.014	Cohesive
	C11A61	4835.6	0.010	Cohesive

TABLE 14. LIST OF ETD 160°F THICK-ADHEREND LAP SHEAR SPECIMENS IN TEST MATRIX 2-B (MGS adhesive—maximum apparent shear strength)

Environmental Condition	Specimen Name	Max. App. Shear Strength (psi)	Avg. Bondline Thickness (in.)	Failure Mode
Elevated Temperature Dry 160°F	C11A24	3306.1	0.013	Cohesive
	C11A34	3248.8	0.014	Cohesive
	C11A52	3642.6	0.014	Cohesive

TABLE 15. LIST OF ETW 160°F THICK-ADHEREND LAP SHEAR SPECIMENS IN TEST MATRIX 2-B (MGS adhesive—maximum apparent shear strength)

Environmental Condition	Specimen Name	Max. App. Shear Strength (psi)	Avg. Bondline Thickness (in.)	Failure Mode
Elevated Temperature Wet 160°F	C11A23	2509.4	0.014	Cohesive
	C11A32	2541.4	0.013	Cohesive
	C11A72	2307.4	0.010	Cohesive
	C11A76	2324.9	0.013	Cohesive

TABLE 16. LIST OF ETD 200°F THICK-ADHEREND LAP SHEAR SPECIMENS IN TEST MATRIX 2-B (MGS adhesive—maximum apparent shear strength)

Environmental Condition	Specimen Name	Max. App. Shear Strength (psi)	Avg. Bondline Thickness (in.)	Failure Mode
Elevated Temperature Dry 200°F	C11A26	1872.4	0.018	Cohesive
	C11A36	1996.9	0.013	Cohesive
	C11A45	2116.0	0.012	Cohesive
	C11A51	2040.1	0.014	Cohesive
	C11A54	2349.2	0.015	Cohesive

TABLE 17. LIST OF ETW 200°F THICK-ADHEREND LAP SHEAR SPECIMENS IN TEST MATRIX 2-B (MGS adhesive—maximum apparent shear strength)

Environmental Condition	Specimen Name	Max. App. Shear Strength (psi)	Avg. Bondline Thickness (in.)	Failure Mode
Elevated Temperature Wet 200°F	C11A25	1590.9	0.012	Cohesive
	C11A35	1683.7	0.013	Cohesive
	C11A62	1365.1	0.010	Cohesive

3.1.2.2 Adhesive Shear Stress-Strain Characterization.

Test matrix 2-B was developed to characterize the adhesive shear stress-strain relationship as a function of environmental condition. Thick-adherend specimens with a bondline thickness of 0.013 inches were tested at four different temperatures and two moisture contents. The results of this series of tests can be seen graphically in figure 30.

The figure shows the averages of several specimens for each temperature. Each individual shear stress-strain curve is shown in appendix F. In addition, each specimens modulus values can be found in tables 18 through 23. Again, these tables show the values for the G_{ASTM}, $G\text{-}F_a$, and $G_{recovered}$. Representative curves from each environmental data set were chosen and plotted in figure 31.

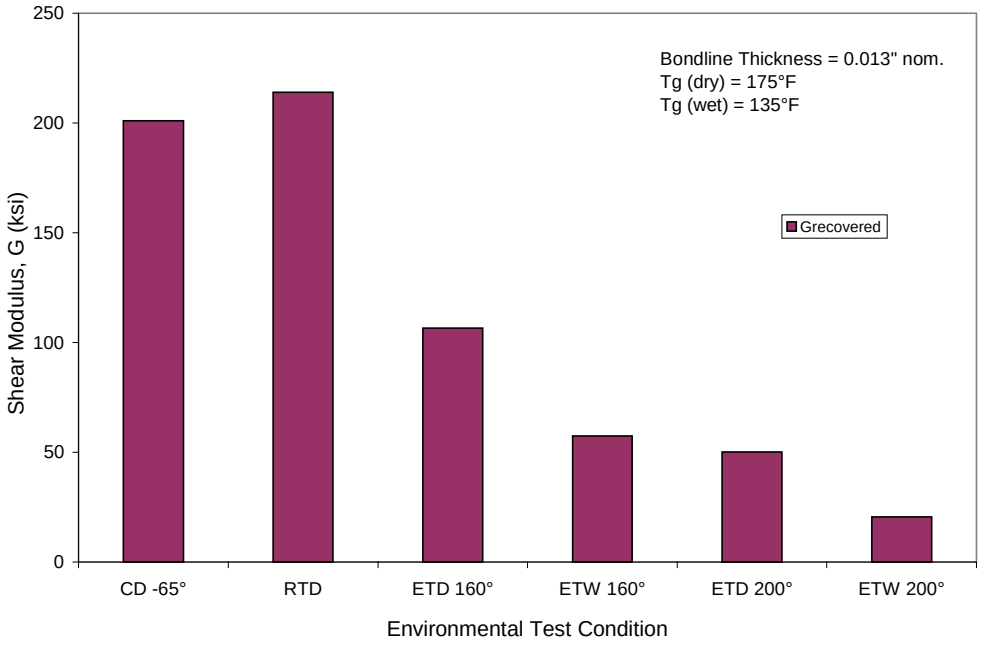

FIGURE 30. ADHESIVE SHEAR MODULUS AS A FUNCTION OF ENVIRONMENT (MGS adhesive)

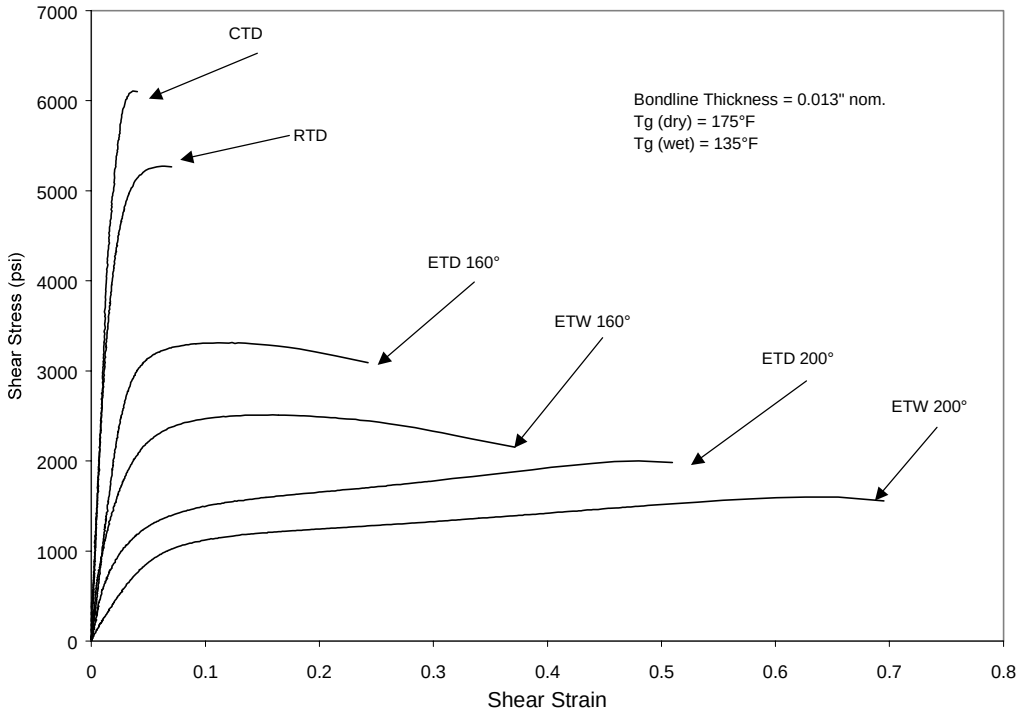

FIGURE 31. REPRESENTATIVE ADHESIVE SHEAR STRESS-STRAIN CURVES AS A FUNCTION OF ENVIRONMENTAL CONDITION (MGS adhesive)

This data is consistent with other studies that have been done [29], in that it shows a decrease in adhesive strength with increasing temperature and an increase in the ductile response of the adhesive. At cold temperatures, the adhesive becomes brittle and has more apparent shear strength, but less strain. As the temperature increases, the adhesive becomes more ductile, resulting in more shear displacement, but less strength. In the extreme cases where the T_g limit of the adhesive has been exceeded, the response of the adhesive is almost totally plastic, resulting in large shear strains as shown in figure 31.

TABLE 18. SHEAR MODULUS DATA FOR MGS A100/B100 PASTE ADHESIVE FROM CD THICK-ADHEREND TEST SPECIMENS (Test Matrix 2-B)

Environmental Condition	Specimen Name	Bondline Thickness (in)	G_{ASTM} (ksi)	G-F_a Corrected (ksi)	$G_{recovered}$ (ksi)
Cold Dry -65°F	C11A22	0.012	196.411	199.518	192.670
	C11A43	0.013	200.181	204.329	198.163
	C11A74	0.011	214.378	220.817	212.375

TABLE 19. SHEAR MODULUS DATA FOR MGS A100/B100 PASTE ADHESIVE FROM RTD THICK-ADHEREND TEST SPECIMENS (Test Matrix 2-B)

Environmental Condition	Specimen Name	Bondline Thickness (in)	G_{ASTM} (ksi)	G-F_a Corrected (ksi)	$G_{recovered}$ (ksi)
Room Temperature Dry	C11A53	0.016	225.255	227.764	222.606
	C11A56	0.014	208.249	210.729	205.163
	C11A61	0.010	218.626	224.398	214.255

TABLE 20. SHEAR MODULUS DATA FOR MGS A100/B100 PASTE ADHESIVE FROM ETD 160°F THICK-ADHEREND TEST SPECIMENS (Test Matrix 2-B)

Environmental Condition	Specimen Name	Bondline Thickness (in)	G_{ASTM} (ksi)	G-F_a Corrected (ksi)	$G_{recovered}$ (ksi)
Elevated Temperature Dry 160°F	C11A24	0.013	104.068	105.193	103.601
	C11A34	0.014	122.728	124.093	122.033
	C11A63	0.013	94.180	95.232	94.136

TABLE 21. SHEAR MODULUS DATA FOR MGS A100/B100 PASTE ADHESIVE FROM ETW 160°F THICK-ADHEREND TEST SPECIMENS (Test Matrix 2-B)

Environmental Condition	Specimen Name	Bondline Thickness (in)	G_{ASTM} (ksi)	G-F_a Corrected (ksi)	$G_{recovered}$ (ksi)
Elevated Temperature Wet 160°F	C11A32	0.013	58.709	59.064	59.768
	C11A72	0.010	49.627	50.056	51.376
	C11A76	0.013	60.032	60.403	61.044

TABLE 22. SHEAR MODULUS DATA FOR MGS A100/B100 PASTE ADHESIVE FROM ETD 200°F THICK-ADHEREND TEST SPECIMENS (Test Matrix 2-B)

Environmental Condition	Specimen Name	Bondline Thickness (in)	G_{ASTM} (ksi)	G-F_a Corrected (ksi)	$G_{recovered}$ (ksi)
Elevated Temperature Dry 200°F	C11A36	0.013	57.128	57.463	58.243
	C11A45	0.012	50.714	51.015	52.160
	C11A51	0.014	38.325	38.459	40.061

TABLE 23. SHEAR MODULUS DATA FOR MGS A100/B100 PASTE ADHESIVE FROM ETW 200°F THICK-ADHEREND TEST SPECIMENS (Test Matrix 2-B)

Environmental Condition	Specimen Name	Bondline Thickness (in)	G_{ASTM} (ksi)	G-F_a Corrected (ksi)	$G_{recovered}$ (ksi)
Elevated Temperature Wet 200°F	C11A25	0.012	19.703	19.743	22.516
	C11A62	0.010	13.164	13.191	16.935
	C11A77	0.013	19.492	19.530	22.207

3.2 THIN-ADHEREND LAP SHEAR RESULTS.

In section 3, two popular thin-adherend lap shear test methods were discussed, as well as the procedures for fabrication and testing of the test specimens for this investigation. The results for all ASTM D 3165 and ASTM D 1002 specimens used in this investigation will be presented in this section.

3.2.1 Test Matrix 1 Results for Thin-Adherend Lap Shear Specimens.

The effect of different adherend types and bondline thicknesses were investigated for three different paste adhesives using the ASTM D 3165 specimens in test matrix 1 (table 1). All tests were carried out in a RTD environment using the procedures outlined in section 2.

Figure 32 shows the results of the of the aluminum adherend tests. Each data point in the figure represents the average of no less than three specimens. Failure modes for the aluminum specimens can be found in tables 24 through 26. It should be noted that failure modes characterized as adhesive occurred when the anodization/bond-primer layer in between the aluminum and adhesive aluminum failed.

It is apparent that as the bondline thickness increases, the apparent shear strength of the adhesive decreases gradually. Moreover, no dramatic drop in the strength is realized, at least in the range tested, as has been speculated.

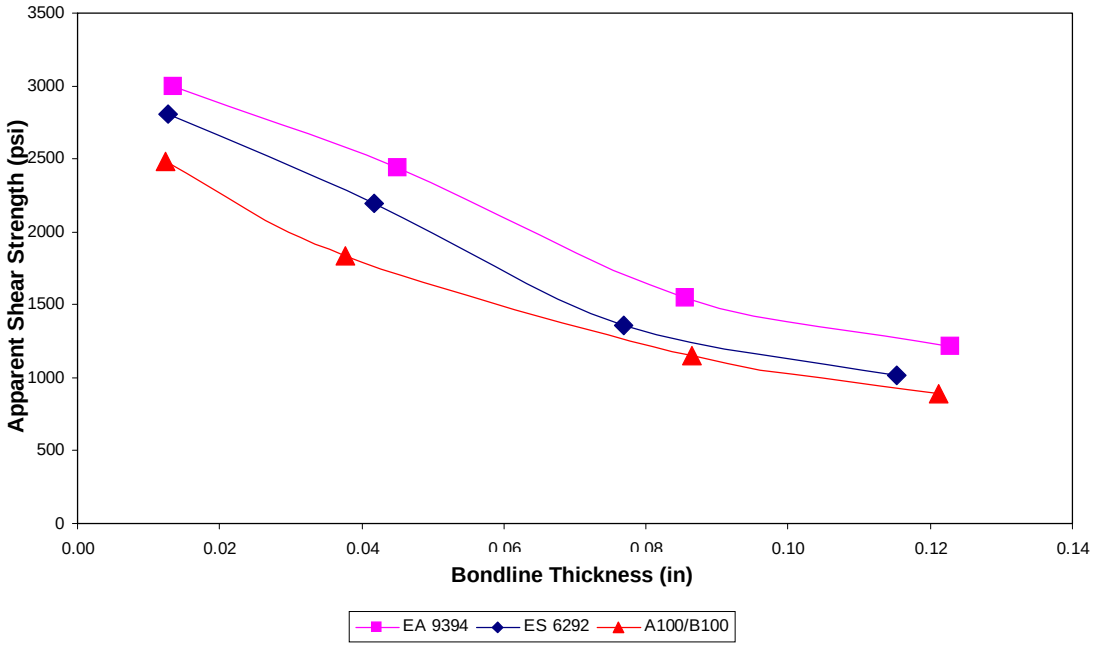

FIGURE 32. APPARENT SHEAR STRENGTH OF ALL THREE ADHESIVES VERSUS BONDLINE THICKNESS WITH ALUMINUM ADHERENDS (ASTM D 3165)
(Failure modes are shown in table 24)

TABLE 24. LIST OF ALUMINUM ASTM D 3165 TEST SPECIMENS FROM TEST MATRIX 1 (Hysol EA9394 paste adhesive)

Adhesive System	Specimen Name	Max. App. Shear Stress (psi)	Avg. Bondline Thickness (in)	Failure Mode (see notes)
Hysol EA9394	A21A11	3051.1	0.0140	Cohesive
	A21A13	2994.7	0.0140	Cohesive
	A21A16	2944.4	0.0130	Cohesive
	A21B23	2439.4	0.0445	Cohesive/Adhesive
	A21B25	2480.2	0.0440	Cohesive/Adhesive
	A21B26	2386.9	0.0465	Cohesive/Adhesive
	A21C13	1566.9	0.0850	Cohesive/Adhesive
	A21C14	1524.5	0.0855	Cohesive/Adhesive
	A21C15	1560.0	0.0860	Cohesive/Adhesive
	A21D11	1207.2	0.1200	Adhesive
	A21D12	1250.1	0.1220	Adhesive
	A21D13	1169.9	0.1240	Adhesive
	A21D14	1217.2	0.1245	Adhesive
	A21D15	1171.2	0.1240	Adhesive
	A21D16	1251.3	0.1225	Adhesive

Notes: Cohesive = 100% Cohesive Failure
Adhesive = 100% Adhesive Failure
Cohesive/Adhesive = >50% cohesive failure, but some adhesive failure present
Adhesive/Cohesive = >50% adhesive failure, but some cohesive failure present

TABLE 25. LIST OF ALUMINUM ASTM D 3165 TEST SPECIMENS FROM TEST MATRIX 1 (PTM&W ES6292 paste adhesive)

Adhesive System	Specimen Name	Max. App. Shear Stress (psi)	Average Bondline Thickness (in)	Failure Mode (see notes)
PTM&W ES6292	B21A11	2748.4	0.0145	Cohesive
	B21A12	2830.3	0.0145	Cohesive
	B21A13	2820.9	0.0110	Cohesive
	B21A14	2825.9	0.0135	Cohesive
	B21A15	2823.6	0.0105	Cohesive
	B21B11	2188.1	0.0415	Cohesive/Adhesive
	B21B12	2219.3	0.0425	Cohesive/Adhesive
	B21B13	2187.0	0.0420	Cohesive/Adhesive
	B21B14	2184.4	0.0420	Cohesive/Adhesive
	B21B15	2206.6	0.0405	Cohesive/Adhesive
	B21C11	1341.0	0.0770	Cohesive/Adhesive
	B21C12	1340.8	0.0770	Cohesive/Adhesive
	B21C13	1386.2	0.0770	Cohesive/Adhesive
	B21C14	1349.6	0.0765	Cohesive/Adhesive
	B21D11	1016.8	0.1155	Cohesive/Adhesive
	B21D12	1039.2	0.1155	Cohesive/Adhesive
	B21D13	1008.7	0.1155	Cohesive/Adhesive
	B21D14	1013.1	0.1145	Cohesive/Adhesive

Notes: Cohesive = 100% Cohesive Failure
Adhesive = 100% Adhesive Failure
Cohesive/Adhesive = >50% cohesive failure, but some adhesive failure present
Adhesive/Cohesive = >50% adhesive failure, but some cohesive failure present

TABLE 26. LIST OF ALUMINUM ASTM D 3165 TEST SPECIMENS FROM TEST MATRIX 1 (MGS A100/B100 paste adhesive)

Adhesive System	Specimen Name	Max. App. Shear Stress (psi)	Avg. Bondline Thickness (in)	Failure Mode (see notes)
MGS A100/B100	C21A11	2471.4	0.0135	Cohesive
	C21A12	2574.7	0.0105	Cohesive
	C21A13	2448.3	0.0125	Cohesive
	C21A14	2457.6	0.0125	Cohesive
	C21A15	2471.5	0.0125	Cohesive
	C21B11	1795.3	0.0385	Adhesive/Cohesive
	C21B12	1797.7	0.0385	Adhesive/Cohesive
	C21B13	1841.4	0.0375	Adhesive/Cohesive
	C21B14	1956.9	0.0350	Adhesive/Cohesive
	C21B15	1766.6	0.0385	Adhesive/Cohesive
	C21B16	1745.7	0.0395	Adhesive/Cohesive
	C21C12	1191.5	0.0845	Cohesive/Adhesive
	C21C14	1135.3	0.0870	Cohesive/Adhesive
	C21C15	1175.2	0.0860	Cohesive/Adhesive
	C21D11	901.9	0.1205	Cohesive/Adhesive
	C21D12	868.3	0.1230	Cohesive/Adhesive
	C21D13	915.5	0.1190	Cohesive/Adhesive
	C21D14	878.9	0.1225	Cohesive/Adhesive
	C21D15	913.4	0.1220	Cohesive/Adhesive
	C21D16	885.6	0.1225	Cohesive/Adhesive

Notes: Cohesive = 100% Cohesive Failure
Adhesive = 100% Adhesive Failure
Cohesive/Adhesive = >50% cohesive failure, but some adhesive failure present
Adhesive/Cohesive = >50% adhesive failure, but some cohesive failure present

The effect of adherend type versus bondline thickness in an RTD environment was studied using the Hysol EA9394 system in test matrix 1 (table 1). Figure 33 shows the results for the apparent shear strength of specimens with three different adherend materials as a function of bondline thickness. The average values shown in the figure comprise no less than three replicates for each bondline thickness. Table 27 lists the apparent shear strength, average bondline thickness, and failure mode for each composite adherend specimen used in figure.

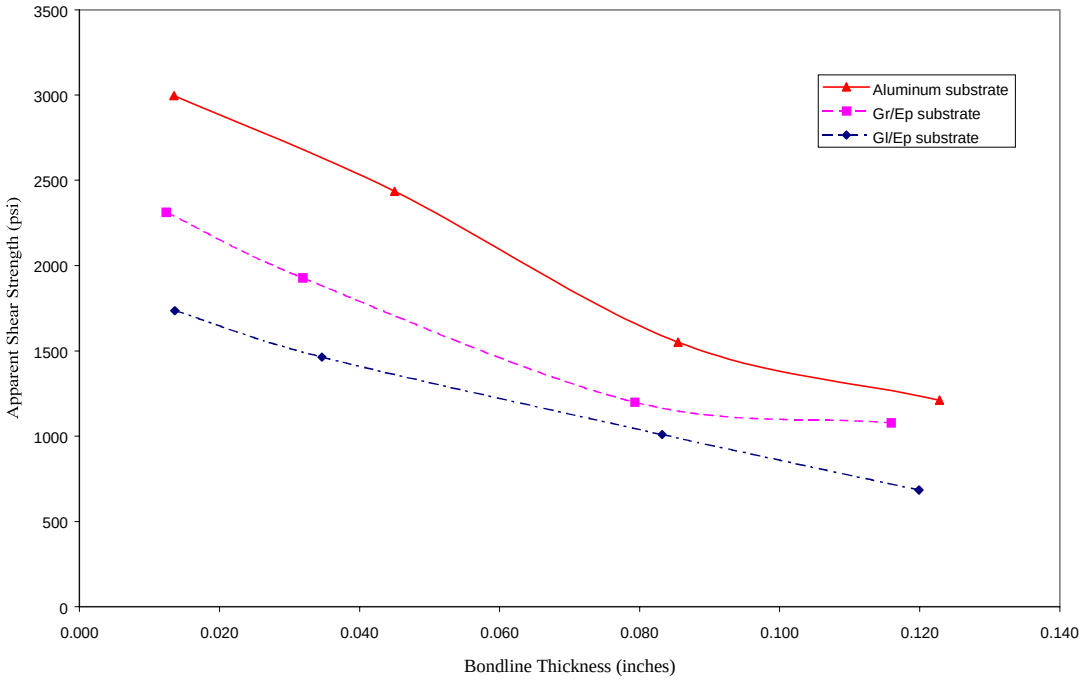

FIGURE 33. APPARENT SHEAR STRENGTH VERSUS BONDLINE THICKNESS FOR DIFFERENT ADHEREND TYPES: ASTM D 3165, HYSOL EA9394 PASTE ADHESIVE

While the general trend remains the same for all three adherend types, i.e., decreasing strength with increasing bondline thickness, there is a significant drop in apparent shear strength of the joint as a function of adherend type. This is better understood when analyzing the failure modes of the specimens. Table 27 shows that the failure mode for all the composite adherend specimens was a result of interlaminar shear failure in the first ply of the substrate. Examples of the first-ply failure for both the C/Ep and Gl/Ep ASTM D 3165 specimens can be seen in figures 34 and 35 respectively, as opposed to the cohesive/adhesive failures in the aluminum specimens as seen in figure 36. As discussed previously, the rotation of the adherends while load is applied induces high peel stresses at the edges of the overlap. In the composite specimens from test matrix 1, the peel stresses exceed the interlaminar shear strength of the matrix before the adhesive in question reaches a critical point. Because of this, the apparent shear strength of the joint is not a measure of the maximum apparent shear strength of the adhesive, but rather a characteristic of the adherend and of the bonded joint.

TABLE 27. LIST OF COMPOSITE ADHEREND ASTM D 3165 RESULTS FROM TEST MATRIX 1 (HYSOL EA9394 paste adhesive)

Adherend Type	Specimen Label	Apparent Shear Strength (psi)	Average Bondline Thickness (in.)	Failure Mode
Fiberglass/Epoxy laminate	A22A11	1757.0	0.0130	Substrate
	A22A12	1733.6	0.0135	Substrate
	A22A13	1702.9	0.0140	Substrate
	A22A14	1751.1	0.0140	Substrate
	A22B11	1456.6	0.0340	Substrate
	A22B12	1558.2	0.0350	Substrate
	A22B13	1437.4	0.0355	Substrate
	A22B14	1402.8	0.0340	Substrate
	A22C11	1103.7	0.0830	Substrate
	A22C12	1143.3	0.0830	Substrate
	A22C13	974.1	0.0830	Substrate
	A22C14	905.5	0.0840	Substrate
	A22C15	920.7	0.0830	Substrate
	A22D11	723.0	0.1205	Substrate
	A22D12	704.1	0.1200	Substrate
	A22D13	664.1	0.1200	Substrate
	A22D14	644.0	0.1190	Substrate
Carbon/epoxy laminate	A23A11	2332.5	0.0120	Substrate
	A23A12	2272.0	0.0125	Substrate
	A23A13	2104.2	0.0125	Substrate
	A23A14	2544.1	0.0125	Substrate
	A23B11	1733.1	0.0310	Substrate
	A23B12	1712.9	0.0315	Substrate
	A23B13	1871.9	0.0310	Substrate
	A23C11	1242.7	0.0785	Substrate
	A23C12	1177.1	0.0825	Substrate
	A23C14	1320.1	0.0780	Substrate
	A23C15	1238.4	0.0780	Substrate
	A23D11	885.2	0.1165	Substrate
	A23D12	937.6	0.1175	Substrate
	A23D13	917.4	0.1165	Substrate

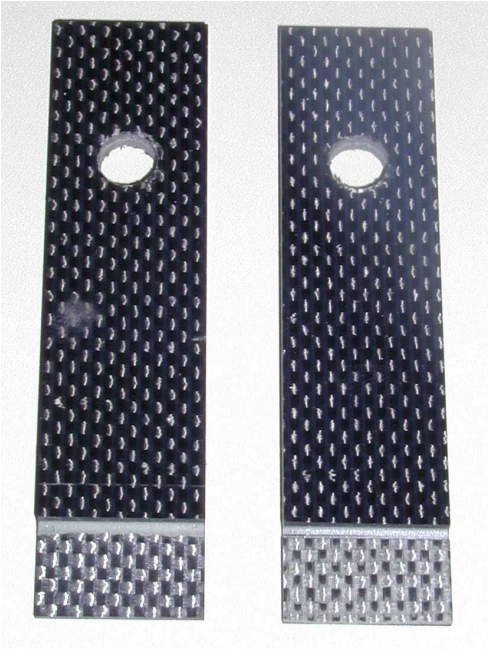

FIGURE 34. EXAMPLE OF FIRST-PLY FAILURE IN CARBON/EPOXY ASTM D 3165 SPECIMEN. THE RIGHT PORTION OF THE SPECIMEN SHOWS PART OF THE FIRST-PLY FROM HE LEFT PORTION STILL ADHERING TO ADHESIVE.

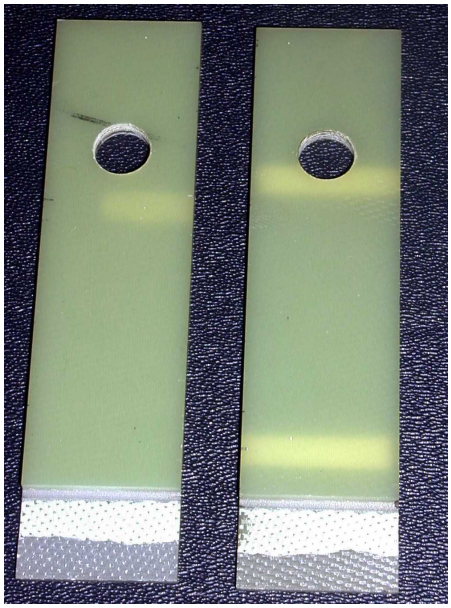

FIGURE 35. EXAMPLE OF FIRST-PLY FAILURE IN FIBERGLASS/EPOXY ASTM D 3165 SPECIMEN. THE FIRST-PLY OF LAMINATE CAN BE SEEN STILL ADHERING TO THE ADHESIVE ON BOTH PORTIONS OF THE SPECIMEN.

FIGURE 36. EXAMPLE OF COHESIVE/ADHESIVE FAILURE OF ALUMINUM ADHEREND ASTM D 3165 SPECIMEN. NOTE THE <50% ADHESIVE FAILURE ON THE UPPER PORTION OF THE RIGHT HALF OF SPECIMEN.

Test matrix 1 (table 1) originally specified testing of the ASTM D 1002 specimens for all three adhesive systems. However, the results from the aluminum adherend D 1002 tests on the Hysol adhesive showed that the apparent shear strengths of the D 1002 specimens only slightly varied from those of the ASTM D 3165 specimen. This can be seen in figure 37, where the results from the Hysol adhesive tests using all three ASTM specimens are shown. It should be noted that ASTM D 1002 specimens with bondlines on the order of 0.010″ failed in bearing of the adherend at the loading pin and are not shown in the figure as the failure is outside the test section. In addition, all other failures of the D 1002 regardless of bondline thickness were adhesive/cohesive or completely adhesive as shown in the figure, whereas the D 3165 configuration led to cohesive failures for thicknesses 0.085″ and less. Based on these results, it was decided that ASTM D 1002 specimens would not be used for the remainder of the investigation, because ASTM D 3165 specimens resulted in more acceptable failure modes and less load path eccentricity due to the sandwich configuration.

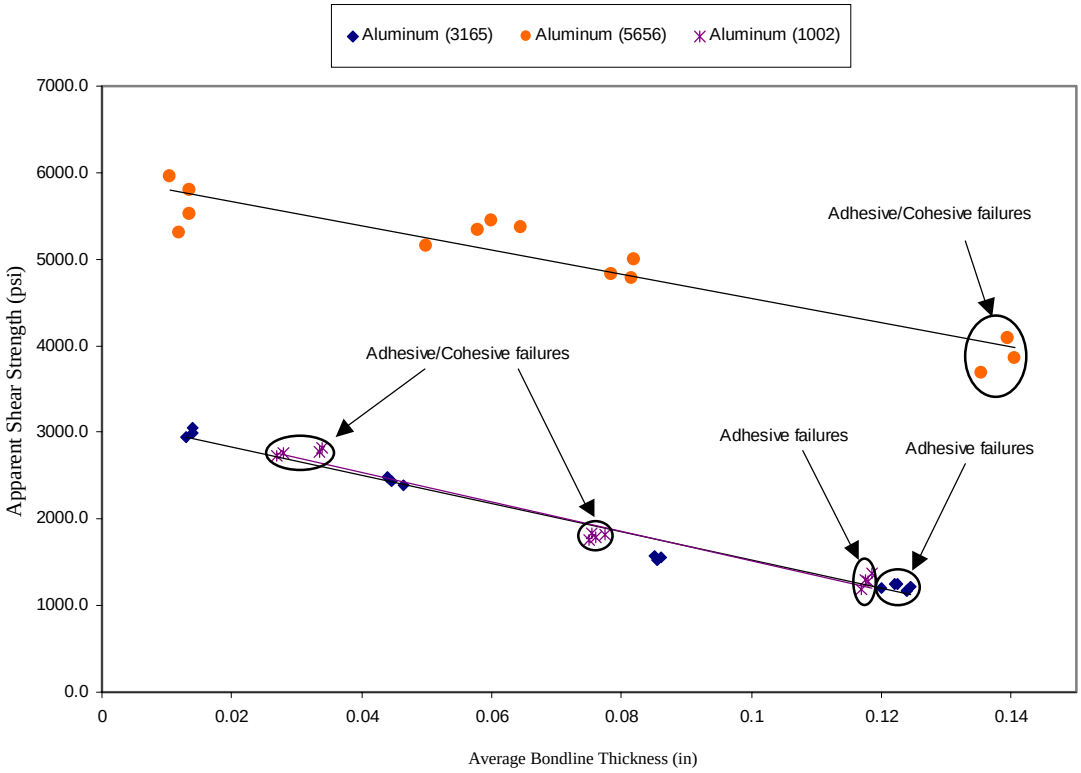

FIGURE 37. COMPARISON OF ASTM D 1002 AND D 3165 APPARENT SHEAR STRENGTH VERSUS BONDLINE THICKNESS (Hysol 9394 adhesive)

3.2.2 Test Matrix 2-A Results for ASTM D 3165 Specimens.

The objective of test matrix 2-A (table 2), studied the effect of different environments on the adhesive apparent shear strength. Based on the results of test matrix 1, the application of this investigation to the GA industry, and on input from various small airplane manufacturers, the C/Ep adherend used previously was chosen as the substrate material for the ASTM D 3165 test specimens in test matrix 2-A. Specimens were tested at four different service temperatures and two moisture levels: CD (-65°F), RTD and ETD (160° and 200°F), and ETW (160°F and 200°F). Both the MGS and PTM&W adhesives were evaluated.

Figures 38 and 39 show the averages of all the ASTM D 3165 environmental tests for the MGS and PTM&W paste adhesives respectively. The averages are computed from no less than three replicate specimens, the actual values for the maximum apparent shear stress, average bondline thickness, and failure mode for all the specimens tested are given in tables 28 through 39.

All RTD and CD specimens failed by first-ply failure of the substrate, while all specimens that had been exposed to moisture failed either cohesively or in a cohesive/substrate combination. Most apparent from the figures is the drop in strength due to moisture absorption, which is most significant for the 0.015″ bondline thicknesses. This trend is more clearly illustrated again in figures 40 and 41, which show the drop in strength due to moisture absorption of the test specimens.

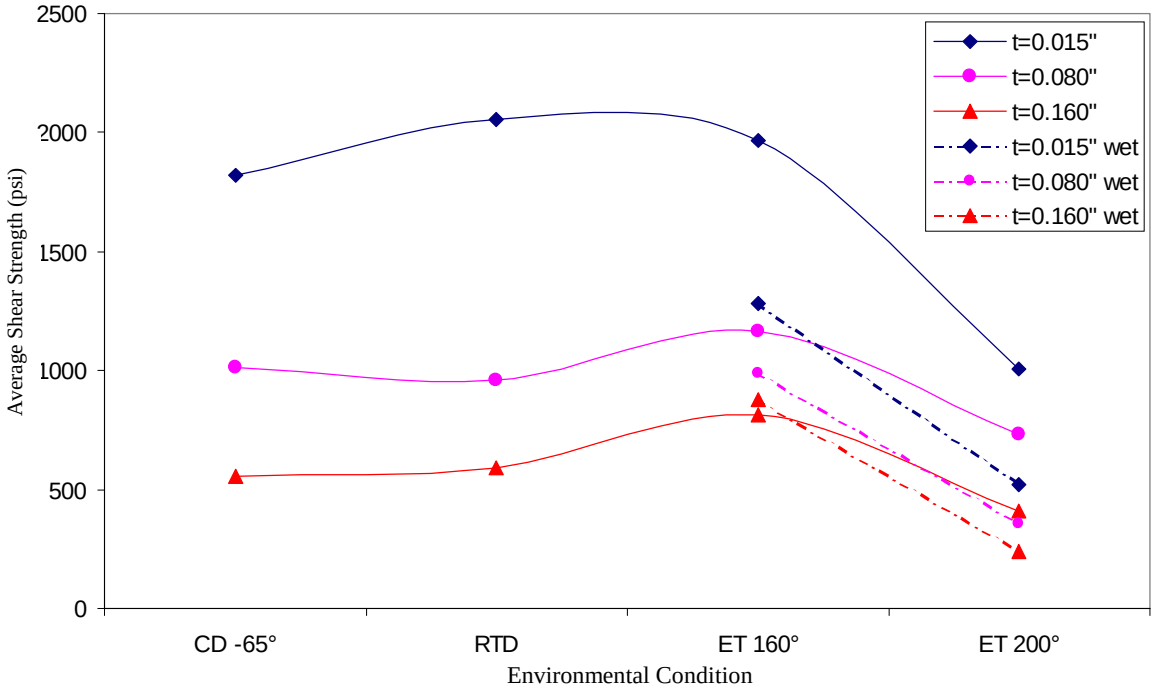

FIGURE 38. AVERAGE APPARENT SHEAR STRENGTH VERSUS ENVIRONMENTAL CONDITION FOR THREE BONDLINE THICKNESSES USING ASTM D 3165 SPECIMENS (C/Ep substrate, MGS adhesive)

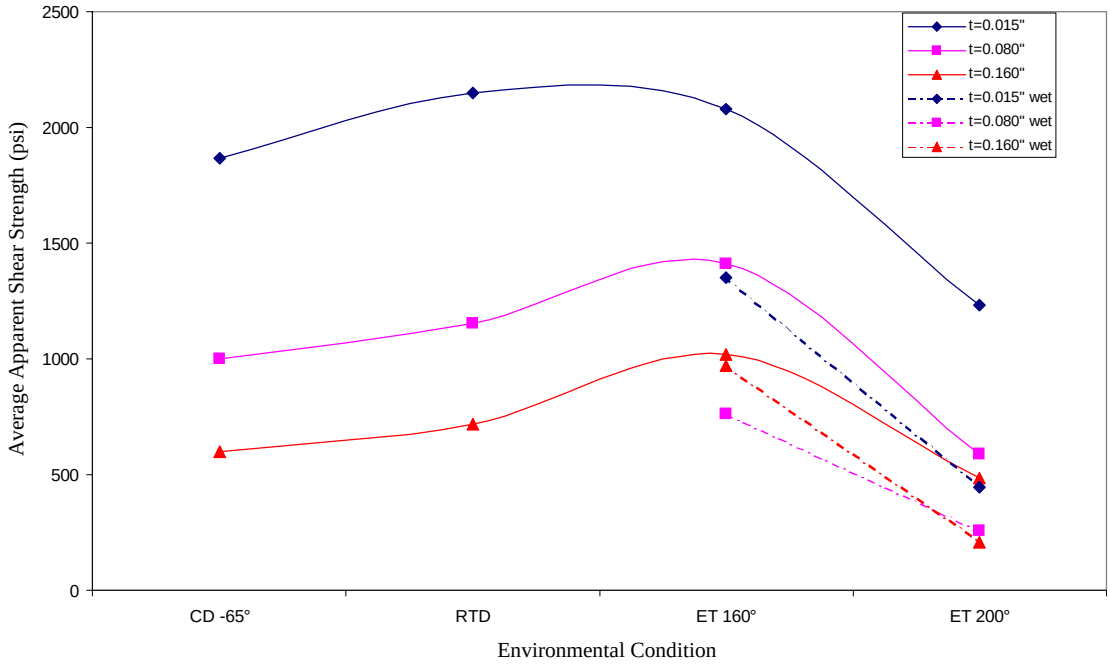

FIGURE 39. AVERAGE APPARENT SHEAR STRENGTH VERSUS ENVIRONMENTAL CONDITION FOR THREE BONDLINE THICKNESSES USING ASTM D 3165 SPECIMENS (C/Ep substrate, PTM&W adhesive)

TABLE 28. ROOM TEMPERATURE DRY RESULTS FOR ASTM D 3165 SPECIMENS
(C/Ep substrate, MGS adhesive)

Specimen Name	Max. Apparent Shear Strength (psi)	Average Bondline Thickness (in.)	Failure Mode
C23A22	2016.2	0.014	Substrate
C23A36	2056.5	0.014	Substrate
C23A45	2128.9	0.014	Substrate
C23A55	2068.3	0.014	Substrate
C23A65	2101.1	0.011	Substrate
C23A73	1948.3	0.013	Substrate
AVG	2053.2	0.013	
STD DEV	64.24	0.0012	
COV (%)	3.13	9.08	
C23C25	949.3	0.079	Substrate
C23C92	979.1	0.082	Substrate
C23C94	963.9	0.081	Substrate
C23C96	995.5	0.082	Substrate
C23C82	917.3	0.083	Substrate
AVG	961.0	0.081	
STD DEV	29.89	0.0015	
COV (%)	3.11	1.86	
C23E27	569.1	0.161	Substrate
C23E42	592.6	0.161	Substrate
C23E47	587.8	0.158	Substrate
C23E53	628.1	0.159	Substrate
C23E61	584.8	0.16	Substrate
C23E67	580.7	0.159	Substrate
AVG	590.5	0.160	
STD DEV	20.06	0.0012	
COV (%)	3.40	0.76	

TABLE 29. COLD DRY (-65°F) RESULTS FOR ASTM D 3165 SPECIMENS
(C/Ep substrate, MGS adhesive)

Specimen Name	Max. Apparent Shear Strength (psi)	Average Bondline Thickness (in.)	Failure Mode
C23A23	1829.714	0.013	Substrate
C23A25	1884.359	0.013	Substrate
C23A27	1781.672	0.013	Substrate
C23A54	1840.912	0.014	Substrate
C23A72	1769.097	0.013	Substrate
C23A75	1812.425	0.014	Substrate
AVG	1819.7	0.013	
STD DEV	41.93	0.0005	
COV (%)	2.30	3.87	
C23C14	946.3065	0.082	Substrate
C23C16	998.1141	0.081	Substrate
C23C51	982.4422	0.078	Substrate
C23C53	995.9776	0.082	Substrate
C23C61	1056.521	0.079	Substrate
C23C65	1084.863	0.082	Substrate
AVG	1010.7	0.081	
STD DEV	50.83	0.0018	
COV (%)	5.03	2.17	
C23E16	539.6841	0.162	Substrate
C23E41	544.8475	0.16	Substrate
C23E71	579.6172	0.16	Substrate
C23E74	567.9537	0.162	Substrate
AVG	558.0	0.161	
STD DEV	18.93	0.0012	
COV (%)	3.39	0.72	

TABLE 30. ELEVATED TEMPERATURE DRY (160°F) RESULTS FOR ASTM D 3165 SPECIMENS
(C/Ep substrate, MGS adhesive)

Specimen Name	Max. Apparent Shear Strength (psi)	Average Bondline Thickness (in.)	Failure Mode
C23A21		0.015	Coh/Sub
C23A35	1934.4	0.013	Coh/Sub
C23A47	1924.8	0.014	Coh/Sub
C23A53	1999.4	0.014	Coh/Sub
C23A67	1975.1	0.013	Coh/Sub
AVG	1958.4	0.014	
STD DEV	34.95	0.0008	
COV (%)	1.78	6.06	
C23C12	1239.4	0.081	Sub/Coh
C23C15	1189	0.082	Sub/Coh
C23C52	1140.7	0.081	Sub/Coh
C23C57	1106.2	0.082	Sub/Coh
C23C64	1159.6	0.081	Sub/Coh
AVG	1167.0	0.081	
STD DEV	50.42	0.0005	
COV (%)	4.32	0.67	
C23E11	749	0.161	Substrate
C23E14	778.6	0.16	Sub/Coh
C23E32	843.6	0.161	Coh/Sub
C23E36	880.8	0.159	Coh/Sub
C23E73	819.1	0.162	Coh/Sub
C23E75	826.6	0.16	Coh/Sub
AVG	816.3	0.161	
STD DEV	46.84	0.0010	
COV (%)	5.74	0.65	

TABLE 31. ELEVATED TEMPERATURE WET (160°F) RESULTS FOR ASTM D 3165 SPECIMENS
(C/Ep substrate, MGS adhesive)

Specimen Name	Max. Apparent Shear Strength (psi)	Average Bondline Thickness (in.)	Failure Mode
C23A26	1259	0.014	Cohesive
C23A32	1353.2	0.011	Cohesive
C23A34	1225	0.014	Cohesive
C23A52	1421.9	0.013	Cohesive
C23A66	1154.8	0.012	Cohesive
AVG	1282.8	0.013	
STD DEV	105.59	0.0013	
COV (%)	8.23	10.19	
C23C22	921.9	0.082	Cohesive
C23C24	1121.8	0.078	Cohesive
C23C26	921	0.081	Cohesive
C23C45	1014.8	0.082	Cohesive
C23C47	964.4	0.082	Cohesive
AVG	988.8	0.081	
STD DEV	83.72	0.0017	
COV (%)	8.47	2.14	
C23E26	905.2	0.162	Coh/Sub
C23E43	953.9	0.162	Coh/Sub
C23E44	901.1	0.162	Cohesive
C23E62	820.8	0.161	Cohesive
AVG	895.3	0.162	
STD DEV	55.12	0.0005	
COV (%)	6.16	0.31	

TABLE 32. ELEVATED TEMPERATURE DRY (200°F) RESULTS FOR ASTM D 3165 SPECIMENS
(C/Ep substrate, MGS adhesive)

Specimen Name	Max. Apparent Shear Strength (psi)	Average Bondline Thickness (in.)	Failure Mode
C23A41	1030.5	0.014	Cohesive
C23A43	1005.9	0.014	Cohesive
C23A51	995.4	0.013	Cohesive
C23A71	1003.7	0.014	Cohesive
AVG	1008.9	0.014	
STD DEV	15.11	0.0005	
COV (%)	1.50	3.64	
C23C13	757.2	0.082	Cohesive
C23C54	702.4	0.082	Cohesive
C23C55	740.4	0.082	Cohesive
C23C62	757.4	0.082	Cohesive
C23C63	700.4	0.082	Cohesive
AVG	731.6	0.082	
STD DEV	28.39	0.0000	
COV (%)	3.88	0.00	
C23E13	448.1	0.161	Cohesive
C23E17	386.6	0.159	Cohesive
C23E35	413.2	0.16	Cohesive
C23E72	418.3	0.16	Cohesive
C23E77	380.3	0.16	Cohesive
AVG	409.3	0.160	
STD DEV	27.19	0.0007	
COV (%)	6.64	0.44	

TABLE 33. ELEVATED TEMPERATURE WET (200°F) RESULTS FOR ASTM D 3165 SPECIMENS
(C/Ep substrate, MGS adhesive)

Specimen Name	Max. Apparent Shear Strength (psi)	Average Bondline Thickness (in.)	Failure Mode
C23A42	517.35	0.014	Cohesive
C23A56	480.56	0.012	Cohesive
C23A62	479.48	0.01	Cohesive
C23A74	550.16	0.014	Cohesive
C23A76	568.99	0.013	Cohesive
AVG	519.3	0.013	
STD DEV	40.35	0.0017	
COV (%)	7.77	13.28	
C23C23	348.77	0.08	Cohesive
C23C44	357.75	0.082	Cohesive
C23C46	365.05	0.082	Cohesive
AVG	357.2	0.081	
STD DEV	8.15	0.0012	
COV (%)	2.28	1.42	
C23E25	274.58	0.163	Cohesive
C23E45	310.19	0.161	Cohesive
C23E55	217.95	0.157	Cohesive
C23E64	185.28	0.161	Cohesive
AVG	247.0	0.161	
STD DEV	56.00	0.0025	
COV (%)	22.67	1.57	

TABLE 34. ROOM TEMPERATURE DRY RESULTS FOR ASTM D 3165 SPECIMENS
(C/Ep substrate, PTM&W adhesive)

Specimen Name	Max. Apparent Shear Strength (psi)	Average Bondline Thickness (in.)	Failure Mode
B23A11	2454.7	0.014	Substrate
B23A26	2172.4	0.015	Substrate
B23A34	1869.1	0.015	Substrate
B23A47	2377.7	0.013	Substrate
B23A52	1864.9	0.017	Substrate
B23A64	2151.4	0.017	Substrate
AVG	2148.4	0.015	
STD DEV	247.13	0.0016	
COV (%)	11.50	10.56	
B23C16	1158.9	0.082	Substrate
B23C24	1176.2	0.081	Substrate
B23C32	1220.9	0.081	Substrate
B23C45	1129.3	0.082	Substrate
B23C56	1131.1	0.078	Substrate
B23C65	1113.2	0.082	Substrate
AVG	1154.9	0.081	
STD DEV	39.46	0.0015	
COV (%)	3.42	1.91	
B23E15	748.47	0.16	Substrate
B23E22	681	0.162	Substrate
B23E32	741.2	0.161	Substrate
B23E34	732.4	0.161	Substrate
B23E47	720.9	0.16	Substrate
B23E65	677.4	0.161	Substrate
AVG	716.9	0.161	
STD DEV	30.63	0.0008	
COV (%)	4.27	0.47	

TABLE 35. COLD DRY (-65°F) RESULTS FOR ASTM D 3165 SPECIMENS
(C/Ep substrate, PTM&W adhesive)

Specimen Name	Max. Apparent Shear Strength (psi)	Average Bondline Thickness (in.)	Failure Mode
B23A23	1819.8	0.017	Substrate
B23A35	1783.8	0.016	Substrate
B23A41	1936.9	0.013	Substrate
B23A42	1848.7	0.016	Substrate
B23A51	1894.1	0.016	Substrate
B23A66	1915.1	0.015	Substrate
AVG	1866.4	0.016	
STD DEV	59.02	0.0014	
COV (%)	3.16	8.89	
B23C71	977.1	0.082	Substrate
B23C72	932.5	0.081	Substrate
B23C73	1035.3	0.082	Substrate
B23C74	1031	0.082	Substrate
B23C76	1031.6	0.082	Substrate
AVG	1001.5	0.082	
STD DEV	45.48	0.0004	
COV (%)	4.54	0.55	
B23E16	618.7	0.161	Substrate
B23E43	599.9	0.161	Substrate
B23E46	597.2	0.162	Substrate
B23E52	587.1	0.162	Substrate
B23E67	585.5	0.16	Substrate
AVG	597.7	0.161	
STD DEV	13.30	0.0008	
COV (%)	2.22	0.52	

TABLE 36. ELEVATED TEMPERATURE DRY (160°F) RESULTS FOR ASTM D 3165 SPECIMENS
(C/Ep substrate, PTM&W adhesive)

Specimen Name	Max. Apparent Shear Strength (psi)	Average Bondline Thickness (in.)	Failure Mode
B23A15	2018.5	0.014	Coh/Sub
B23A25	2173.9	0.017	Coh/Sub
B23A37	2028.5	0.013	Coh/Sub
B23A45	2057.4	0.015	Coh/Sub
B23A61	2120.3	0.017	Coh/Sub
AVG	2079.7	0.015	
STD DEV	65.93	0.0018	
COV (%)	3.17	11.77	
B23C13	1441.2	0.082	Coh/Sub
B23C27	1369.1	0.08	Coh/Sub
B23C37	1426.5	0.078	Cohesive
B23C47	1340.4	0.08	Coh/Sub
B23C63	1469.5	0.082	Coh/Sub
AVG	1409.3	0.080	
STD DEV	53.15	0.0017	
COV (%)	3.77	2.08	
B23E12	1026.1	0.16	Substrate
B23E27	1007.5	0.159	Sub/Coh
B23E44	1009.3	0.162	Sub/Coh
B23E55	1093.2	0.161	Sub/Coh
B23E66	973.4	0.161	Sub/Coh
AVG	1021.9	0.161	
STD DEV	44.21	0.0011	
COV (%)	4.33	0.71	

TABLE 37. ELEVATED TEMPERATURE WET (160°F) RESULTS FOR ASTM D 3165 SPECIMENS
(C/Ep substrate, PTM&W adhesive)

Specimen Name	Max. Apparent Shear Strength (psi)	Average Bondline Thickness (in.)	Failure Mode
B23A12	1336.5	0.015	Cohesive
B23A14	1342.8	0.015	Cohesive
B23A22	1301.5	0.017	Cohesive
B23A43	1345.6	0.016	Cohesive
B23A53	1405	0.017	Cohesive
B23A65	1378.4	0.016	Cohesive
AVG	1351.6	0.016	
STD DEV	35.84	0.0009	
COV (%)	2.65	5.59	
B23C21	834.6	0.081	Cohesive
B23C23	742.6	0.081	Cohesive
B23C25	770.9	0.082	Cohesive
B23C35	766	0.082	Cohesive
B23C46	692.7	0.082	Cohesive
B23C53	775.2	0.08	Cohesive
AVG	763.7	0.081	
STD DEV	46.27	0.0008	
COV (%)	6.06	1.00	
B23E11	1077.9	0.16	Coh/Sub
B23E42	1043.7	0.162	Coh/Sub
B23E45	825	0.162	Cohesive
B23E56	940.3	0.161	Coh/Sub
B23E64	739.3	0.162	Cohesive
AVG	925.2	0.161	
STD DEV	143.34	0.0009	
COV (%)	15.49	0.55	

TABLE 38. ELEVATED TEMPERATURE DRY (200°F) RESULTS FOR ASTM D 3165 SPECIMENS
(C/Ep substrate, PTM&W adhesive)

Specimen Name	Max. Apparent Shear Strength (psi)	Average Bondline Thickness (in.)	Failure Mode
B23A21	1221.5	0.017	Cohesive
B23A32	1110.4	0.015	Coh/Sub
B23A44	1246.4	0.016	Coh/Sub
B23A54	1243.4	0.016	Coh/Sub
B23A63	1338.9	0.017	Coh/Sub
AVG	1232.1	0.016	
STD DEV	81.64	0.0008	
COV (%)	6.63	5.16	
B23C15	738.1	0.082	Coh/Sub
B23C34	478.3	0.082	Coh/Sub
B23C52	504.3	0.081	Cohesive
B23C54	520.8	0.079	Coh/Sub
B23C67	693.6	0.08	Coh/Sub
AVG	587.0	0.081	
STD DEV	119.62	0.0013	
COV (%)	20.38	1.61	
B23E14	419.9	0.16	Substrate
B23E41	462.6	0.162	Sub/Coh
B23E51	510.2	0.159	Sub/Coh
B23E53	563.8	0.162	Sub/Coh
B23E61	457.6	0.16	Sub/Coh
AVG	482.8	0.161	
STD DEV	55.48	0.0013	
COV (%)	11.49	0.84	

TABLE 39. ELEVATED TEMPERATURE WET (200°F) RESULTS FOR ASTM D 3165 SPECIMENS
(C/Ep substrate, PTM&W adhesive)

Specimen Name	Max. Apparent Shear Strength (psi)	Average Bondline Thickness (in.)	Failure Mode
B23A16	418.2	0.013	Cohesive
B23A24	426.7	0.017	Cohesive
B23A36	412.1	0.015	Cohesive
B23A46	499.5	0.014	Cohesive
B23A56	452.7	0.014	Cohesive
B23A62	458.1	0.017	Cohesive
AVG	444.6	0.015	
STD DEV	32.67	0.0017	
COV (%)	7.35	11.16	
B23C12	277.2	0.082	Cohesive
B23C17	297.9	0.08	Cohesive
B23C33	214.1	0.082	Cohesive
B23C55	230.1	0.079	Cohesive
B23C66	279.2	0.082	Cohesive
AVG	259.7	0.081	
STD DEV	35.71	0.0014	
COV (%)	13.75	1.75	
B23E17	203.1	0.158	Cohesive
B23E25	194.6	0.161	Cohesive
B23E33	206.7	0.162	Cohesive
B23E35	222.1	0.161	Cohesive
B23E53	216.8	0.162	Cohesive
B23E62	196.7	0.161	Cohesive
AVG	206.7	0.161	
STD DEV	10.94	0.0015	
COV (%)	5.29	0.92	

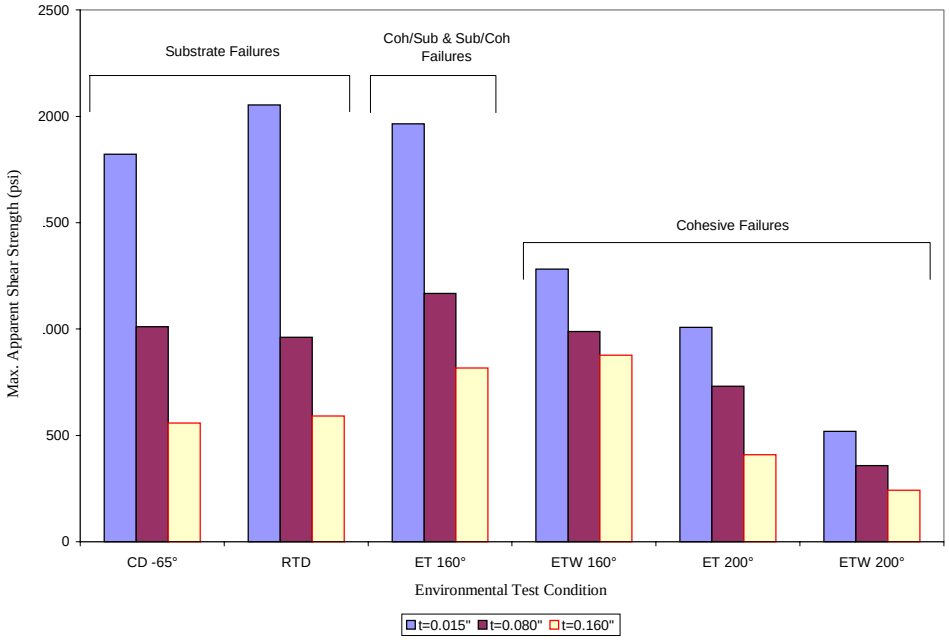

FIGURE 40. AVERAGE MAXIMUM APPARENT SHEAR STRENGTH VERSUS ENVIRONMENTAL CONDITION FOR THREE DIFFERENT BONDLINE THICKNESSES (ASTM D 3165, C/Ep adherends, MGS adhesive)

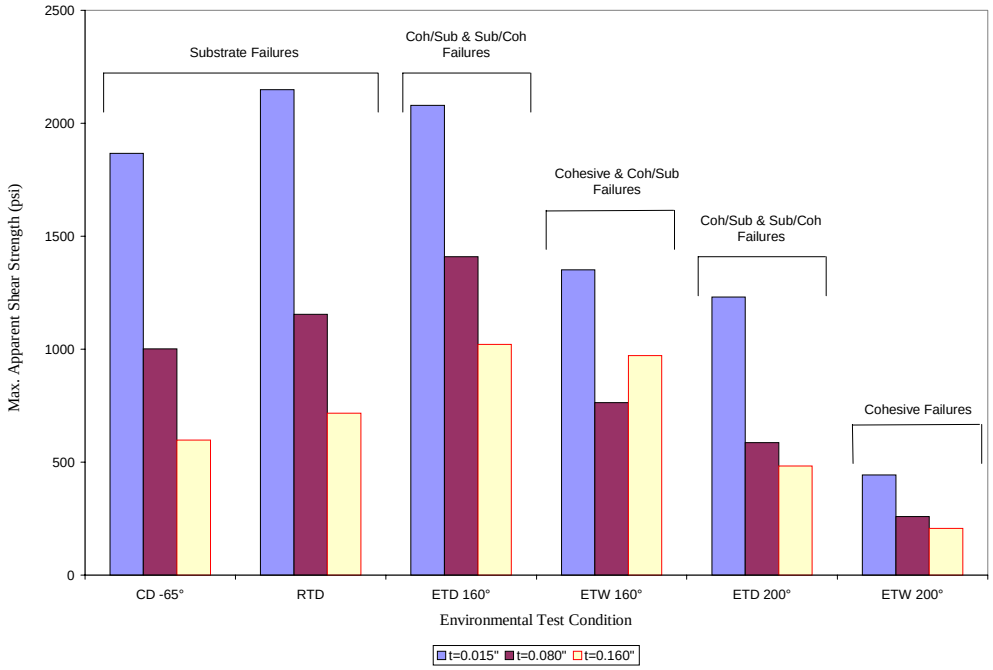

FIGURE 41. AVERAGE MAXIMUM APPARENT SHEAR STRENGTH VERSUS ENVIRONMENTAL CONDITION FOR THREE DIFFERENT BONDLINE THICKNESSES (ASTM D 3165, C/Ep adherends, PTM&W adhesive)

The T_g values of the adhesive should also be taken into consideration. For both adhesives, the dry T_g value (see table D-1) is just above the 160°F threshold, which explains the drastic drop in apparent shear strength between the ETD 160°F values and the ETD 200°F values. Initially, the 200°F condition was chosen to evaluate the performance of the adhesives well above their T_g limits. The wet T_g value for both adhesives was found to be well below the 160°F testing environment. This explains the drastic drop in strength values between the ETD 160°F and ETW 160°F. Indeed, gross shear deformation was seen during all the ETW tests and the ETD 200°F tests due to the rubbery nature of the post-T_g adhesive.

3.3 COMPARISONS.

The results from all three test methods and all three adherend types versus bondline thickness for the Hysol adhesive are shown in figure 42. This figure shows the effect that adherend stiffness has on the failure mode and apparent shear strength of the bonded joint. The stiffest specimen, mostly due to adherend cross-sectional area, is the ASTM D 5656 specimen, which in turn yields the largest apparent shear strength. For the ASTM D 3165 specimens, the aluminum adherend has the highest bending stiffness, followed by the C/Ep laminate and finally the Gl/Ep laminate. The trends confirm analytical models which show that as the bending stiffness of the adherend decreases, the peel stresses increase and the apparent shear strength decreases accordingly. These results are in agreement with previous experiments and analytical models for thin bondlines, but it can be seen from this investigation that the same holds true for thick bondlines also. The increased peel stresses induced by thicker bondlines do not effect the state of stress enough to change this trend.

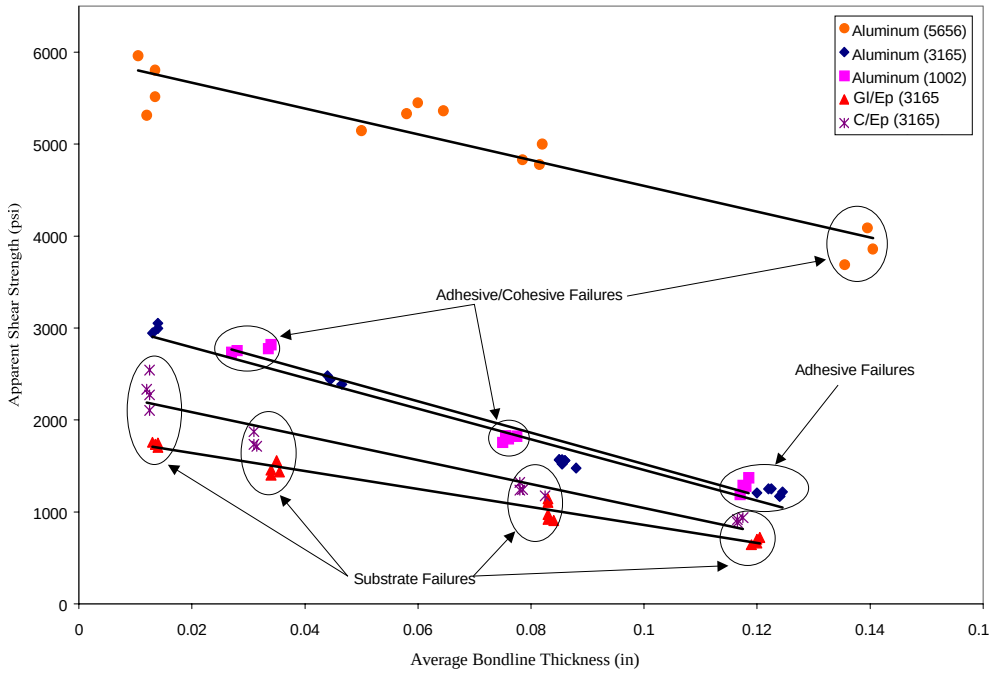

FIGURE 42. APPARENT SHEAR STRESS VERSUS BONDLINE THICKNESS FOR EA9394 PASTE ADHESIVE. COMPARISON OF ALL THREE TEST METHODS AND ALL THREE ADHEREND TYPES AT RTD.

When comparing the results from the thin-adherend tests to the thick-adherend tests, an interesting phenomenon is seen. For the thick-adherend specimens, the maximum apparent shear strength of the MGS adhesive is larger than the PTM&W adhesive. Yet, for the thin-adherend specimens, this situation is reversed. This trend can be seen in figure 43 as a function of bondline thickness. Guess, et al. observed this same phenomenon for thin bondlines using a film adhesive [14]. The results from this investigation show the same occurrence in paste adhesives of similar strengths for thin bondlines as well as for very thick bondlines. This occurrence is most likely due to the bending deformations in the thin adherend specimens as stated earlier. While the thick-adherend specimens come closest to a purely shear loading, the thin-adherend specimens have a combined state of shear and large peel stresses, which in turn produce a different state of stress in the adhesive bond than the 1 present in the thick-adherend specimens. Structural adhesives with similar strengths, but different stiffnesses, will react to this combined loading state differently as can be seen in figure 43.

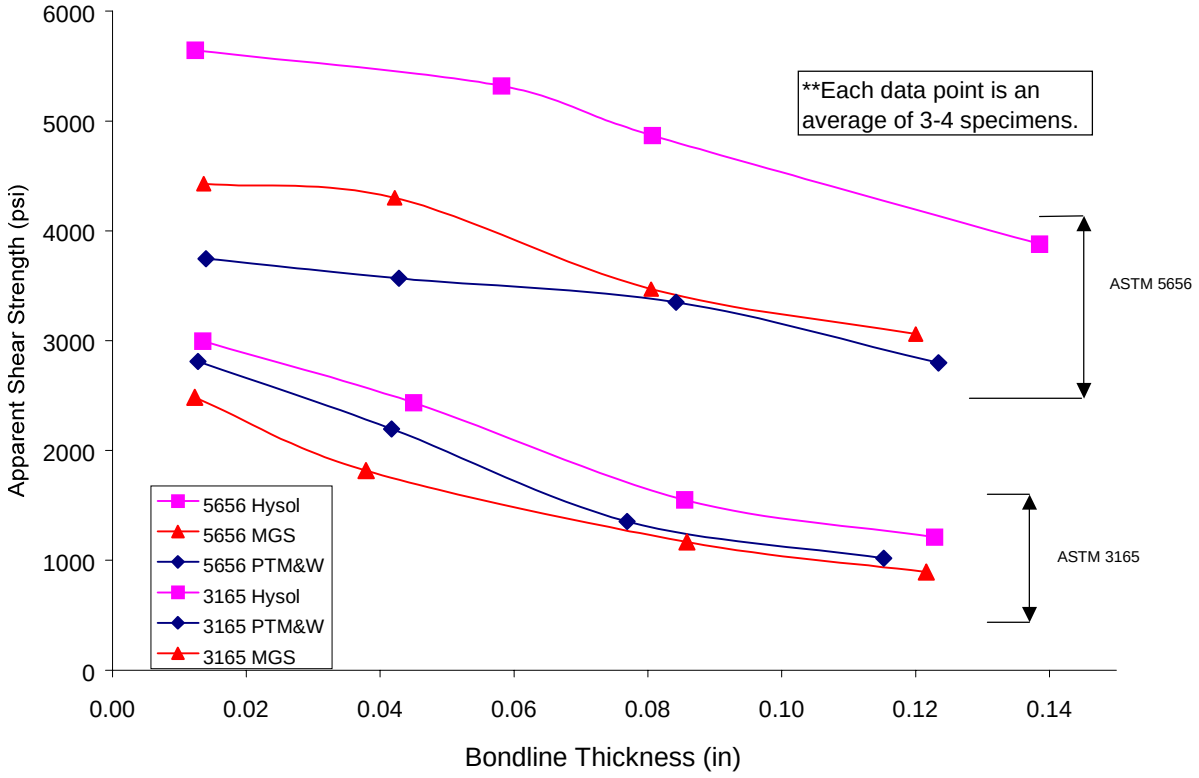

FIGURE 43. COMPARISON OF APPARENT SHEAR STRENGTH RESULTS FROM THIN- AND THICK-ADHEREND SPECIMENS AS A FUNCTION OF BONDLINE THICKNESS FOR ALL THREE ADHESIVES USING ALUMINUM ADHERENDS
(Note that the apparent shear strength of the MGS adhesive is larger than the PTM&W adhesive for the thick-adherend configuration, yet, less than the PTM&W adhesive for the thin-adherend configuration.)

Figure 44 shows the apparent shear strength of the MGS adhesive for various environmental conditions using two different test methods (ASTM D 5656 and ASTM D 3165). As seen from figure 44, the noncohesive failures were predominant in the cold dry conditions for both specimen configurations. As the temperature was increased, these failures modes changed to cohesive. It should also be noted that the cohesive failures of the ASTM D 5656 specimen with aluminum adherends occurred sooner (as a function of temperature) than observed with the ASTM D 3165 specimen with carbon/epoxy adherends.

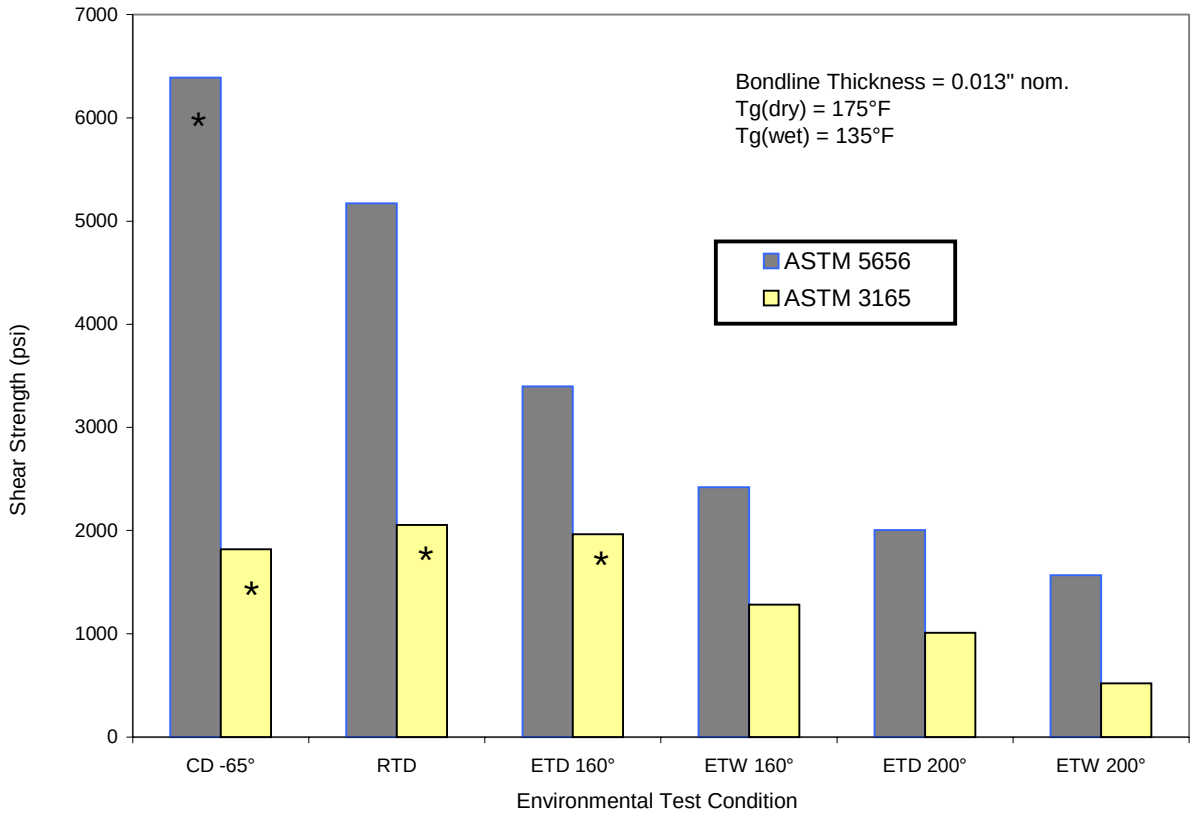

FIGURE 44. APPARENT SHEAR STRENGTH OF MGS ADHESIVE VERSUS ENVIRONMENTAL CONDITION FOR ALUMINUM THICK-ADHEREND SPECIMENS AND C/Ep THIN-ADHEREND SINGLE-LAP SHEAR SPECIMENS
(Starred data denotes noncohesive failures)

Also of significance is the drop in relative strength between the three adhesive systems. In the thick-adherend specimens, the difference in strength between the Hysol adhesive and the other two adhesives is substantially larger than the difference between the three in the thin-adherend specimens. This shows the adverse effects that the bending deformations in the thin-adherend specimen have on strength values. The significant peel stresses in the thin-adherend specimen, can lead to unseasonably low shear strength values. For this reason, it is important that the thin-adherend specimens should only be used with extreme caution when comparing different adhesive systems because they do not give a clear picture of the shear strength of the adhesive. They are more suitable for quality control purposes, when only one adhesive is being compared against itself.

4. CONCLUSIONS.

The objectives of this project were to:

- Investigate various test methods for the evaluation of adhesive shear properties.
- Evaluate the effect of bond thickness and environmental conditions on adhesive joint strength.
- Characterize the adhesive shear stress-strain relationship over a spectrum of environmental conditions and bond thicknesses using the KGR-type extensometers.

Three adhesives were tested using three different test methods, three adherend types, and four different bondlines. Several conclusions were made from these results. First, it was verified that as the adhesive bondline increases, the apparent shear strength decreases. However, this drop in strength was not as large as has been speculated, even for the extremely thick bonds. It was also found that the failure modes of the thick-adherend specimens were still largely cohesive in nature even for large bondline thicknesses.

The apparent shear strength of a given adhesive was found to be highly dependent on adherend bending stiffness, regardless of bondline thickness. Thin-adherend specimens gave lower apparent shear strengths due to the bending of the adherend and increased peel stresses in the overlap region due to the bending. As a result of the combined shear and peel stress state, it was shown that using the thin-adherend configuration for comparing different adhesives can lead to false information about the apparent shear strength of the adhesive systems. ASTM D 3165 specimens were found to have similar strengths as the ASTM D 1002 specimens, but failure modes were more acceptable in the ASTM D 3165 specimens. For the composite test specimens, failure of the joint occurred in the first ply of the substrate due to interlaminar failure. Decreases in apparent shear strength due to thicker bondlines can be attributed to the greater eccentricity of the load path as the bondline grows thicker. It was observed that thicker bondlines decrease the strength of a joint by increasing the load path eccentricity and, in so doing, increase the peel stresses in the joint. Indeed, the increased peel stresses are most likely the only contributor to the decrease in apparent strength of thicker bonds.

In the adhesive strength comparison tests, it was found that the thin-adherend tests gave different comparative results than the thick-adherend tests. Using the thick-adherend specimens, the MGS adhesive was found to have higher apparent shear strength than the PTM&W adhesive. However, the thin-adherend results showed that the PTM&W adhesive had higher apparent shear strength than the MGS adhesive. Thus, thin-adherend specimen results should be closely examined when used to compare different adhesives, since high-peel stresses lead to a combined peel-shear state of stress. This combined state of stress does not give the tester a true view of the apparent shear stress, but rather an indication of the adhesive behavior under this type of loading. It is recommended that thick adherends be used when comparing different adhesive systems for apparent shear strength, and that thin adherends should be used for qualitative tests only.

The adhesive shear stress-strain behavior was evaluated over the range of bondline thicknesses using the thick-adherend test specimen and the KGR-type extensometers. It was found that the KGR-type extensometers could correctly characterize the stress-strain relationship of the adhesive. The average adhesive modulus found by the thick-adherend test method differed slightly with the bulk adhesive test samples, but nowhere near that as found in previous studies [14 and 26]. In addition, it was found that the KGR-type extensometers provided more accurate information, especially in the linear elastic region of the adhesive, when a fourth measuring pin was added and small mounting holes were drilled in the adherends. A factor proposed by Yang, et al. [23] was used to correct for adherend deflection during loading of the thick-adherend specimen. Other correction factors were offered for both a three-pin and four-pin configuration to correct for the effect of bondline thickness on the modulus results.

The ASTM D 3165 test method with C/Ep adherends was used to evaluate the effect of environmental conditions on adhesive joint characteristics. Specimens with bondlines from 0.015-0.160 inch were tested over a range of environmental conditions. Apparent shear strengths were found to decrease as the adhesive was exposed to heat and moisture. The dry and wet T_g values of the adhesive were also found to have a significant effect on the apparent shear strength of the adhesive joint. Failure modes of the specimen were found to be dependent on the environmental condition and strongly dependent on the adhesives ductility at different environments.

Thick-adherend specimens were used to characterize the adhesive shear stress-strain behavior for a bondline thickness of 0.015″. It was found that the KGR-type extensometer could provide reliable data over the entire environmental spectrum. The MGS adhesive was characterized for a variety of environmental conditions, showing similar results to other epoxy adhesives.

5. REFERENCES.

1. Kuno, J.K., *Structural Adhesives and Bonding*, Proceedings of the Structural Adhesives Bonding Conference, El Segundo, CA, 1979.

2. Tsai, M.Y., Morton, J., Krieger, R.B., and Oplinger, D.W., “Experimental Investigation of the Thick-Aherend Lap Shear Test,” *Journal of Advanced Mechanics*, April 1996, pp. 28-36.

3. Vinson, J.K., “Adhesive Bonding of Polymer Composites,” *Polymer Engineering and Science*, Vol. 29, No. 19, 1989, pp. 1325-1331.

4. MIL-HDBK-17-3E, “Chapter 5—Structural Behavior of Joints.”

5. “Standard Test Method for Apparent Shear Strength of Single-Lap-Joint Adhesively Bonded Metal Specimens by Tension Loading,” *Annual Book of ASTM Standards*, Vol. 15.06, 1997, pp. 45-48.

6. “Standard Test Method for Strength Properties of Adhesives in Shear by Tension Loading of Single-Lap-Joint Laminated Assemblies,” *Annual Book of ASTM Standards,* Vol. 15.06, 1997, pp. 199-202.

7. "Standard Test Method for Thick-Adherend Metal Lap-Shear Joints for Determination of the Stress-Strain Behavior of Adhesives in Shear by Tension Loading." *Annual Book of ASTM Standards,* Vol. 15.06, 1997, pp. 470-475.

8. Krieger, R.B., Jr., "Stress Analysis Concepts for Adhesive Bonding of Aircraft Primary Structure," *Adhesively Bonded Joints: Testing, Analysis, and Design,* ASTM STP 981, W.S. Johnson, ed., American Society for Testing and Materials, Philadelphia, Pennsylvania, 1988, pp. 264-275.

9. Volkersen, O., "Die Neitkraftverteilung in Zugbeanspruchten Neitverbindungen mit Konstanten Laschenquerschnitten," *Luftfahrtforschung*, Vol. 15, 1938, pp. 4-47.

10. Goland, M., and Reissner, E., "The Stresses in Cemented Joints," *Journal of Applied Mechanics*, March 1944, pp. A.17-A.27.

11. Kutscha, D., "Mechanics of Adhesive-Bonded Lap-Type Joints: Survey and Review," Technical Report AFML-TDR-64-298, 1964.

12. Kutscha, D. and Hofer, K.E. Jr., "Feasibility of Joining Advanced Composite Flight Vehicles," Technical Report AFML-TR-68-391, 1969.

13. Adams, R.D. and Wake, W.C., *Structural Adhesive Joints in Engineering*, Elsevier Applied Science Publishers, London, England, 1984.

14. Guess, T.R., Allred, R.E., and F.P. Gerstle, Jr., "Comparison of Lap Shear Tests," *Journal of Testing and Evaluation*, Vol. 5, No. 3, p. 1977, p. 84-93.

15. Hart-Smith, L.J., "Adhesive-Bonded Single-Lap Joints," Douglas Aircraft Co., NASA Langley Report CR 112236, 1973.

16. Hart-Smith, L.J., "Adhesive-Bonded Double-Lap Joints," Douglas Aircraft Co., NASA Langley Report CR 112235, 1973.

17. Hart-Smith, L.J., "Adhesive-Bonded Scarf and Stepped-Lap Joints," Douglas Aircraft Co., NASA Langley Report 112237, 1973.

18. Hart-Smith, L.J., "Analysis and Design of Advanced Composite Bonded Joints," Douglas Aircraft Co., NASA Langley Report CR-2218, 1974.

19. Oplinger, D.W., Proceedings of the Fourth Army Materials Technology Conference—Advances in Joining Technology, September 1975.

20. Oplinger, D.W., "Effects of Adherend Deflections in Single-Lap Joints," *International Journal of Solids and Structures*, Vol. 31, 1994, pp. 2565-2587.

21. Yang, C., Pang, S.S., and Griffen, S.A., "Failure Analysis of Adhesive-Bonded Double-Lap Joints Under Cantilevered Bending," *Polymer Engineering and Science*, Vol. 31, pp. 533-538, 1992.

22. Yang, C. and Pang, S.S. "Stress-Strain Analysis of Single-Lap Composite Joints Under Cylindrical Bending," *Composites Engineering*, Vol. 3, pp. 1051-1063, 1993.

23. Yang, C., Huang, H., Tomblin, J.S., and Oplinger, D. W., "Evaluation and Adjustments for ASTM D 5656 Standard Test Method for Thick-Adherend Metal Lap-Shear Joints for Determination of the Stress-Strain Behavior of Adhesives in Shear by Tension Loading," *Journal of Testing and Evaluation*, JTEVA, Vol. 29, No. 1, pp. 36-43, January 2001.

24. Yang, C., Huang, H., Tomblin, J.S., and Harter, P.F., "Stress Analysis and Failure Load Prediction of Thick Adhesive Single-Lapped Composite Joint Under Tension," in progress.

25. Post, D., Czarnek, R., Wood, J.D., and Job, D., "Deformations and Strains in a Thick-Adherend Lap Joint," Adhesively Bonded Joints: Testing, Analysis and Design, ASTM STP 981, American Society for Testing and Materials, Philadelphia, PA, 1988, pp. 107-118

26. Kassapoglou, C. and Adelmann, J.C., "KGR-1 Thick-Adherend Specimen Evaluation for the Determination of Adhesive Mechanical Properties," 23rd International SAMPE Technical Conference, October 21-24, 1991.

27. "Standard Guide for Preparation of Aluminum Surfaces for Structural Adhesives Bonding (Phosphoric Acid Anodizing)," *Annual Book of ASTM Standards*, ASTM D 3933, Vol. 15.06, 1997, pp. 287-290.

28. Bohlmann, R.E., "Development of Adhesive Design Allowables," MIL-HDBK-17 Input, September 1997.

29. MIL-HDBK-17-1E, Bonded Joints, pp. 7-45 – 7-63.

APPENDIX A—CALIBRATION PROCEDURE FOR THE KGR-TYPE DEVICES

This appendix discusses the procedure used for calibrating the KGR-type devices. The extensometers that the KGR-type fixtures are attached to are calibrated over a 1-inch gage section. However, once the fixtures are attached to the extensometers, this calibration is invalid. The point of measurement of the KGR-type fixtures is at the pins, so a calibrating fixture was devised to check the reading from the extensometers when fitted with the KGR-type fixtures.

The calibrating fixture was attached to the MTS test stand via the clevis arrangement. The KGR-type devices were attached in the same manner as an actual ASTM D 5656 test, and a simple calibration was run. The initial value for the actuator displacement and both KGR-type devices were recorded. Then the actuator was moved slightly and all three readings were recorded again. This continues for approximately 100 readings over a total displacement of at least 0.010″. A total of ten calibrations cycles were run and plotted.

The KGR-type devices displacements were plotted versus the actuator displacement. A linear curve fit was applied to each curve so that the correction factor could be found. The slope of the curve gives the correction factor for each device. An example of this process is seen in figure A-1. The slopes for each device from the ten different calibration runs were averaged and are can be seen in table A-1. The average for each device is used as the correction factor when reducing data. It can be seen that the addition of the KGR-type fixtures to the extensometers produces an error of roughly 3% and is device dependent.

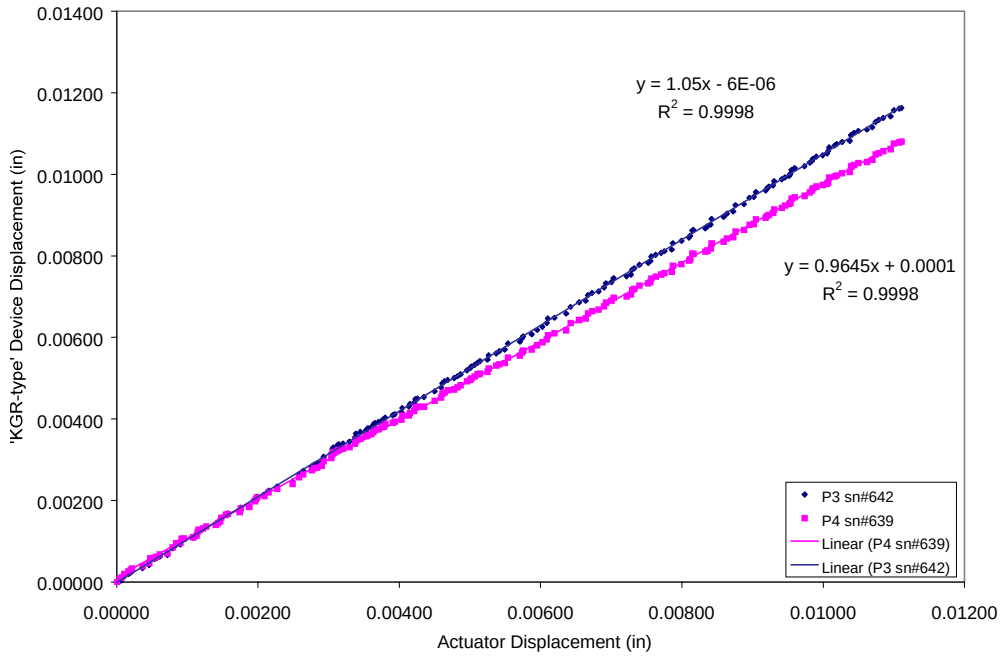

FIGURE A-1. EXAMPLE OF CALIBRATION CURVES FOR THE KGR-TYPE DEVICES CALIBRATION FACTOR (Note that actual displacement and the measured displacement from the devices are not a 1:1 correlation.)

TABLE A-1. KGR-TYPE DEVICE CORRECTION FACTORS IN TABULAR FORM
(Data is shown for the average of ten calibration runs and also the standard deviation.)

	Correction for device 642	Correction for device 639
cal1 8/30/99	1.00190	0.96590
cal2 8/30/99	0.98740	0.95420
cal3 8/30/99	1.00350	0.96690
cal4 8/30/99	1.03630	0.98310
cal5 8/30/99	0.99610	0.96880
cal6 8/30/99	1.00280	0.96430
cal7 8/30/99	1.02400	0.96940
cal8 8/30/99	1.05000	0.96450
cal9 8/30/99	1.00910	0.98150
cal10 8/30/99	1.04040	0.99740
Average	1.01515	0.97160
Std. Deviation	2.1%	1.2%

APPENDIX B—PASTE ADHESIVE MIXING PROCEDURE

The procedure used for mixing the paste adhesives in this investigation is outlined below. This procedure is used as a standard at the Witchita State University (WSU) National Institute for Aviation Research (NIAR) Composites Lab. The mixing ratios for the paste adhesives used in this investigation are given in table B-1.

TABLE B-1. ADHESIVE MIXING RATIOS FOR ALL THREE PASTE ADHESIVES USED IN THIS INVESTIGATION

Adhesive System Constituents	Manufacturers Designation	Resin Mix Ratio (Parts by Weight)	Resin Mix Ratio (Parts by Volume)
Base resin	PTM&W ES6292-A	100	4
Curing agent	PTM&W ES6292-B	28	1
Base resin	MGS A100	100	100
Curing agent	MGS B100	30	36
Base resin	Hysol EA9394-A	100	N/A
Curing agent	Hysol EA9394-B	17	N/A

Equipment:

- Triple beam balance or other measuring device accurate to 0.1 grams.
- Mixing cups—paper or cardboard preferably
- Mixing utensil—wooden or plastic, wooden tongue depressors are cheap and work well

Procedure:

- Place empty mixing cup on balance and tare.
- Dispense approximate amount needed of part of base resin (part A) into mixing cup.
- Weigh and calculate amount of curing agent (part B) and set balance to that amount.
- Add appropriate amount of curing agent to mixing cup.
- Remove cup from balance and mix thoroughly by hand.
- Mix until a homogeneous appearance is achieved and no swirls or contrasting colors or consistency are visible or present in the cup. This is usually achieved after 3-4 minutes of mixing. Pay special attention to the sidewalls and bottom of cup. A flat utensil is recommended for mixing.
- Dispense mixture into a new mixing cup and continue mixing with a new utensil. This is commonly called double-cupping and aids in the mixing of any residual base constituents left on the walls of the first mixing cup.

- Mixing is complete after this step. Make sure and check for a homogeneous appearance. Mixed adhesive should have no swirls or color variations.

- Adhesive should be applied within 30-45 minutes after mixing is complete. Because pot life differs from adhesive to adhesive, manufacturers specification should be consulted concerning usable pot life of adhesive after mixing.

APPENDIX C—LABELING SCHEME FOR ALL SPECIMENS USED IN THIS INVESTIGATION

All specimens for this investigation were labeled using the format shown below in figure C-1. This six-digit, alphanumeric code provided a unique label for each specimen tested in this investigation.

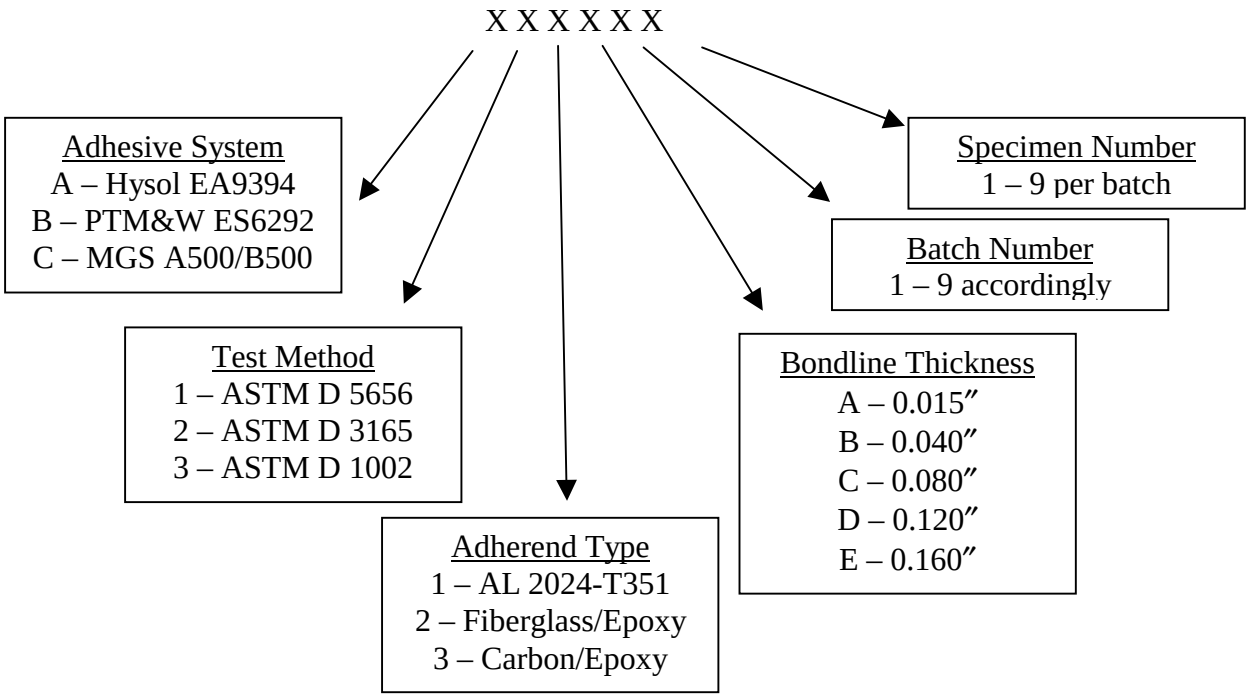

FIGURE C-1. LABELING SCHEME FOR ALL SPECIMENS USED IN THIS INVESTIGATION

APPENDIX D—"NEAT" ADHESIVE PROPERTIES

This appendix will discuss the different procedures used to characterize the mechanical properties of the neat adhesive. As stated previously, three paste adhesives were used for this investigation. For the Hysol EA9394 system, the manufacturer provided data. However, at the time of this study, the MGS and PTM&W adhesive systems were relatively new and had no technical data supplied with them. It was necessary to find the neat adhesive properties of these adhesives for use in analytical modeling and in quantifying the experimental results. The tensile modulus, Poissons ratio, and the wet and dry glass transition (T_g) temperatures were found using bulk adhesive specimens.

The wet and dry T_g temperatures for the MGS and PTM&W adhesive systems were found using Dynamic Mechanical Analysis (DMA). Specimens for these tests were cut from a block of solid adhesive, which was prepared and cured as described in appendix B. The dry specimens were tested as-fabricated, while the wet specimens were conditioned in an environmental chamber for 1000 hours at 145°F and 85% relative humidity. Table D-1 shows the T_g values for both adhesives and both conditions. It should be noted that there is no exact value for the T_g, but rather a range. The DMA tests provide two curves from which the range can be found. However, a fixed value is usually needed for design purposes. Typically, the storage modulus curve defines the lower bound of the T_g range, and this value is chosen as the glass transition temperature. Representative curves from the DMA tests are shown in figures D-1 through D-4.

TABLE D-1. T_g VALUES FOR BOTH ADHESIVE SYSTEMS TESTED

Adhesive System	Storage Modulus		Tan δ Peak	
	dry T_g	wet T_g	dry T_g	wet T_g
MGS A100/B100	175°F	135°F	207°F	164°F
PTM&W ES6292	167°F	127°F	198°F	153°F

The neat adhesive tensile modulus and Poisson's ratio were found using neat adhesive specimen. An adhesive plate was cast and specimens were machined out of it with dimensions 9 inches long by 2 inches wide by 0.375 inch thick. This approach was also used by Kassapoglou and Adelmann and was adopted for this study [D-1]. Each specimen was fitted with two sets of longitudinal and transverse strain gages, which where used to record the axial and transverse strain during the test. The specimens were gripped and pulled in tension to approximately 500 lbs, well within the elastic region of the test specimen. This was repeated a total of five times for each specimen, and data were gathered for the load and strain data for each test. Two specimens for each adhesive were tested for redundancy. From the data that was gathered, a stress-strain chart was created for each specimen, from which the elastic modulus was found. In addition, Poisson's ratio was found by plotting the lateral strain vs the longitudinal strain. Ten values for both the tensile modulus and Poisson's ratio were found for each adhesive system. From this data, an accurate measure of the shear modulus was then obtained using the formula for isotropic materials shown in equation D-1. The averages for each neat adhesive property are given in table D-2.

TABLE D-2. SUMMARY OF BULK ADHESIVE TEST SPECIMEN RESULTS FOR MODULUS AND POISSON'S RATIO

Adhesive System	Tensile Modulus *E* (ksi)	Poisson's Ratio ν	Calcluated Shear Modulus *G* (ksi)*
MGS A100/B100	509	0.343	189.6
PTM&W ES6292	229.4	0.306	87.9
Hysol EA9394	615	0.450	212

*Shear modulus was calculated using equation D-1

$$G = \frac{E}{2(1+\nu)} \qquad \text{(D-1)}$$

where: *E* is the tensile modulus, *G* is the calculated shear modulus, and ν is Poisson's ratio.

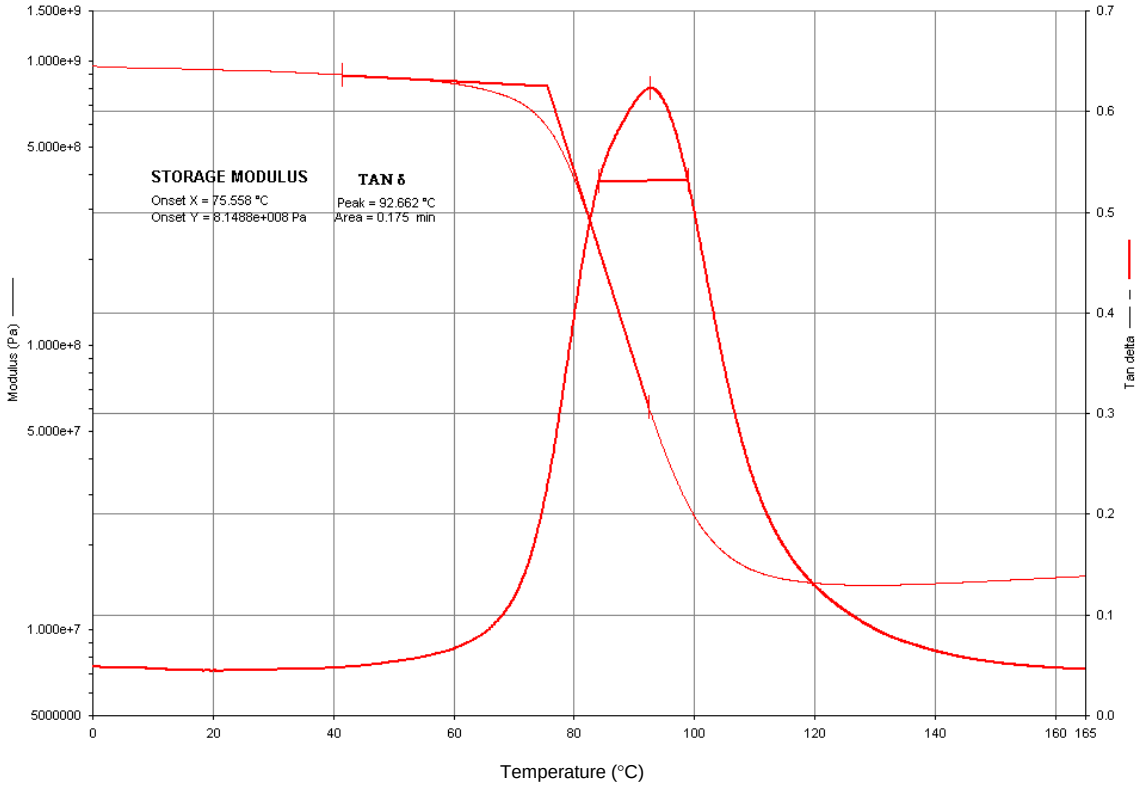

FIGURE D-1. GRAPH OBTAINED FROM DMA TEST OF A DRY PTM&W ADHESIVE BULK SPECIMEN SHOWING THE RANGE OF T_g VALUES

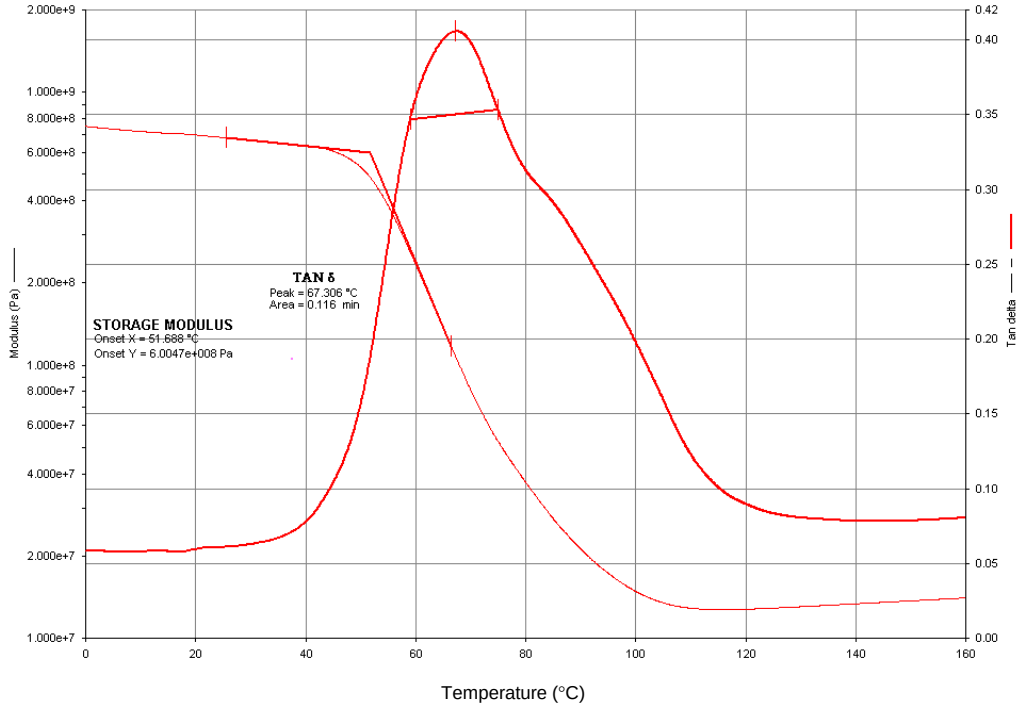

FIGURE D-2. GRAPH OBTAINED FROM DMA TEST OF A WET PTM&W ADHESIVE BULK SPECIMEN SHOWING THE RANGE OF T_g VALUES

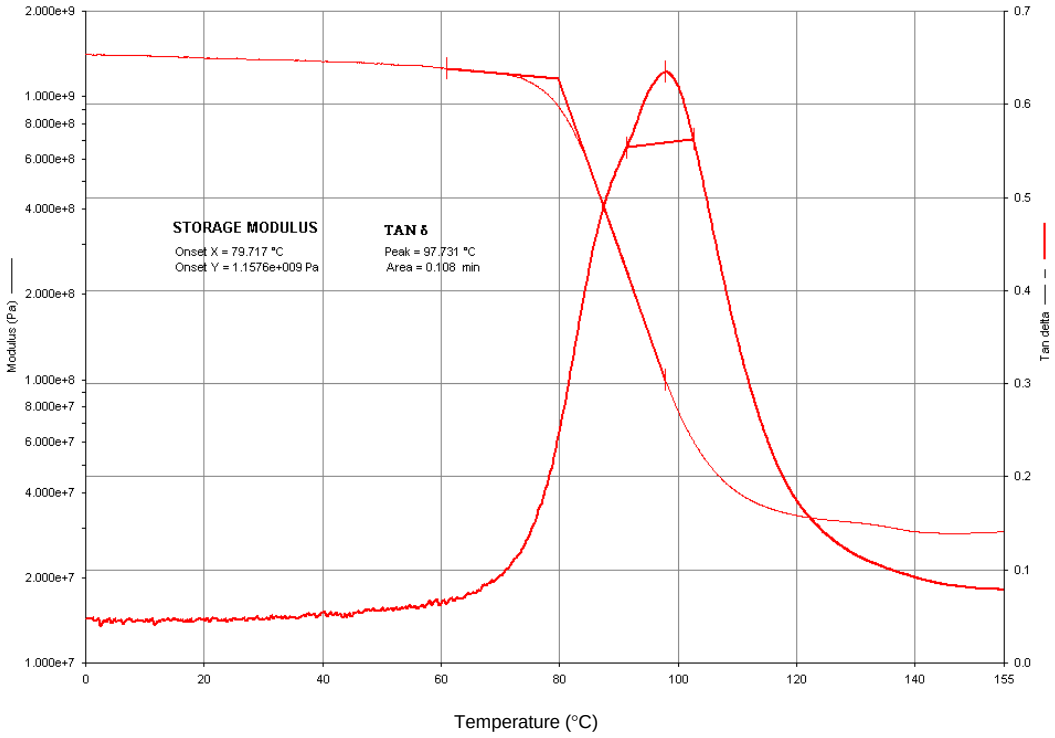

FIGURE D-3. GRAPH OBTAINED FROM DMA TEST OF A DRY MGS ADHESIVE BULK SPECIMEN SHOWING THE RANGE OF T_g VALUES

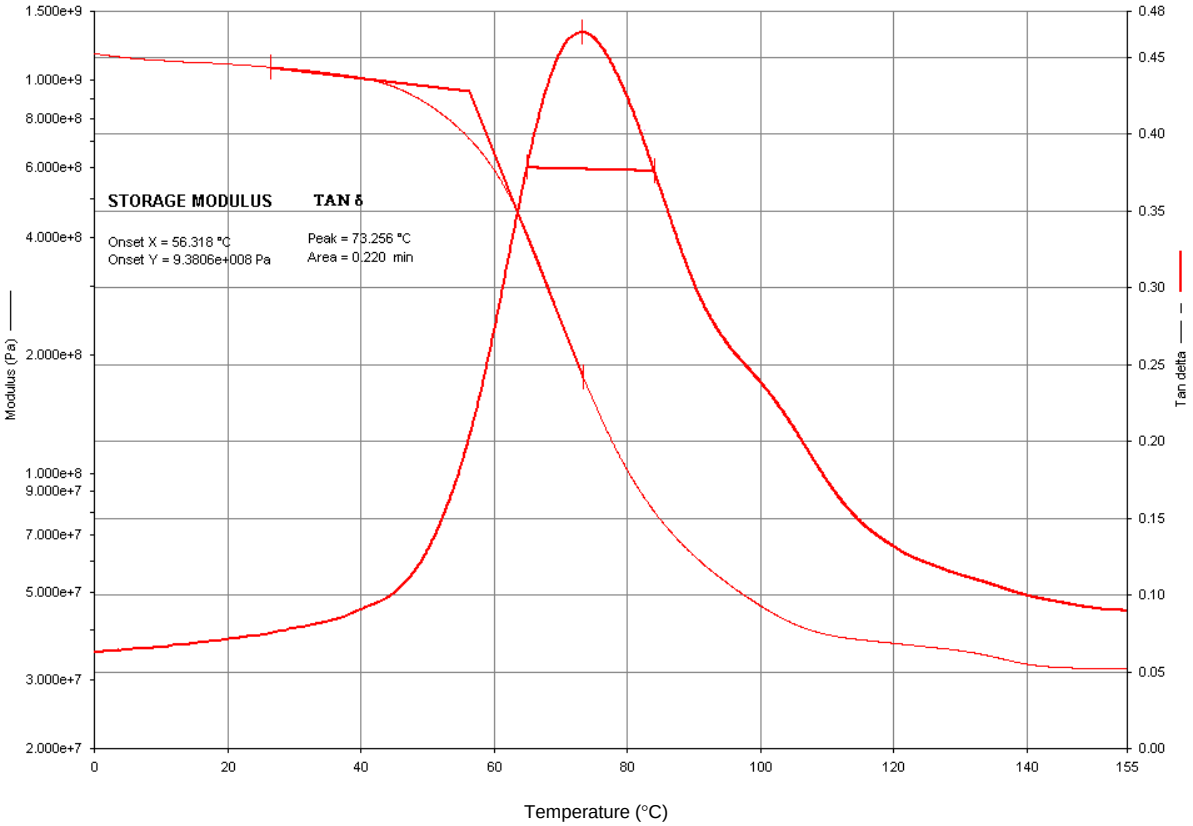

FIGURE D-4. GRAPH OBTAINED FROM DMA TEST OF A WET MGS ADHESIVE BULK SPECIMEN SHOWING THE RANGE OF T_g VALUES

REFERENCE

D-1 Kassapoglou, C. and Adelmann, J.C., "KCR-1 Thick-Adherend Specimen Evaluation for the Determination of Adhesive Mechanical Properties," 23rd International SAMPE Technical Conference, October 23-24, 1991.

APPENDIX E—LAY-UP AND FABRICATION PROCEDURE FOR COMPOSITE LAMINATES

In order to investigate the effect of adherend type on the apparent shear strength of the ASTM D 3165 and D 1002 lap shear joints, two different composite laminates were used in this investigation and the analytical analyses carried out by Yang, et al [E-1]. The composite laminates were designed to be quasi-isotropic, while remaining of similar thickness to the ASTM D 3165 and D 1002 test configurations. Two composite prepregs of interest to the AGATE consortium were chosen:

- FiberCote E765/T300 3KPW Plain Weave Carbon Fabric
- FiberCote E765/7781 E-Glass Satin Weave Fabric

The lamina mechanical properties for C/Ep and Gl/Ep are given in tables E-1 and E-2 respectively. Both prepregs were designed for vacuum-bag oven cure at 275°F. The lay-up of both the C/Ep and Gl/Ep laminates was [0°/60°/-60°/0°/-60°/60°/0°]. Lay-up and fabrication of the composite laminates was carried out using the procedure discussed below, which applies to both types of material unless specified otherwise.

- Individual plies were cut into 20-inch squares for each angle, taking care to designate fiber direction and reference edge.

- Plies were aligned and stacked individually on a large, thick aluminum plate covered with separator film according to the lay-up sequence. Rollers were used to eliminate any wrinkling. In the case of the satin weave glass fabric, care was taken to assure that the warp face was mirrored to assure balance in the laminate.

- Separator film was used to cover the stacked prepreg, followed by a thin aluminum call sheet, breather material, and a vacuum bag.

- After assuring vacuum bag integrity, the assembly was placed in an oven and cured under vacuum pressure at 275°F for 2 hours according to manufacturers specifications.

- The vacuum bag was removed after the assembly reached room temperature and each 20-inch-square laminate was cut into either four 9″ by 9″ subpanels for ASTM D 3165 specimens or 4″ by 6″ subpanels for ASTM D 1002 specimens. A reference edge was clearly marked on each subpanel designating an edge perpendicular to the 0° direction of the subpanel.

At this point, the subpanels were ready for bond preparation as discussed in section 2.11.1.2.

TABLE E-1. LAMINA MECHANICAL PROPERTIES FOR FIBERCOTE E765/T300 3KPW CARBON FABRIC (Normalized by CPT= 0.0089 in)

	CTD		RTD		ETD		ETW	
	B-Basis	Mean	B-Basis	Mean	B-Basis	Mean	B-Basis	Mean
F_1^{tu} (ksi)	75.73 (74.76)	83.36 (82.55)	82.18 (80.59)	90.46 (88.99)	85.10 (83.73)	93.68 (92.45)	87.84 (87.20)	96.69 (96.29)
E_1^t (Msi)	---	8.55 (8.46)	---	8.20 (8.09)	---	7.94 (7.83)	---	8.02 (7.97)
ν_{12}^{tu}	---	0.078	---	0.076	---	0.064	---	0.061
F_2^{tu} (ksi)	64.36 (64.15)	74.39 (73.67)	67.34 (67.54)	77.82 (77.56)	71.26 (71.38)	82.35 (81.96)	71.14 (71.56)	82.22 (82.17)
E_2^t (Msi)	---	8.29 (8.25)	---	8.01 (7.98)	---	7.80 (7.78)	---	7.82 (7.83)
F_1^{cu} (ksi)	98.57 (95.46)	109.86 (107.01)	86.42 (87.59)	96.31 (98.19)	57.66 (58.76)	77.80 (78.79)	51.73 (52.42)	57.66 (58.76)
E_1^c (Msi)	---	7.78 (7.40)	---	7.27 (7.37)	---	7.52 (7.58)	---	7.46 (7.51)
F_2^{cu} (ksi)	85.79 (86.24)	98.04 (97.01)	76.58 (78.98)	87.52 (88.84)	61.76 (63.74)	70.59 (71.70)	47.49 (48.66)	54.28 (54.74)
E_2^c (Msi)	---	7.52 (7.38)	---	7.37 (7.37)	---	7.58 (7.64)	---	7.48 (7.55)
F_{12}^{su} (ksi)	20.47	22.07	17.49	18.86	13.29	14.33	11.31	12.19
G_{12}^s (Msi)	---	0.90	---	0.56	---	0.50	---	0.41
F_{13}^{su*} (ksi)	10.18	10.82	9.77	10.38	7.86	8.35	4.82	5.12

* Apparent interlaminar shear strength
CPT = cured ply thickness

TABLE E-2. LAMINA MECHANICAL PROPERTIES FOR FIBERCOTE E765/7781 E-GLASS FABRIC (Normalized by CPT = 0.0109 in)

	CTD (-65°F)		RTD		ETD (160°F)		ETW (160°F) 1000 hrs 85% R.H.	
	B-Basis	Mean	B-Basis	Mean	B-Basis	Mean	B-Basis	Mean
F_1^{tu} (ksi)	50.75 (46.20)	56.81 (49.77)	46.12 (42.70)	51.63 (46.08)	44.15 (40.39)	49.42 (43.58)	38.58 (35.92)	43.19 (38.76)
E_1^t (Msi)	---	3.86 (3.39)	---	3.83 (3.41)	---	3.64 (3.21)	---	3.45 (3.09)
ν_{12}^{tu} (ksi)	---	0.207	---	0.167	---	0.145	---	0.124
F_2^{tu} (ksi)	48.14 (46.25)	53.99 (50.66)	41.83 (40.80)	46.92 (44.69)	40.13 (38.17)	45.01 (41.80)	34.51 (33.07)	38.71 (36.22)
E_2^t (Msi)	---	3.72 (3.51)	---	3.43 (3.26)	---	3.31 (3.07)	---	3.18 (2.95)
F_1^{cu} (ksi)	57.03 (62.23)	69.55 (71.68)	55.46 (59.56)	67.64 (68.59)	44.99 (47.86)	54.87 (55.12)	35.21 (37.50)	42.94 (43.19)
E_1^c (Msi)	---	3.46 (3.61)	---	3.49 (3.48)	---	3.32 (3.36)	---	3.36 (3.38)
F_2^{cu} (ksi)	64.87 (67.99)	72.89 (74.14)	53.94 (54.87)	60.60 (59.84)	40.08 (41.12)	45.03 (44.85)	33.15 (34.10)	37.25 (37.19)
E_2^c (Msi)	---	3.44 (3.49)	---	3.36 (3.34)	---	3.19 (3.13)	---	3.30 (3.25)
F_{12}^{su} (ksi)	20.61	22.67	16.02	17.62	12.93	14.22	9.57	10.52
G_{12}^s (Msi)	---	0.60	---	0.60	---	0.44	---	0.35
F_{13}^{su**} (ksi)	9.22	10.88	7.80	9.21	6.03	7.12	4.26	5.02

** Apparent interlaminar shear strength
CPT = cured ply thickness

REFERENCE

E-1. Yang, C., Huang, H., Tomblin, J.S. and Hartter, P.F., “Stress Analysis and Failure Load Prediction of Thick Adhesive Single-Lapped Composite Joint Under Tension,” in progress.

APPENDIX F—ADHESIVE SHEAR STRESS-STRAIN CHARTS

This section shows the graphical data for all thick-adherend specimens that modulus data was taken from. These graphs show the adhesive shear stress-strain behavior for a particular adhesive organized by bondline thickness. Each curve is labeled by the specimen name that it originated from. Also included is the extensometer(s) reading that the curve came from, i.e., port-side extensometer, starboard extensometer, or the average of the two.

Figures F-1 through F-12 show the shear stress-strain curves for all modulus specimens from test matrix 1. In each figure, the curves that were used to obtain the adhesive shear modulus, *G*, are shown. Figures F-13 through F-18 show the results from test matrix 2-B. These figures show the curves that were used to obtain the shear modulus as a function of environment. Some notes to the reader:

- All charts do not have the same scale.
- Shear stress values are in psi.
- Bondline thicknesses are averages of all specimens shown on each chart.

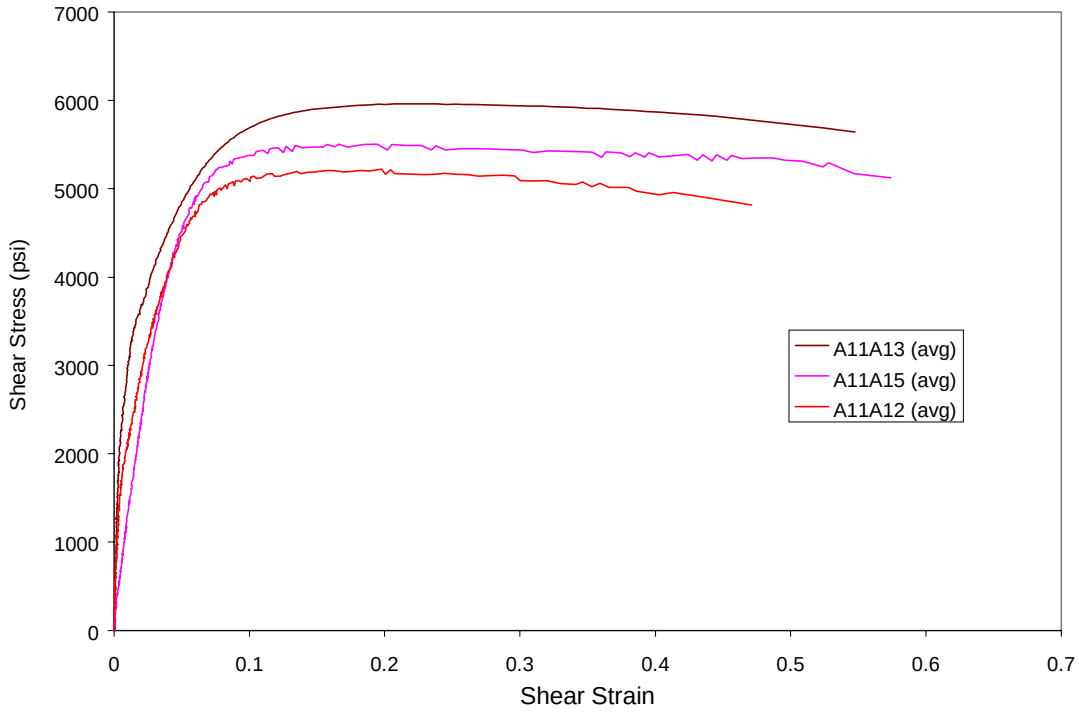

FIGURE F-1. HYSOL EA9394 ADHESIVE SHEAR STRESS-STRAIN CHART FOR T≈0.013 in. RTD

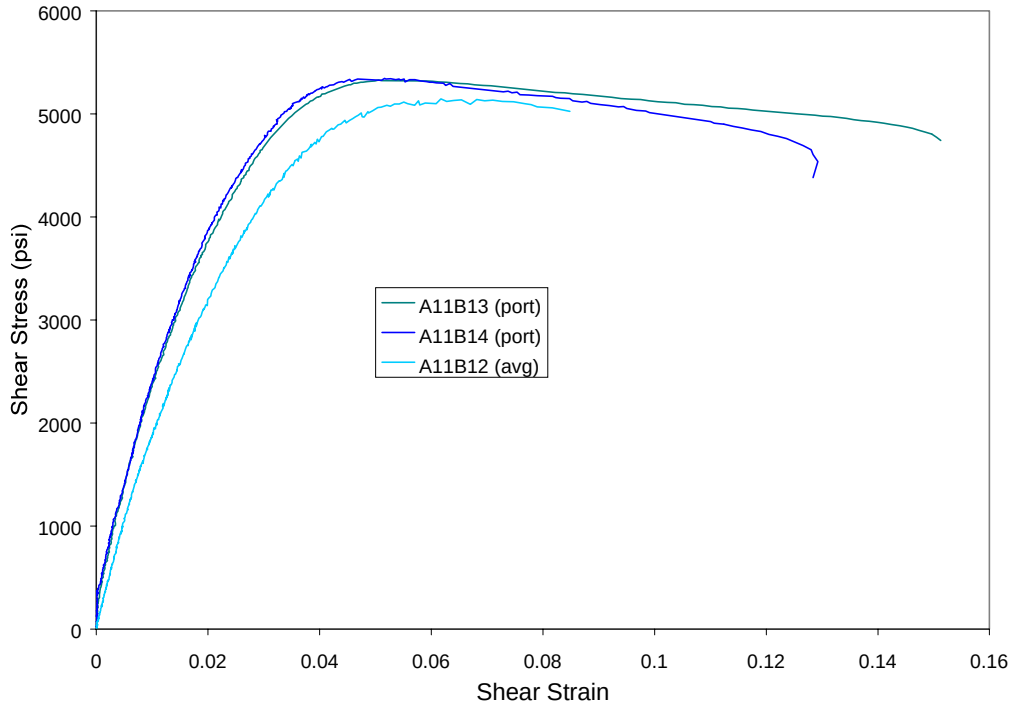

FIGURE F-2. HYSOL EA9394 ADHESIVE SHEAR STRESS-STRAIN CHART FOR T≈0.060 in. RTD

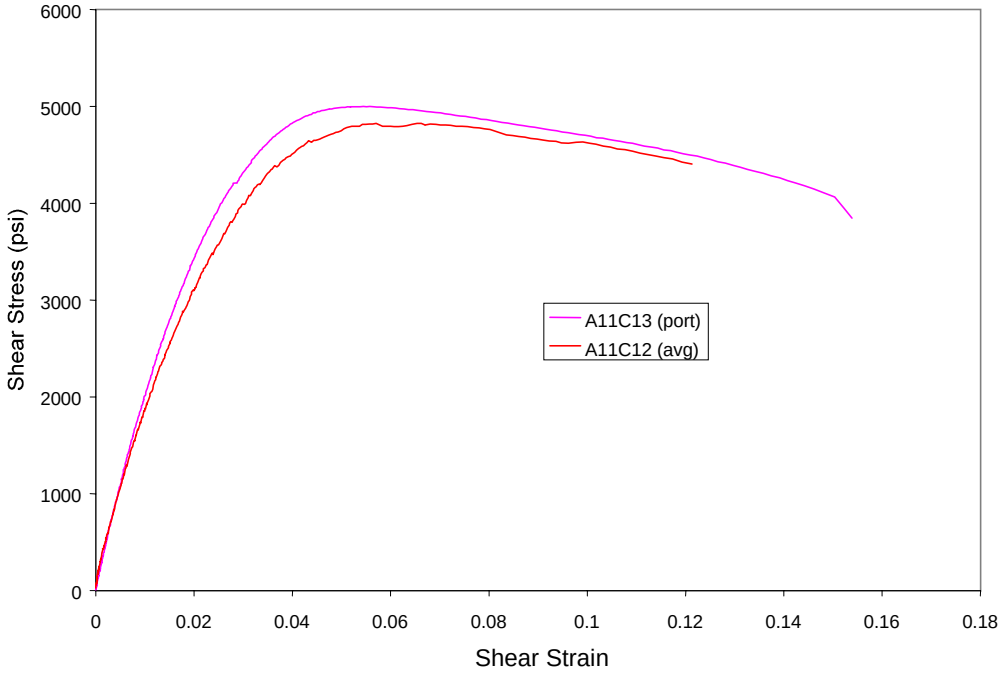

FIGURE F-3. HYSOL EA9394 ADHESIVE SHEAR STRESS-STRAIN CHART FOR T≈0.080 in. RTD

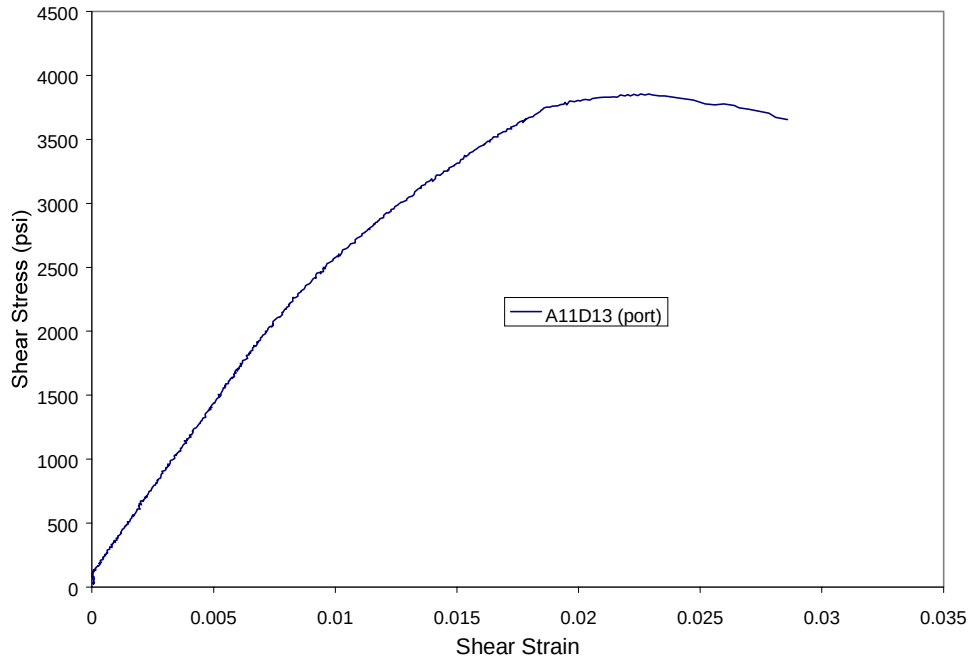

FIGURE F-4. HYSOL EA9394 ADHESIVE SHEAR STRESS-STRAIN CHART FOR T≈0.135 in. RTD

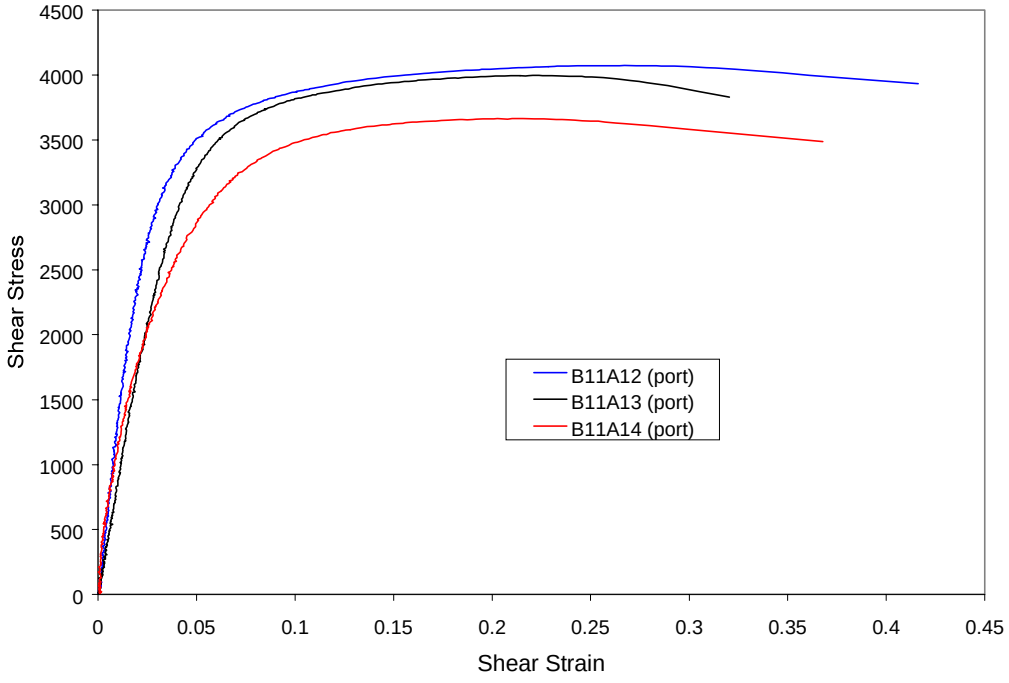

FIGURE F-5. PTM&W ES6292 ADHESIVE SHEAR STRESS-STRAIN CHART FOR T≈0.013 in. RTD

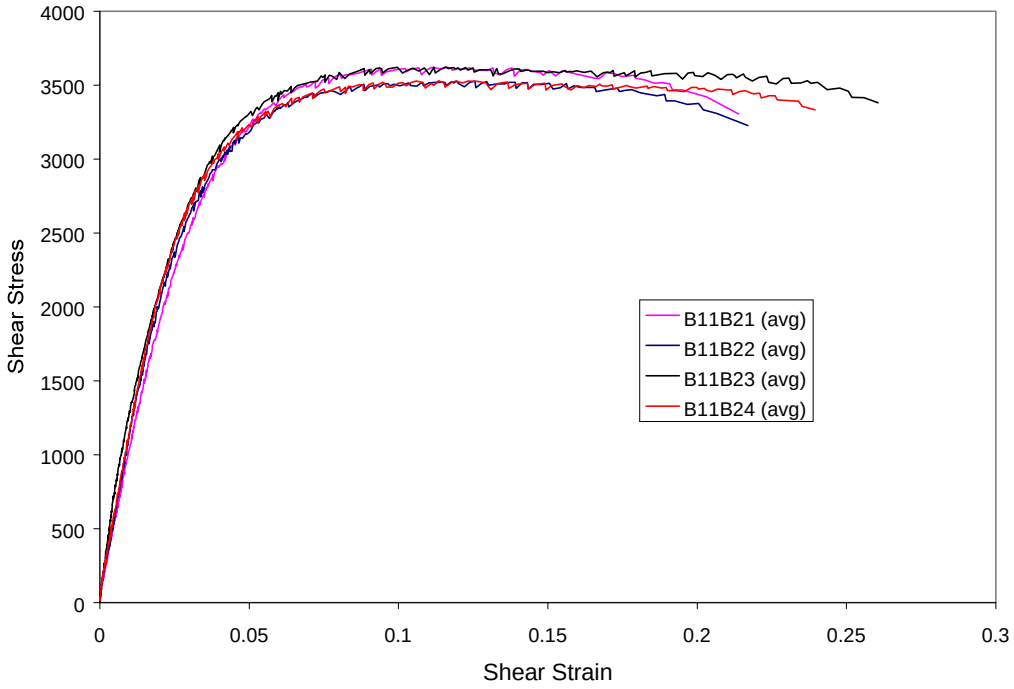

FIGURE F-6. PTM&W ES6292 ADHESIVE SHEAR STRESS-STRAIN CHART FOR T≈0.042 in. RTD

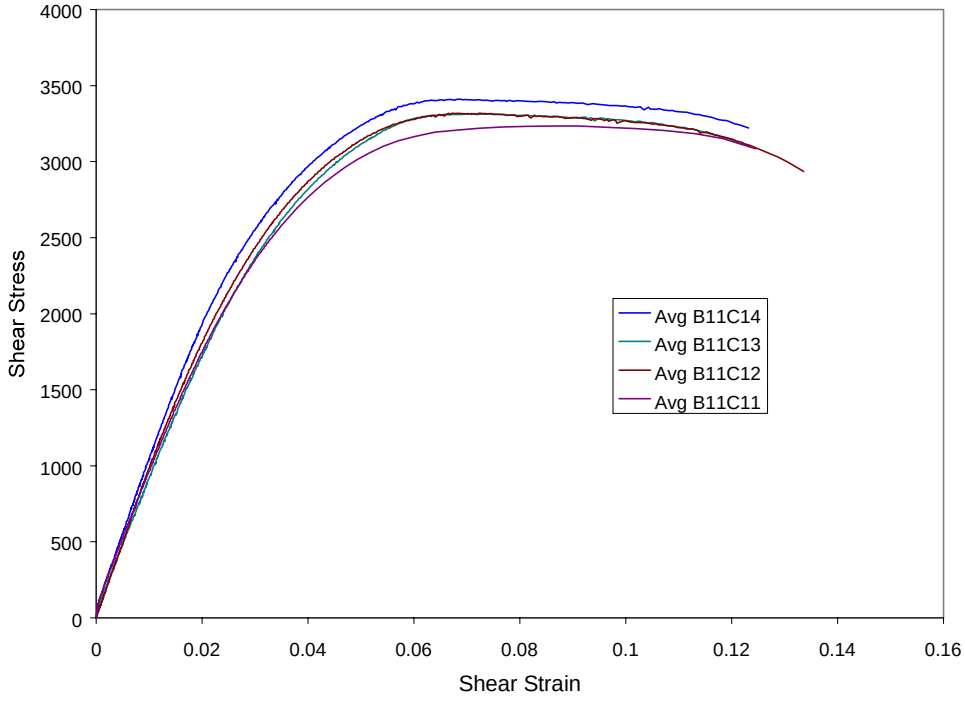

FIGURE F-7. PTM&W ES6292 ADHESIVE SHEAR STRESS-STRAIN CHART FOR T≈0.082 in. RTD

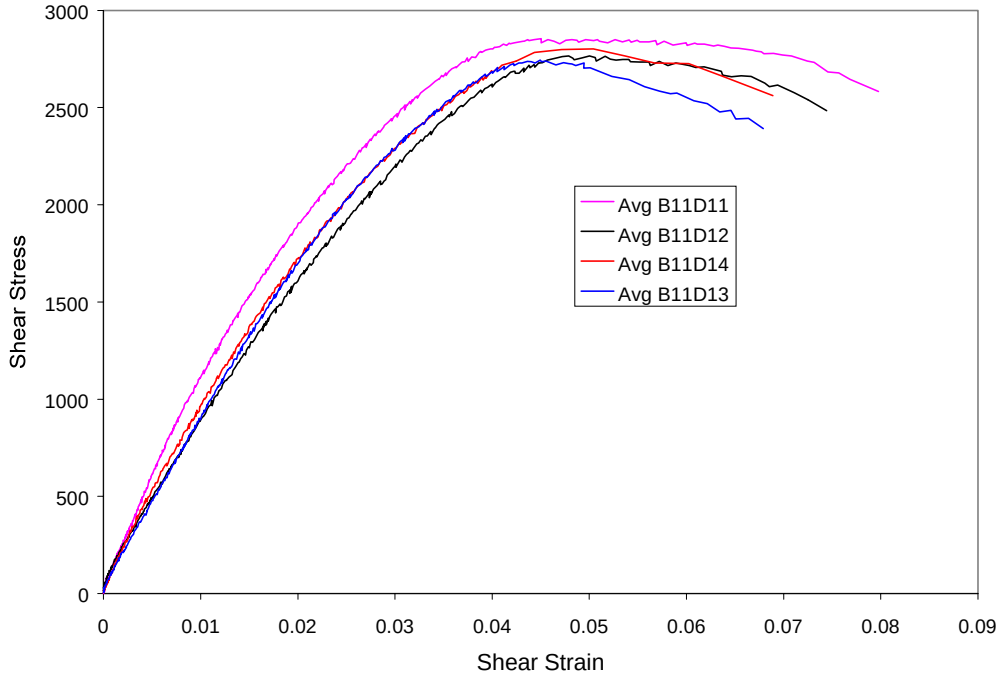

FIGURE F-8. PTM&W ES6292 ADHESIVE SHEAR STRESS-STRAIN CHART FOR T≈0.120 in. RTD

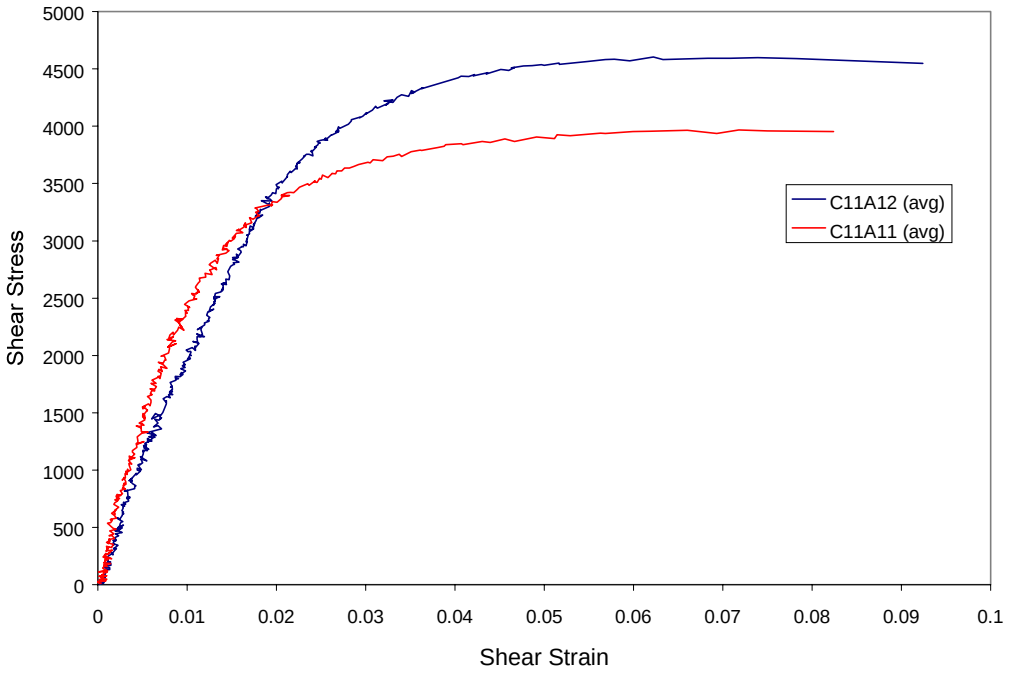

FIGURE F-9. MGS A100/B100 ADHESIVE SHEAR STRESS-STRAIN CHART FOR T≈0.013 in. RTD

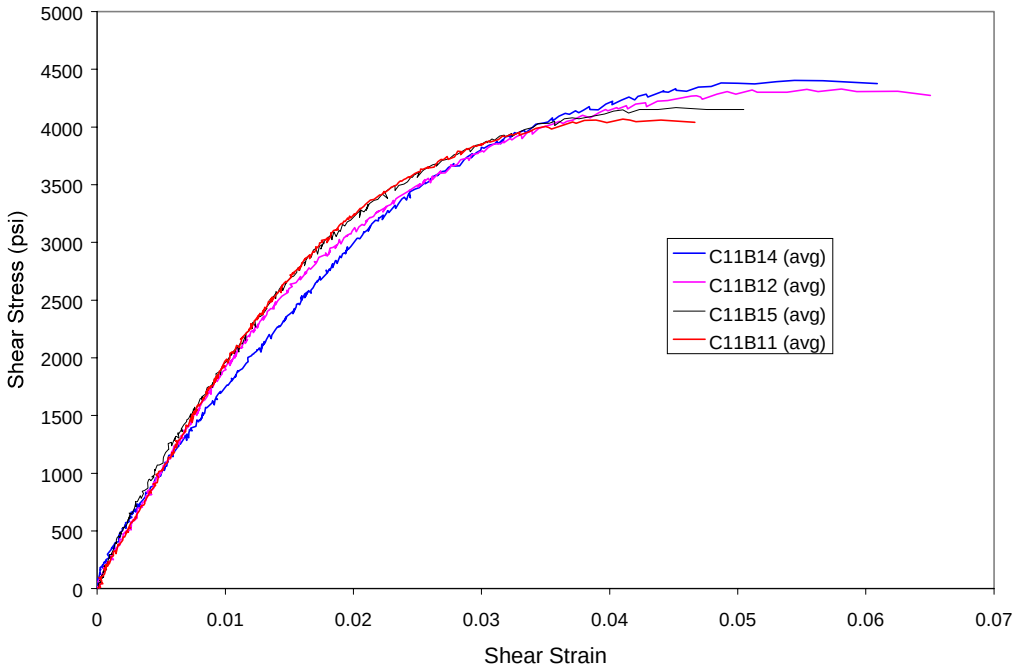

FIGURE F-10. MGS A100/B100 ADHESIVE SHEAR STRESS-STRAIN CHART FOR T≈0.042 in. RTD

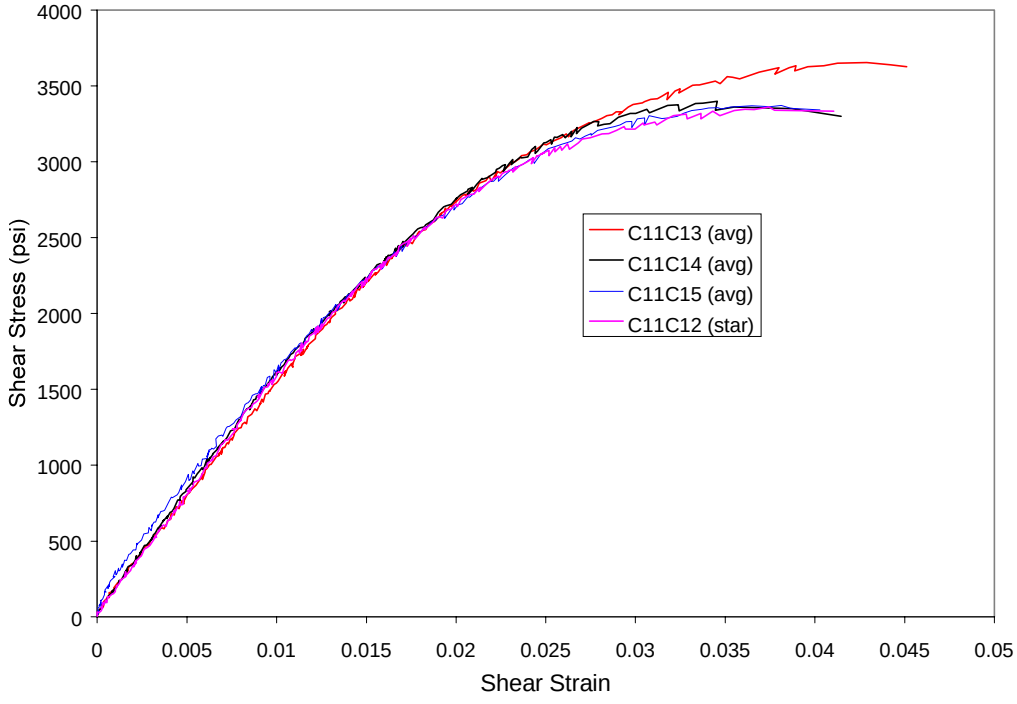

FIGURE F-11. MGS A100/B100 ADHESIVE SHEAR STRESS-STRAIN CHART FOR T≈0.082 in. RTD

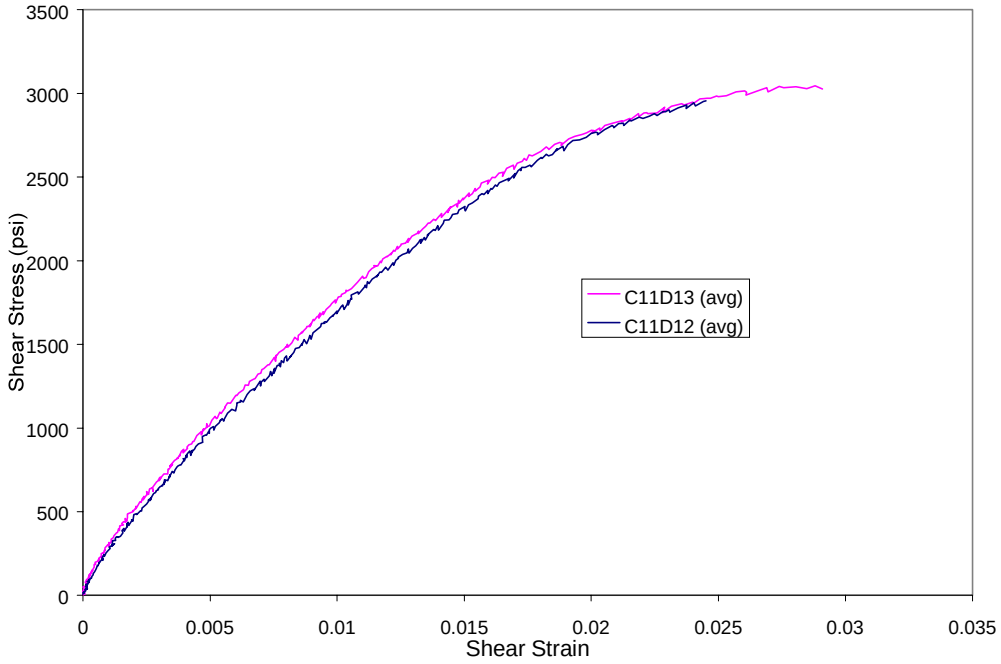

FIGURE F-12. MGS A100/B100 ADHESIVE SHEAR STRESS-STRAIN CHART FOR T≈0.120 in. RTD

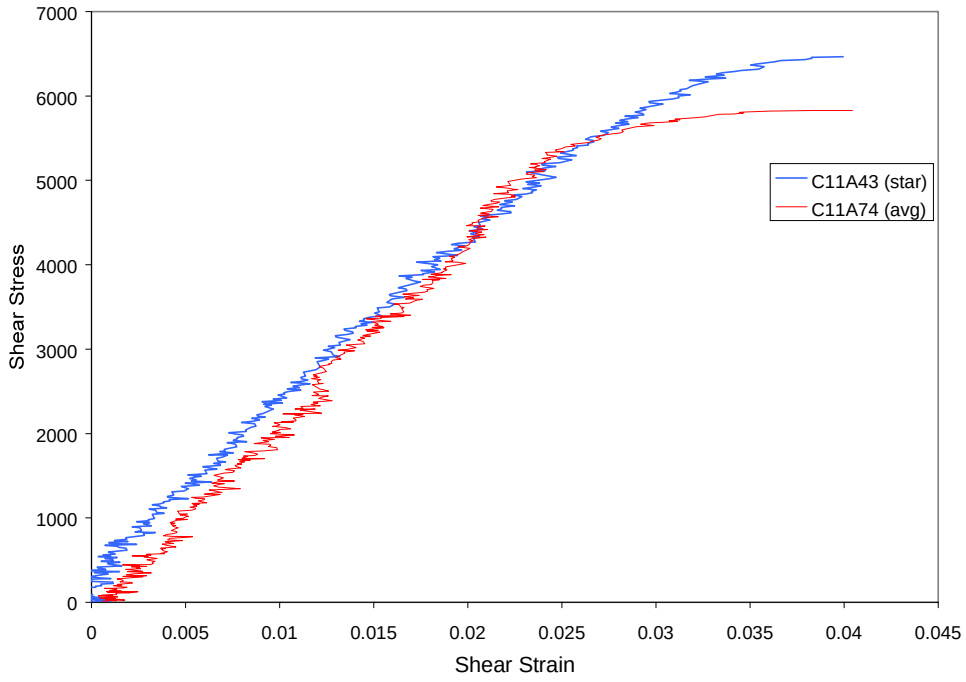

FIGURE F-13. MGS A100/B100 ADHESIVE SHEAR STRESS-STRAIN CHART FOR T≈0.013 in. CD

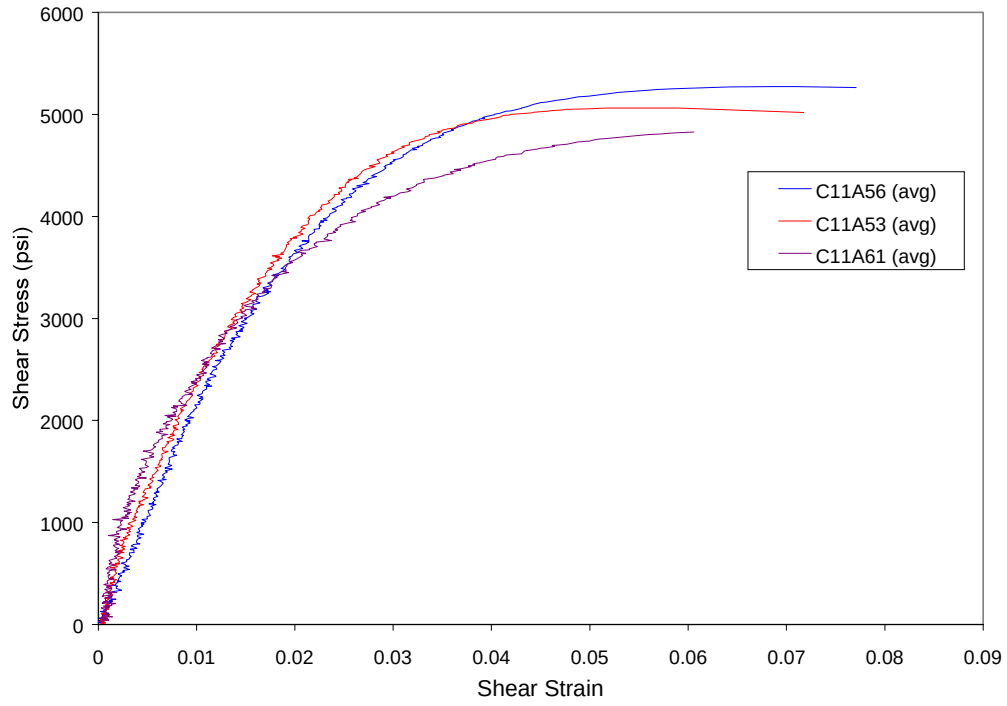

FIGURE F.14. MGS A100/B100 ADHESIVE SHEAR STRESS-STRAIN CHART FOR T≈0.013 in. RTD

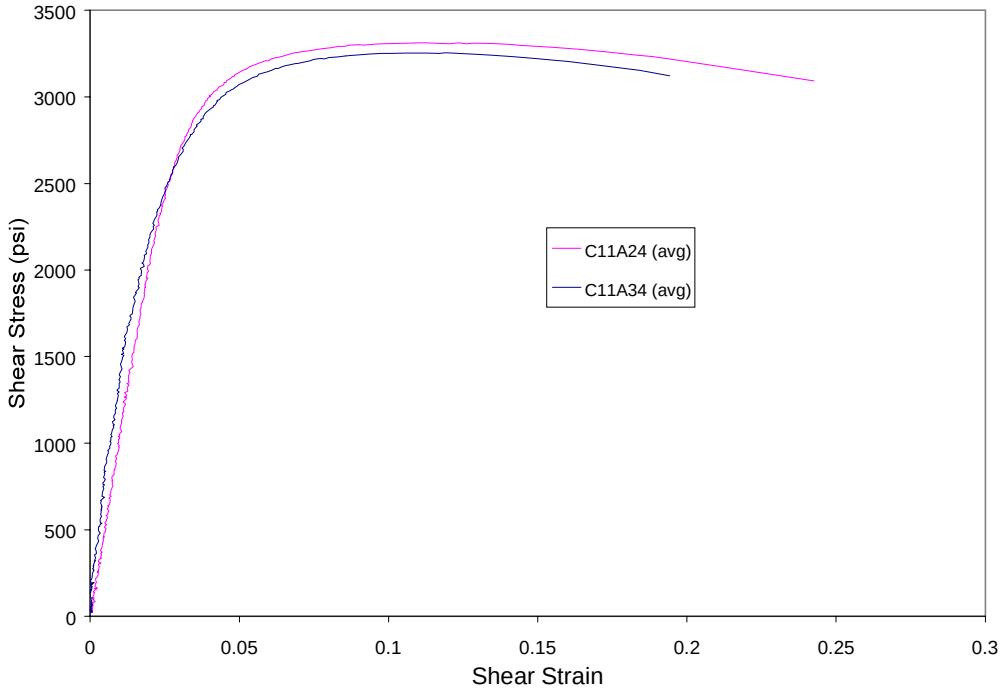

FIGURE F-15. MGS A100/B100 ADHESIVE SHEAR STRESS-STRAIN CHART FOR T≈0.013 in. ETD 160°F

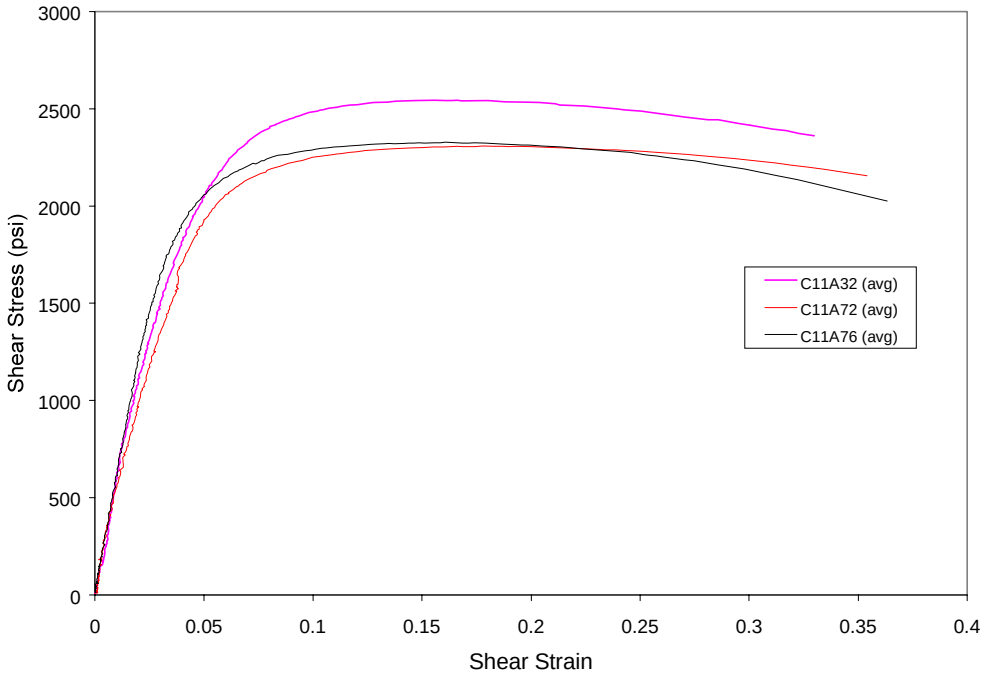

FIGURE F-16. MGS A100/B100 ADHESIVE SHEAR STRESS-STRAIN CHART FOR T≈0.013 in. ETW 160°F

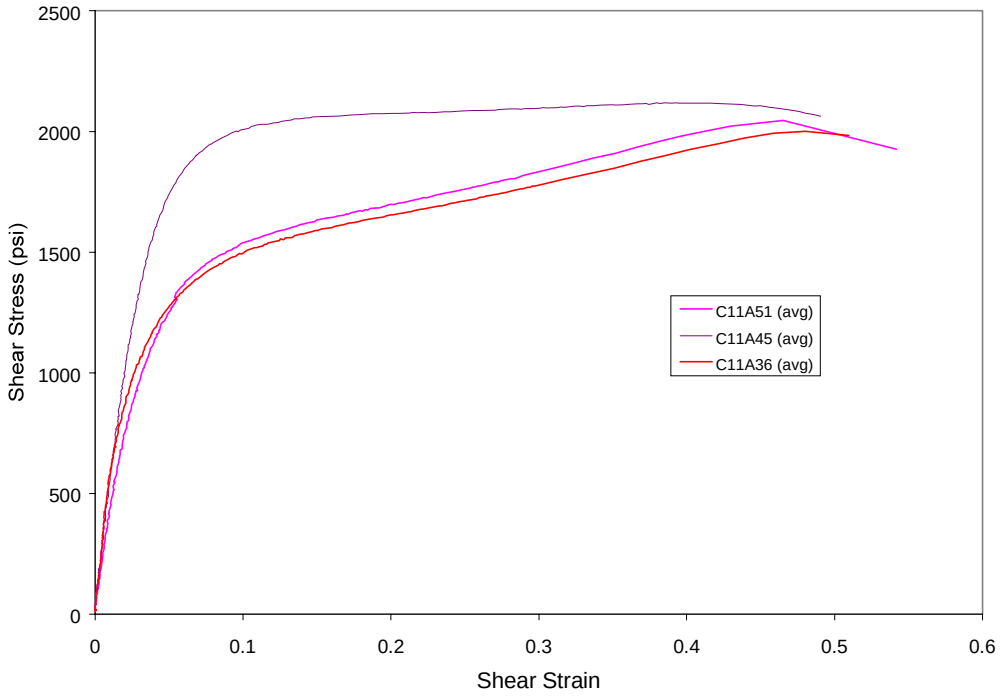

FIGURE F-17. MGS A100/B100 ADHESIVE SHEAR STRESS-STRAIN CHART FOR T≈0.013 in. ETD 200°F

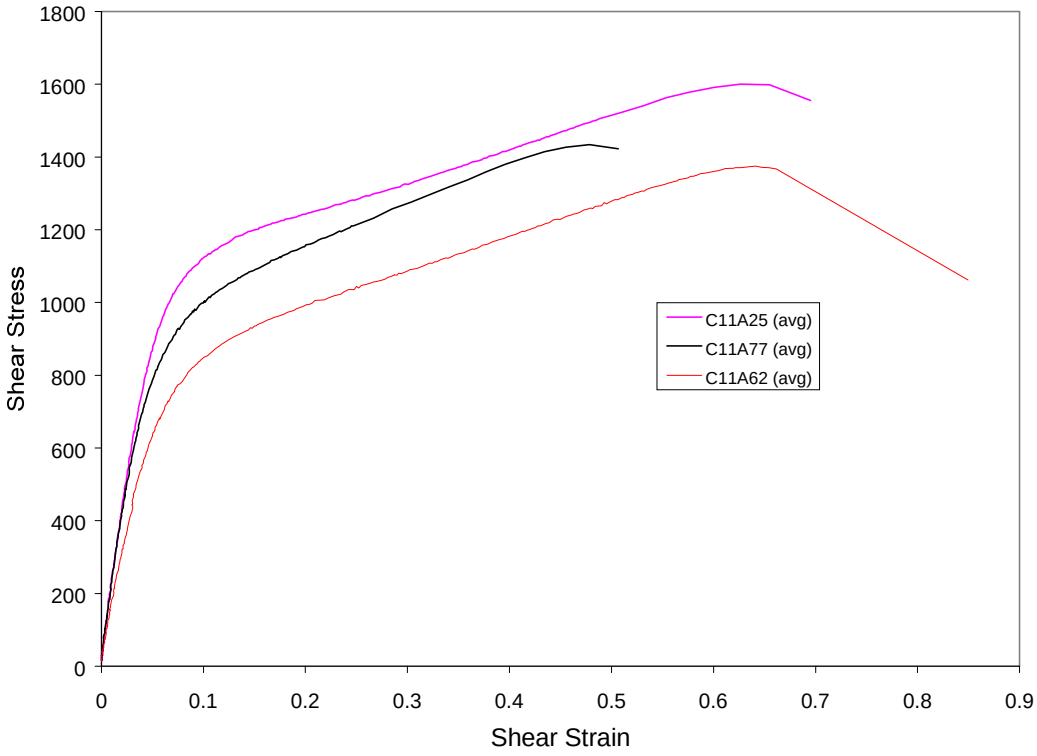

FIGURE F-18. MGS A100/B100 ADHESIVE SHEAR STRESS-STRAIN CHART FOR T≈0.013 in. ETW 200°F